Computer simulation of pedestrian dynamics at high densities

Inaugural - Dissertation

zur

Erlangung des Doktorgrades

der Mathematisch-Naturwissenschaftlichen Fakultät

der Universität zu Köln

vorgelegt von

Christian Eilhardt

aus Rosenheim

Köln

2014

Berichterstatter: Prof. Dr. Andreas Schadschneider

Prof. Dr. Armin Seyfried

Tag der mündlichen Prüfung: 17. Oktober 2014

ACKNOWLEDGEMENTS

During the last few years, I met, worked with, and have been inspired by far too many people to explicitly mention all of them here. I am grateful for the support!

First of all, I want to thank my supervisor Prof. Andreas Schadschneider for introducing me to the exciting topic of pedestrian dynamics and giving me the opportunity to write this dissertation. I have learned a lot in our discussions. His advice and guidance have been invaluable to my work.

I am very grateful to Prof. Armin Seyfried for acting as my second supervisor and also for welcoming me into his working group and supporting me when the continuation of my dissertation was uncertain. I also want to thank Mohcine Chraibi for his advice and for many interesting and constructive discussions about my work and beyond.

Thanks to all of my colleagues at Cologne University and Jülich Research Centre, in particular to Stefan Nowak and Ulrich Kemloh, for providing a pleasant and constructive working atmosphere and for interesting discussions about physics and the world in general.

For proofreading, I want to thank Kanut Kirches and Jonathan Weskott. Your effort made this work better. I am grateful to my friends for their understanding and sympathy when I – once again – worked late into the night.

Finally, I want to express my deepest thanks to my family for their unwavering support at all times. This work would not have been possible without the love and care of my wonderful wife, Gesa. Thank you!

ABSTRACT

Computer simulation of pedestrian dynamics at high densities

by

Christian Eilhardt

The increasing importance and magnitude of large-scale events in our society calls for continuous research in the field of pedestrian dynamics. This dissertation investigates the dynamics of pedestrian motion at high densities using computer simulations of stochastic models.

The first part discusses the successful application of the Floor Field Cellular Automaton (FFCA) in an evacuation assistant that performs faster than real-time evacuation simulations of up to $50,000$ persons leaving a multi-purpose arena. A new interpretation of the matrix of preference improves the realism of the FFCA simulation in U-turns, for instance at the entrance to the stands.

The focus of the second part is the experimentally observed feature of phase separation in pedestrian dynamics into a slow-moving and a completely jammed phase. This kind of phase separation is fundamentally different to known instances of phase separation in e.g. vehicular traffic. Different approaches to modeling the phase separation are discussed and an investigation of both established and new models of pedestrian dynamics illustrates the difficulties of finding a model able to reproduce the phenomenon. The Stochastic Headway Dependent Velocity Model is introduced and extensively analyzed, simulations of the model evolve into a phase-separated state in accordance with the experimental data. Key components of the model are its slow-to-start rule, minimum velocity, and large interaction range.

KURZZUSAMMENFASSUNG

Computersimulation von Fußgängerdynamik bei hohen Dichten

von

Christian Eilhardt

Die zunehmende Bedeutung und die wachsenden Besucherzahlen von Großveranstaltungen in unserer Gesellschaft erfordern kontinuierliche Forschung im Bereich der Fußgängerdynamik. Diese Dissertation untersucht das Verhalten von Fußgängerströmen bei hohen Dichten mit Computersimulationen stochastischer Modelle.

Der erste Teil der Arbeit beschreibt die erfolgreiche Anwendung des 'Floor Field Cellular Automaton' (FFCA) Modells in einem Evakuierungsassistenten, der Simulationen von bis zu 50.000 Personen schneller als in Echtzeit durchführt. Eine neue Interpretation der Präferenzmatrix des Modells verbessert den Realismus der Simulation in U-Turns, zum Beispiel vor Mundlöchern in einem Stadion.

Der Schwerpunkt des zweiten Teils ist die experimentell beobachtete Separation in eine sich langsam bewegende und eine stehende Phase in Fußgängerströmen bei hohen Dichten, die grundlegend anders ist als z.B. die aus dem Fahrzeugverkehr bekannte Phasenseparation. Eine Untersuchung von etablierten und neuen Modellen der Fußgängerdynamik veranschaulicht die Schwierigkeiten, ein geeignetes Modell zur Reproduktion des Phänomens zu finden. Schließlich wird das 'Stochastic Headway Dependent Velocity' (SHDV) Modell vorgestellt und umfassend analysiert. Simulationen des Modells entwickeln einen phasenseparierten Zustand in Übereinstimmung mit den experimentellen Daten. Die wichtigsten Komponenten des Modells sind seine slow-to-start-Regel, Mindestgeschwindigkeit und große Wechselwirkungsreichweite.

TABLE OF CONTENTS

CHAPTER I

Introduction

The world population steadily increases and more people than ever before live in urban areas. Large-scale events grow in both magnitude and frequency and even daily commuting travel may exhibit high-density crowds at train stations. Clearly a detailed understanding of the underlying dynamics of pedestrian crowds should be pursued in order to appropriately design locations where high densities are expected and adequately act in case of an emergency. Crowd disasters such as the tragic catastrophe during the Love Parade 2010 in Duisburg (Germany) where 21 people died and many more were injured further illustrate that improving the safety of large-scale events is an important research topic.

The development of elaborate models and computer simulations is an established method to describe phenomena in many complex systems including pedestrian dynamics. Computer simulations are used to predict evacuation times and ideally also critical areas where dangerously high densities might be reached and accidents are more likely to happen. Realistic models require careful calibration and validation with the help of empirical or experimental data. Because every model is necessarily limited in scope, occasionally, some detail of the experimental data cannot be described by existing models. While this does not generally invalidate the established models, new knowledge might be gained by developing a model that is capable of reproducing the

new phenomenon. To gain insight into such an experimentally observed but not yet understood phenomenon, a typical approach is trying to find the simplest system that exhibits the relevant behavior ('minimal model'). After the simple system has been understood, it can be expanded into a more complex and potentially more realistic system.

This dissertation is structured as follows: The rest of this chapter introduces general concepts of pedestrian dynamics, gives a short overview of common modeling approaches, and discusses the experimental data relevant for this work. In Chapter II, the established Floor Field Cellular Automaton [1, 2, 3, 4] (FFCA) as well as a new modification of the model are presented. The application of the FFCA within the Hermes project [5, 6] is discussed in Chapter III. As part of an evacuation assistant for a multi-purpose arena the FFCA performs faster than real-time evacuation simulations of up to $50,000$ persons. Chapter IV explains the notion of phase separation that has been observed in one-dimensional pedestrian motion at high densities. Several established and novel models are examined as to whether they can successfully reproduce the effect. In Chapter V, a new one-dimensional model is defined and extensively analyzed. The Stochastic Headway Dependent Velocity (SHDV) Model is able to reproduce the experimentally observed phase separation in pedestrian dynamics. A discussion of the model characteristics that are required for this kind of phase separation concludes the chapter. Finally, the contribution of this work is summarized and possible future work is proposed in Chapter VI.

1.1 General concepts of pedestrian dynamics

1.1.1 Collective phenomena

The dynamics of pedestrian motion gives rise to a multitude of self-organization phenomena that are briefly presented here. A more detailed discussion can be found

e.g. in [7, 8, 9].

- Lane formation [10, 11, 12, 13, 14]: Bidirectional pedestrian movement, e.g. in a corridor, causes distinct lanes to emerge in which pedestrians only move in one direction. The order and quantity of these lanes dynamically varies. The formation of lanes reduces interactions with pedestrians moving in the opposite direction and thus leads to higher velocities. While cultural bias toward walking on a specific side influences this effect, it is not required to observe lane formation in pedestrian counterflow.

- Jamming: In high-density situations where many people want to move through a bottleneck limiting the flow, jamming (clogging) occurs [1, 15, 16]. Another example for jamming is counterflow at very high densities where pedestrian moving in opposite directions completely hinder each others movement (deadlock) [14, 17].

- Oscillations at bottlenecks [10, 11, 18]: Counterflow at bottlenecks leads to an oscillating direction of flow through the bottleneck.

- Faster-is-slower effect [8, 19]: A stronger desire[1] of a crowd of pedestrians to leave a room or building e.g. during an evacuation leads to a reduced flow.

- Freezing-by-heating effect [8, 20]: In pedestrian counterflow, larger fluctuations lead to a transition from movement in lanes to a deadlock.

- Patterns at crossings: Intersecting pedestrian streams can form patterns such as diagonal stripes in which pedestrians move in the same direction with the same velocity [12, 15] or short-lived roundabouts [7, 8, 21, 22]. Recently performed

[1] In models, this is typically represented by increasing the desired velocity and reducing cooperation.

experiments[2] investigate whether the flow through a crossing can be increased by encouraging or enforcing the roundabout motion.

1.1.2 Basic quantities in pedestrian dynamics

In addition to the qualitative characteristics described above, a thorough study of pedestrian dynamics also requires quantitative investigation. The basic quantities describing pedestrian motion are briefly introduced here.

- The velocity v of a pedestrian is straightforwardly defined as the traveled distance over time or more precise as the derivative of the traveled distance with respect to the time. An actual measurement necessarily records the average velocity over a short period of time.

- The average flow[3] J during a time interval T is defined as the number of pedestrians N passing a measurement line during the time interval:

$$J = \frac{N}{T} \,. \tag{1.1}$$

- The density ρ is in general given by the number of pedestrians N within a measurement area of size A:

$$\rho = \frac{N}{A} \,. \tag{1.2}$$

  This simple definition is difficult to employ in a meaningful way because the fluctuations in the measurement can be of the same order of magnitude as the density itself. To analyze microscopic behavior, the measurement area should be small. Consider e.g. a measurement area of approximately the size of a pedestrian. The number of pedestrians inside is either 0 or 1 and fluctuations

[2]The experiments have been performed within the BaSiGo project briefly discussed in Section 1.2.2. The analysis of the results is ongoing.

[3]The precise notation for the average would be $\langle J \rangle$; in the following the brackets are omitted to simplify the notation.

play an important part. If, on the other hand, the measurement area is large, the fluctuations are much smaller. However, the density can only be measured as an average over the macroscopic measurement area. Section 1.1.3 briefly discusses a few other possible density definitions.

1.1.3 Density concepts

As discussed, the density heavily fluctuates in naive measurements. To prevent these fluctuations, other density concepts can be used. A thorough discussion of different measurement methods can be found in [23].

1.1.3.1 Global density

The simplest way to define the density is by considering the whole experimental (or simulation) setup. The density is given by the number of people over the total area, equivalent to the naive definition with the largest possible measurement section. Using the global density precludes a microscopic analysis. It is, however, still useful for gaining macroscopic insights. The global density is an easy-to-implement and thus natural choice for computer simulations where it can also be used as an easily adjustable parameter.

1.1.3.2 Θ-density

To reduce fluctuations, the density in a measurement section at time t can be defined as

$$\rho(t) = \frac{\sum_{i=1}^{N} \Theta_i(t)}{L} \tag{1.3}$$

where L is the length of the measurement section, N the total number of agents, and

$$\Theta_i(t) = \frac{L_{i,i+1}(t)}{x_{i,i+1}(t)} \tag{1.4}$$

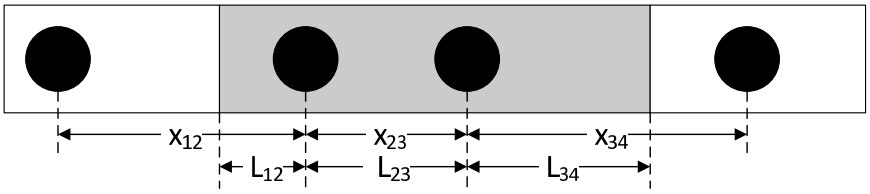

Figure 1.1: Definition of Θ. The shaded region is the measurement section.

the fraction of space between the pedestrians i and $i+1$ which is inside the measurement section, see Figure 1.1. The Θ-density [24, 25] that can then be assigned to an individual pedestrian i is defined as the average of all $\rho(t)$ with $t \in [t_i^{\text{in}}, t_i^{\text{out}}]$.

1.1.3.3 Voronoi density

The Voronoi density concept is based on Voronoi diagrams [26] and has been adapted to the analysis of pedestrian dynamics in [27]. Each point in space is assigned to a Voronoi cell A_i associated with a specific pedestrian i such that every point inside the cell is closer to the corresponding pedestrian than to any other pedestrian. The density $\rho_{x,y}$ of a single point (x, y) in space is given by A_i^{-1} with A_i such that $(x, y) \in A_i$. The density inside an arbitrarily small measurement area A is then given as the integral

$$\rho = \frac{1}{A} \int_A \mathrm{d}A \, \rho_{x,y} \, . \tag{1.5}$$

The Voronoi measurement method allows to reduce the size of the measurement area without increasing the resulting scatter [13, 28, 29] and thus improves the investigation of pedestrian dynamics on a microscopic scale.

The local/individual (Voronoi) density of a pedestrian in a one-dimensional system can easily be calculated by taking the inverse of the average distance to the person in front and behind,

$$\rho_i = \frac{2}{d_{i-1,i} + d_{i,i+1}} \tag{1.6}$$

where $d_{i,i+1}$ denotes the distance between pedestrian i and pedestrian $i+1$, measuring

from the center of each person. Note that this line density measures pedestrians per meter instead of the two-dimensional pedestrians per square meter.

1.1.4 Fundamental diagram

The fundamental diagram is one of the most important quantities to characterize the behavior of pedestrians, or traffic flow in general. In the classical formulation it depicts the flow as a function of the density. Because velocity v, flow J, and density ρ are not independent but linked by the hydrodynamic relation

$$J = \rho \cdot v \,, \tag{1.7}$$

it can also be presented as velocity vs. density or velocity vs. flow. The fundamental diagram is often referred to as the most basic observable in pedestrian dynamics and used as a tool for the calibration of computer simulation models that describe pedestrian motion [3, 30, 31].

The precise form of the pedestrian fundamental diagram is a heavily discussed topic. An often cited study of fundamental diagrams has been done by Weidmann [32]. Experimentally measured fundamental diagrams are affected by many factors such as the cultural background of participants [33, 34], psychological factors like the pedestrian's motivation [35], or the type of traffic [36]. Another important influence is the difference between unidirectional and bidirectional flow [9, 37, 38, 39]. Unfortunately, the exact experimental conditions have not always been documented in sufficient detail which is understandable considering that the importance of some effects has only been discovered after the experiments have been performed.

As outlined in Section 1.1.3, the density (and the velocity as well) can be measured in many different ways. The characteristics of the measurement method influence the resulting fundamental diagram [40]. This should be considered when the fundamental

diagram is used to calibrate models.

Two variants of the fundamental diagram for one-dimensional movement are primarily used in this work, namely the global fundamental diagram which uses velocity and density values averages over the whole system and the local fundamental diagram. The latter uses the local density defined in Section 1.1.3.3 and the individual velocity. Note that the lack of averaging leads to a very large number of data points as each pedestrian contributes one data point for each timestep in a simulation (or for each frame in experimental data).

1.1.5 Trajectories

The dynamics in a one-dimensional system can be visualized using a space-time plot that depicts the trajectories of individual pedestrians. Typical trajectories of the Stochastic Headway Dependent Velocity (SHDV) Model developed in this work (see Chapter V) are given in Figure 1.2. The left image shows local trajectories zoomed

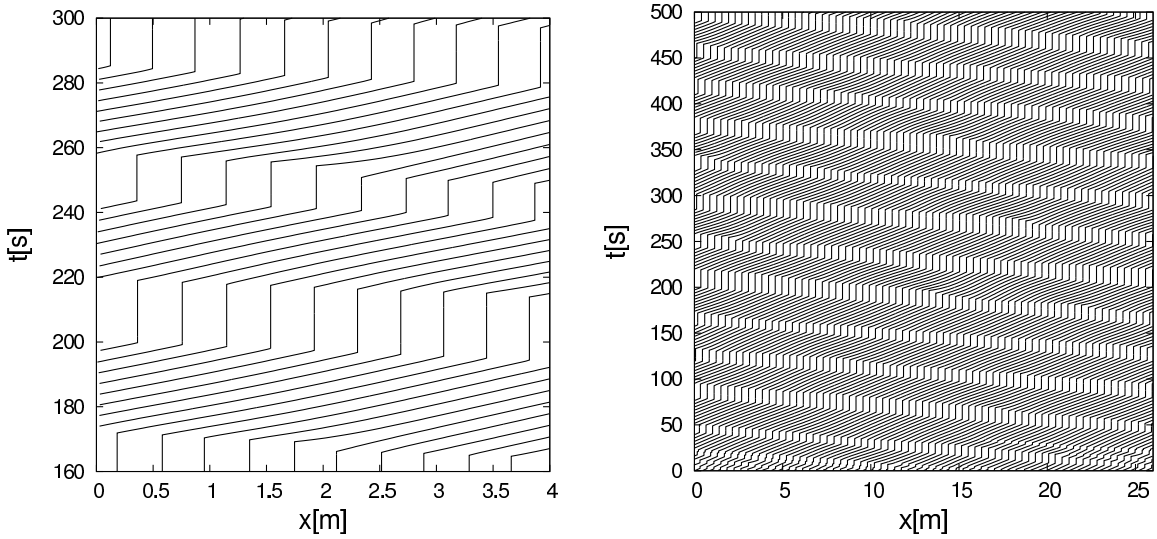

Figure 1.2: Trajectories of the SHDV model: local (left) and global (right).

in to cover only a small part of the system that, incidentally, corresponds to the size of the measurement area of the experimental data discussed in Section 1.2.1. The

right image shows global trajectories covering the whole simulated course[4]. Each line corresponds to one pedestrian moving from left to right and from bottom to top. The vertical parts of the lines correspond to jams: Time passes but the position of the pedestrian does not change. One advantage of studying trajectories instead of e.g. the fundamental diagram is that they contain the complete information of the dynamics and allow to gain further microscopic insights.

1.2 Experimental situation

To allow insights into pedestrian dynamics, either empirical data or data from laboratory experiments has to be studied. A typical approach to gather quantitative data is the analysis of video footage [41, 42, 43, 44, 45, 46]. This can be done 'by hand' or automatically by using e.g. the software PeTrack[5] [45, 46] to extract precise trajectories of individual pedestrians. The latter, however, requires special markers to detect the exact pedestrian positions and can at this point only be used in laboratory experiments. Quantitative data of pedestrian dynamics can be used to calibrate mathematical or computer simulation models aiming to describe pedestrian motion [42, 47, 48, 49, 50] and search for 'laws of nature' characterizing pedestrian dynamics.

1.2.1 Experiment 'Bergische Kaserne'

For this work, one series of experiments is of particular importance. In 2006, Seyfried et al. [25, 39] performed experiments with up to 70 pedestrians that examine one-dimensional (single-file) pedestrian movement. A similar experiment had already been executed in 2005 [51] and evaluated manually to obtain the fundamental diagram. The participants were instructed to 'move normally' and not allowed

[4] A larger version of this image can be found in Appendix A.
[5] PeTrack has been used in both the Hermes and BaSiGo projects.

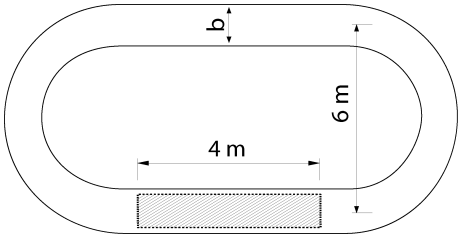

Figure 1.3: Experimental setup [25, 39].

to overtake. The experimental setup depicted in Figure 1.3 had a length of approximately 26 m including a 4 m long measurement section in which the pedestrian trajectories have been measured by automatically tracking the pedestrian heads [45, 46]. The positions of pedestrians outside the measurement section have not been captured. Several runs with different numbers of pedestrians and thus different density have been conducted.

The fundamental diagram can be obtained using either the Θ-density [24, 25] discussed in Section 1.1.3.2 or the Voronoi [27] (individual) density. Both variants are depicted in Figure 1.4. The negative velocities in the local fundamental diagram come

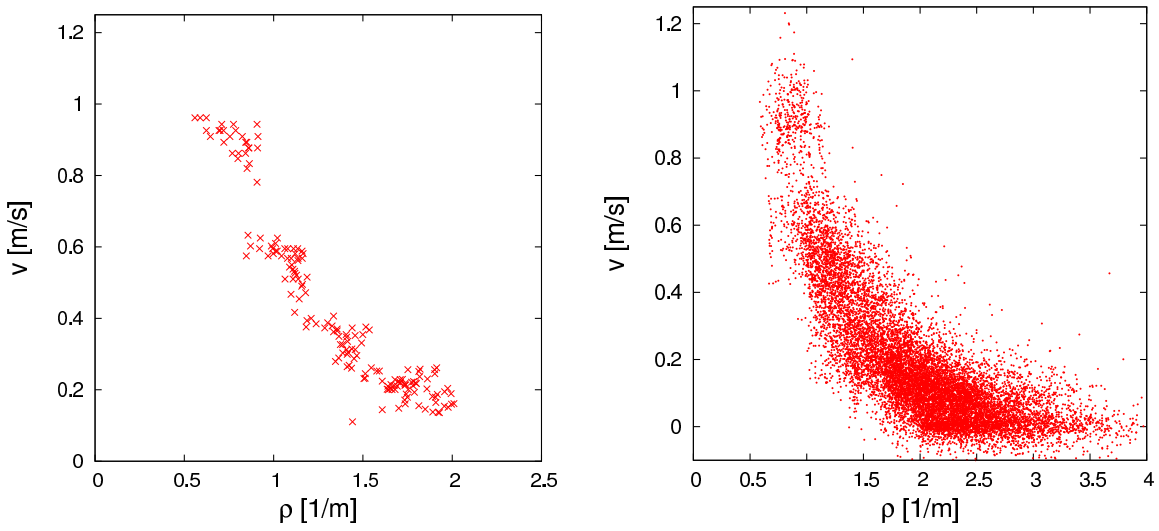

Figure 1.4: Fundamental diagram of the experimental data using the Θ-density (left) and the Voronoi density (right).

from the backward-moving heads of standing pedestrians. This effect results from not tracking the center of mass, but the head of each pedestrian. The local fundamental

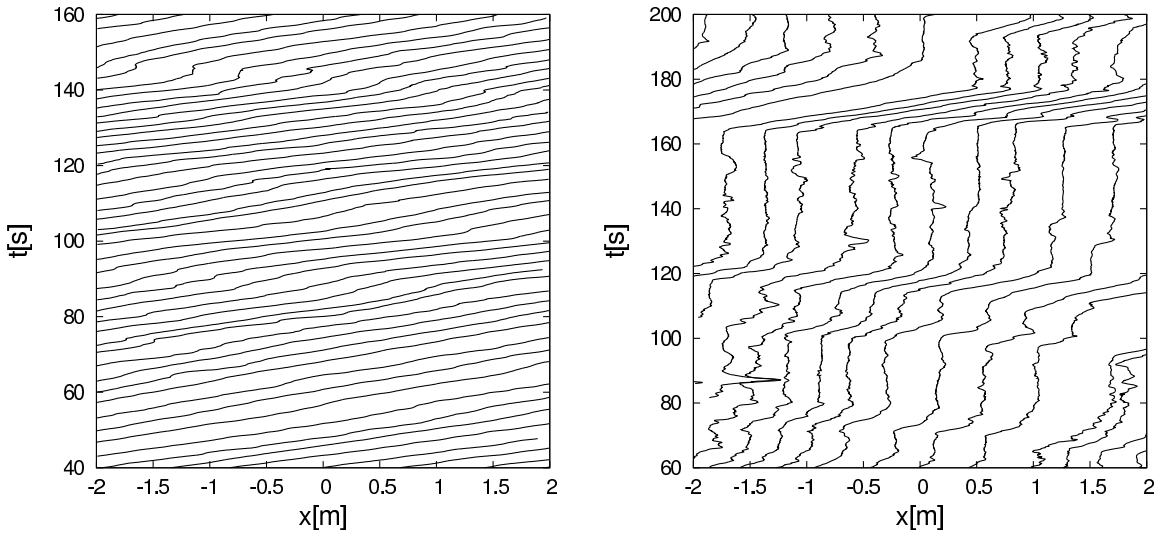

Figure 1.5: Experimental trajectories for $N = 45$ (left) and $N = 70$ (right).

diagram contains much higher densities. This can be explained by considering that the local fundamental diagram contains unaveraged data and the distance between two heads can be much smaller than between two persons. The macroscopic fundamental diagram on the other hand averages over multiple pedestrians as discussed in Section 1.1.3.2.

The resulting trajectories of two typical runs are shown in Figure 1.5 (left) as a space-time plot. At very high densities, a separation into phases with standing pedestrians (vertical lines) and phases with moving pedestrians can be observed. The velocity in the moving phase can be obtained by estimating the slope of the trajectories, it is about 0.15 $\frac{\mathrm{m}}{\mathrm{s}}$ and thus much smaller than the free-flow velocity, which is about 1.2 $\frac{\mathrm{m}}{\mathrm{s}}$. From vehicular traffic a similar effect is known, namely a separation into a jammed and free-flowing phase. This will be discussed in more detail in Section 4.1. Small (backward) movements in the trajectories come from the head movement of standing pedestrians.

The existence of a jam in the system raises the question whether the system contains multiple jams or the observed jam in the measurement section is the only jam in the experimental setup. The trajectories are compatible with both scenarios because

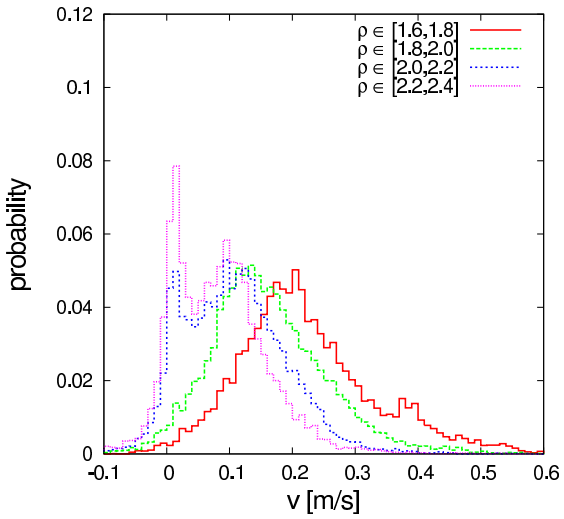

Figure 1.6: Experimental velocity distribution [25].

the experimental data only extends over the small time-scale of 140 s and spatial scale of 4 m. This also prevents judging the stability of the empirical phase separation, it is unclear whether the phases remain separate for longer timescales. The existence of additional jams would be an indication that jams might be forming and decaying dynamically. Even though it has not been formally documented, the experimenters assume[6] that there was probably only one jam in the system. To analyze the phase separation of high-density pedestrian traffic, one has to study microscopic quantities (trajectories). It does not suffice to study the fundamental diagram which not necessarily contains information about the microscopic characteristics of a system. A more detailed analysis of the observed phase separation will be conducted in Chapters IV and V by comparing the experimental data to computer simulations.

The velocity distribution of the experimental data is given in Figure 1.6 for several density intervals. At high densities, it exhibits a double peak structure with one maximum at 0 $\frac{\mathrm{m}}{\mathrm{s}}$ and the other at about 0.1 $\frac{\mathrm{m}}{\mathrm{s}}$, depending on the density. This suggests a coexistence of moving and standing pedestrians and can also be interpreted

[6]The goal of the experiment was to obtain a precise fundamental diagram. The very specific question about the number of jams in the system during a few high-density runs arose during the evaluation of the data, after the experiments had been performed.

as an indication of a minimum velocity.

1.2.2 BaSiGo experiments

The project BaSiGo [52] – Safety and Security Modules for Large Public Events[7] is funded by the German Federal Ministry of Education and Research. The goal of the project is to improve the evaluation and planning of mass events using a modular approach. One aspect of BaSiGo is the realization of large-scale experiments with up to 1000 participants.

For this work only one of the experiments conducted within the BaSiGo project is relevant, namely an almost exact replication of the experiment discussed in Section 1.2.1. The sole difference is that during the new experiment the whole experimental setup has been covered by the camera grid which allows to extract the complete set of trajectories instead of only capturing a subset due to the confined measurement section. The new data allows to also consider global experimental trajectories and thus check whether there is indeed only one jam in the system. Unfortunately, the analysis of the raw data leading to the extraction of the trajectories is not yet finished. Therefore the quantitative results of the new experiment are not incorporated into this work. The visual impression during the experiment[8], however, suggests that there is indeed only one jam in the high-density system at any time.

1.3 Modeling of pedestrian dynamics

1.3.1 Classification of modeling approaches

An enormous number of different models has been used to describe pedestrian motion, therefore any attempt to list the numerous different approaches will probably

[7] in German: Bausteine für die Sicherheit von Großveranstaltungen

[8] The author was part of the team responsible for the planning and execution of the experiments and therefore able to observe this particular experiment live from a well-suited vantage point.

remain incomplete. Nevertheless, this work presents a possible classification based on basic characteristics of pedestrian models. A more detailed discussion can be found in e.g. [53]. For all of the properties discussed below, there are models that do not belong to either pure category but can be placed somewhere in between.

- **Macroscopic** models describe a system as a whole, typically using aggregated quantities such as density and flow. **Microscopic** models on the other hand describe the motion of individual agents and track their individual properties such as position and velocity; they also allow to personalize the agents by using different parameter values for different agents. **Mesoscopic** models include features of both macroscopic and microscopic models.

- Variables such as time, position, or velocity can either take integer (**discrete**) or real (**continuous**) values. An important advantage of discrete models is the efficiency in computer simulations. However, in some situations the limited resolution in contrast to continuous models can be problematic. Some models such as the Stochastic Headway Dependent Velocity (SHDV) Model discussed in Chapter V use a mix of discrete and continuous variables.

- In **force-based** models, the dynamics is defined in analogy to Newtonian mechanics, agents are accelerated by 'social' forces. The behavior of agents in **rule-based** models is governed by a set of rules based on the state of the agent, its neighborhood, and possibly other factors as well. Again, some models use a mixed approach.

- In models with **deterministic** dynamics, the evolution of a system depends only on the starting configuration. In **stochastic** models, agents in the same situation can behave differently, the dynamics is governed by probabilities. Some models combine deterministic dynamics with an additional external noise.

The two most commonly used model classes are force-based models and cellular automata (CA). Microscopic force-based models [10, 30, 48, 54, 55] are usually defined in a continuous geometry and use deterministic dynamics; CA models [1, 53, 56, 57, 58] are microscopic, discrete, rule-based, and usually stochastic.

The discrete space used in CA models can be realized in multiple ways. The simplest and most popular lattice consists of square cells that typically have a size of 0.4×0.4 m^2 [32]. In models utilizing the **von-Neumann** neighborhood agents are allowed to move to the four non-diagonal neighbors [1]; the **Moore** neighborhood allows agents to move to all eight neighbors including the adjacent diagonal cells [58]. Another choice for CA models is to use a hexagonal lattice [59, 60, 61, 62]. An advantage of the hexagonal lattice is its improved isotropy. However, as the vast majority of buildings contains mainly right angles, for many simulations the square lattice is a more natural choice.

1.3.2 Initial conditions

Experimental initial conditions are usually difficult to control and therefore only known approximately. The participants can e.g. be instructed to distribute evenly in an experimental area, yet even in the best case the distribution is only nearly homogeneous. Simulations, in contrast, can use precisely defined initial conditions which allow to exactly reproduce their results.

In the following, typical starting configurations for periodic one-dimensional simulations are discussed. After a sufficiently long simulation time, many models reach a stationary state that is independent from the initial condition. Depending on the model and the parameter choice there may be several distinct stationary states that the model can converge to, e.g. a homogeneous stationary state at low densities and an inhomogeneous stationary state at high densities. Additionally, for applications such as evacuation simulations or replication of experimental results it is also inter-

esting to consider the non-stationary state. Pedestrian experiments might not last long enough to ensure the convergence to a stationary state.

Initial conditions for two-dimensional simulations can be defined similarly. They will not be discussed in detail because for the two-dimensional simulations discussed in this work the initial distribution of agents is relatively unimportant in comparison to other factors determining the simulation results as will be discussed in Section 3.5.

1.3.2.1 Homogeneous initial condition

One possible initial condition is a homogeneous state in which all agents are spaced out evenly in the simulation area. If the model does not include some kind of stochastic influence it will typically stay in the homogeneous state in which it started. Note that models with discrete space such as CA models can in general not use a truly homogeneous initial condition. Consider for example a simulation with two agents and an area of five cells. In that case it is impossible to homogeneously distribute the agents. Models with continuous space, on the other hand, can easily implement this.

1.3.2.2 Inhomogeneous initial condition

Alternatively, the system can start in an inhomogeneous state, e.g. a megajam. This is especially easy to implement for CA models: Assuming a total of N agents in the simulation, the first N cells are occupied and the other cells are empty. For space-continuous models either the size of an agent or a minimum distance between point-like agents has to defined. The distance between agents in the simulation is then set accordingly. Depending on the details of the model, this distance can either be a well-defined quantity or not. For simulations with inhomogeneous initial conditions and less than maximum density both discrete and continuous models feature a single larger distance between two agents in the system, namely between the end of the megajam and its beginning.

1.3.2.3 Random initial condition

The agents can be distributed randomly in the system. For CA models this is very straightforward: Every agent gets assigned to a random empty cell which is then occupied and blocked for other agents. For pedestrian models with continuous space, random initial conditions work well for relatively empty systems but can be problematic when the density is close to the maximum allowed density.

Assuming that each agent has a finite size[9], overlapping has to be considered. A straightforward idea is to place every agent at a random position such that the distance to the neighboring agents is big enough to avoid overlapping. However, at some point there might not be enough space between any two adjacent agents to allow the placement of the next agent. This becomes clear for the extreme case of considering the maximum possible density[10]. To allow the placement of every agent, the headway of each agent has to be equal to the agent size. A truly random distribution of agents however can and most likely will lead to headways that are larger than the agent size but not twice as large, meaning that no other agent can be placed in between. Due to the 'wasted' space at least one agent cannot be placed at all. There are some methods[11] to avoid this problem, but there is no obvious way to transfer the random distribution from a CA model to space-continuous models.

1.3.2.4 Almost homogeneous initial condition

The final starting configuration discussed here is intended for space-continuous models. It is designed to be very similar to the experimental initial condition and resembles an 'almost homogeneous' state, which is achieved via a two-step process: First the agents are distributed homogeneously. Then each agent's position is shifted

[9] The same argument can be made for point-like agents that have to respect a minimum distance.

[10] For simplicity's sake the system size is assumed to be a multiple of the agent size; the same argument is valid for a more general system size.

[11] One approach is to randomly distribute headways instead of positions.

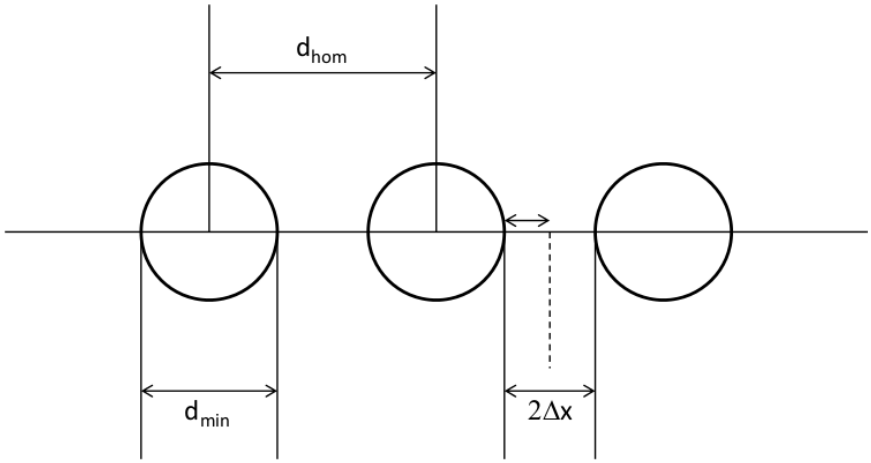

Figure 1.7: Almost homogeneous initial condition after the first step. In the second step each agent is shifted by up to Δx.

a little according to a Gauss-distributed random variable. The Gauss-distribution is cut off at 2σ in such a way that overlapping of agents is impossible, see Figure 1.7. The maximum distance Δx which an agent can be shifted to either side is equal to half of the free space in between two adjacent agents:

$$|\Delta x| \leq \frac{d_{\text{hom}} - d_{\text{min}}}{2}\,, \tag{1.8}$$

where d_{hom} is the headway or distance between the homogeneously spaced agents and d_{min} is the size of an agent or, depending on the model, the minimum distance between point-like agents. This means the agents are indeed 'almost homogeneously' distributed, resulting in a realistic starting configuration.

CHAPTER II

Floor Field Cellular Automaton (FFCA)

The Floor Field Cellular Automaton (FFCA) [1, 2, 3, 4] is a microscopic, agent-based model. Space is partitioned into small non-overlapping cells which can either be empty or occupied by a pedestrian or an obstacle such as a wall. The exclusion principle is enforced: No cell can be occupied by more than one pedestrian. The size of one cell corresponds to the space requirement for a single person. A common value for the maximum density in highly crowded areas is 6.25 persons per square meter which leads to a typical cell size of 0.4×0.4 m^2 [32]. In each timestep t all pedestrians are updated in parallel. Since a reaction to the motion of other agents is only possible in the next timestep $t + \Delta t$, the size of a timestep Δt can be identified with the reaction time of a pedestrian. A typical choice is $\Delta t = 0.3$ s which is of the same order of magnitude as the reaction time [1].

The rule-based dynamics of the model are defined by the transition probabilities p_{ij} to neighboring cells including the cell currently occupied by the pedestrian in consideration. As discussed in Section 1.3.1, there are several possibilities regarding the choice of the neighborhood. The most common ones are the von-Neumann neighborhood used in this work (Figure 2.1) and the Moore neighborhood.

These transition probabilities are in general determined by three factors: the desired direction of motion, the interaction with other pedestrians and the interaction

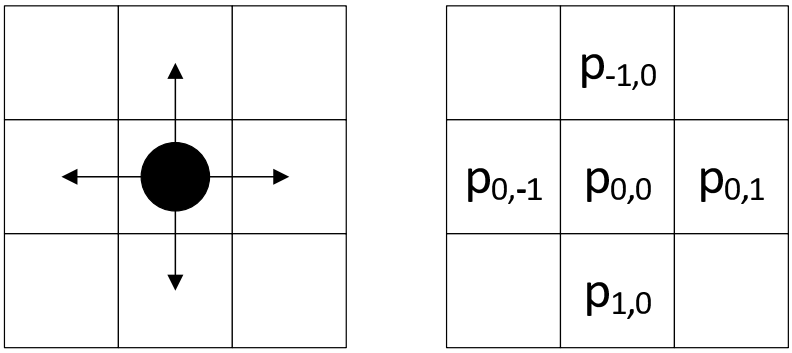

Figure 2.1: Definition of the transition probabilities p_{ij} in the von-Neumann neigborhood.

with the infrastructure. For this purpose the model uses two discrete floor fields S_{ij} and D_{ij}.

2.1 Floor fields

The **static floor field** S_{ij} contains the information about the preferred direction of motion. It does not change in time but is calculated for each lattice site at the beginning of the simulation. It can be interpreted as a potential and describes the shortest distance to the destination site which typically corresponds to an exit. It is possible to have multiple destination cells. For complex geometries the static floor field is usually calculated with a flooding algorithm such as the Dijkstra algorithm [63].

The **dynamic floor field** D_{ij} transforms the long-ranged interaction between agents into a local interaction with memory. It represents a virtual trace created by moving pedestrians and corresponds to the tendency of pedestrians to follow other (moving) pedestrians. The dynamic floor field is inspired by the process of chemotaxis which is e.g. responsible for the formation of ant trails [64]. At the start of a simulation, the field has a value of zero on each site (ij), $D_{ij} = 0$. This value increases by one whenever a pedestrian leaves the site. The increase does not affect the leaving pedestrian in the next timestep in order to avoid a negative feedback loop by preventing the agent from being drawn backwards by its own forward movement.

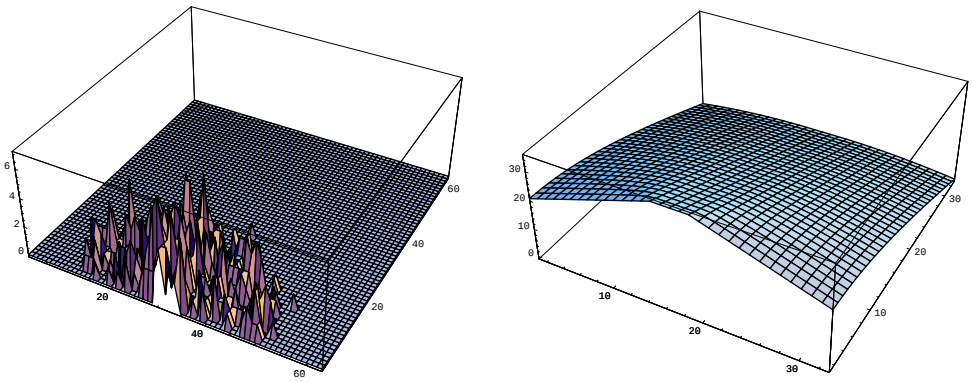

Figure 2.2: Dynamic floor field (left) and static floor field (right) during the final stage of the simulation of a large room with a single door [2].

Due to the dynamic floor field the FFCA features dynamic transition probabilities that depend on the history of the simulation.

The dynamic floor field can only have non-negative integer values, it can therefore be loosely interpreted as a bosonic field in the following sense: The non-negative integer value of the dynamic floor field at a given cell can be interpreted as the number of bosons on this cell. The model dynamics then leads to varying numbers of bosons at each cell at different timesteps. These bosons are unrelated to quantum statistics and quantum mechanics but help visualizing the update procedure. The increase of the dynamic floor field triggered by a moving agent then corresponds to the creation of a boson. Additionally, the bosonic field is subject to diffusion and decay processes. At the beginning of each timestep, every boson has a probability δ to decay, leading to $D_{ij} \to D_{ij} - 1$. Every remaining boson has a diffusion probability α to move to a random neighboring cell. This leads to a diluting and widening trace and determines the effective interaction range: Except for local interaction via the exclusion-principle, an agent can only interact with another agent if one of the agents is influenced by a boson that the other agent created. The range of the interaction therefore corresponds to the average distance a boson travels via the diffusion process before it decays. A small decay probability and a big diffusion probability allow a boson to travel relatively far and thus lead to a large interaction range.

2.2 Transition probabilities

The unnormalized transition probabilities (weights) $\widehat{p}_{ij}$ of the standard FFCA model for the movement of an agent to the site with relative coordinates (i, j) are given by

$$\widehat{p}_{ij} = \exp(k_S S_{ij}) \cdot \exp(k_D D_{ij}) \cdot \xi_{ij} \tag{2.1}$$

where the parameters k_S and k_D are coupling constants which control the influence of the floor fields S and D. The factor ξ_{ij} ensures that movement is only possible to allowed sites. It prevents movement to sites that are occupied by either a pedestrian or an obstacle,

$$\xi_{ij} = \begin{cases} 0, & (i,j) \text{ empty} \\ 1, & (i,j) \text{ blocked.} \end{cases} \tag{2.2}$$

The normalized transition probabilities p_{ij} are given by

$$p_{ij} = N \cdot \widehat{p}_{ij} = N \cdot \exp(k_S S_{ij}) \cdot \exp(k_D D_{ij}) \cdot \xi_{ij} \tag{2.3}$$

where the factor

$$N = \frac{1}{\sum_{ij} \widehat{p}_{ij}} \tag{2.4}$$

assures the normalization $\sum_{ij} p_{ij} = 1$ of the transition probabilities.

2.3 Matrix of preference

The matrix of preference is a way to encode the preferred direction of motion of the pedestrians. It is a 3 x 3 matrix whose entries modify the transition probabilities depending on the direction of the movement. For the von Neumann neighborhood,

only five entries are different from zero:

$$M = \begin{pmatrix} 0 & M_{-1,0} & 0 \\ M_{0,-1} & M_{0,0} & M_{0,1} \\ 0 & M_{1,0} & 0 \end{pmatrix} \quad . \tag{2.5}$$

When the Moore neighborhood is used, the diagonal matrix entries corresponding to diagonal movement are also nonzero[1]. The transition probabilities p_{ij} including the matrix of preference are given by

$$p_{ij} = N \cdot \exp(k_S S_{ij}) \cdot \exp(k_D D_{ij}) \cdot \xi_{ij} \cdot M_{ij} \quad . \tag{2.6}$$

In many cases it is sufficient to use the static and dynamic floor fields to describe the behavior of the simulated pedestrians and the matrix of preference is not necessary. This is equivalent to setting all matrix entries to $M_{ij} = 1$ in which case the matrix of preference does not influence the model dynamics.

2.4 Friction

Due to the parallel update in the FFCA it is possible for two or more pedestrians to choose the same target cell. This is called a conflict. The simplest solution to a conflict is to randomly choose one of the agents which is allowed to move and let the other agents stand still for the timestep. However, a more realistic behavior of the pedestrians at high densities e.g. in a bottleneck can be obtained by introducing friction [65, 66].

Friction provides a probability μ for each conflict cell that none of the conflicting pedestrians move to the chosen destination, see Figure 2.3. With probability $1 - \mu$

[1] Their values can actually be related to observable quantities such as the average velocities and their fluctuations [1].

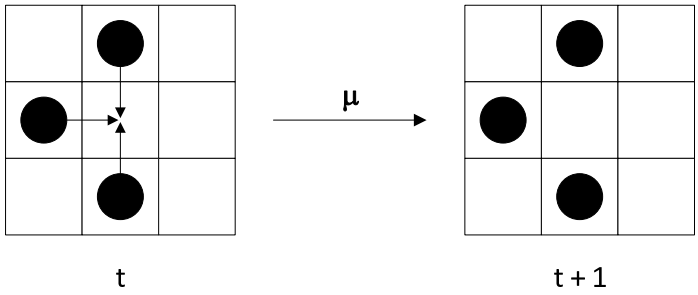

Figure 2.3: Friction prevents the movement of conflicting agents with probability μ.

one pedestrian is allowed to move to the target cell while the others are forbidden to move. The moving pedestrian is chosen randomly from the conflicting agents. Friction can be interpreted as a kind of local pressure between agents that results in agents disrupting each others movement such that with probability μ all conflicting agents remain in their cell.

More intuitively, friction can be interpreted as nonverbal communication between conflicting pedestrians which takes a little time. As an example, consider two pedestrians who want to walk through a door and arrive at the same time. They might look at each other briefly, then one of them moves through the door and the other one follows. On the other hand, both pedestrians might try to move simultaneously and block each other for a short time: friction.

2.5 FFCA algorithm overview

In each timestep the following steps are performed in parallel for each agent:

- Calculate diffusion and decay of the dynamic floor field.
- Calculate the transition probabilities to the cells with relative coordinates (i, j).
- Choose a target cell using these transition probabilities.
- Resolve potential conflicts and move the agents who are allowed to move.
- Increase the value of the dynamic floor field according to the moving agents.

Typical parameter values for the diffusion probability α, the decay probability δ, the coupling constants k_S and k_D of the static and dynamic floor field, respectively, and the friction parameter μ are given in Table 2.1. The specific values of the parameters generally depend on the scenario that is analyzed.

parameter	value
α	0.2
δ	0.2
k_S	2.5
k_D	2.0
μ	0.3

Table 2.1: Parameter values for the FFCA model.

2.6 Possible model extensions

There are several possibilities to extend the FFCA model:

- Higher velocities ($v_{\max} > 1$): Pedestrians are allowed to move more than one cell in each timestep. This leads to an increased interaction range and a more complex pedestrian behavior such as possible crossings of trajectories within a single timestep [65, 67].

- Politeness factor: An additional factor $p_{ij}^{(P)} = \exp(-k_P N_{ij})$ is added to the probabilities in Equation (2.3), where N_{ij} is the number of nearest neighbors on site (i, j). This leads to a suppression of motion into the direction of crowded areas [3, 58].

- Smaller cell sizes: In order to represent the infrastructure of a building in more detail, smaller cells are used. For 20×20 cm^2 cells each pedestrian occupies 2×2 cells [65, 67].

- Inertia: Inertia effects suppress abrupt changes in the direction of motion [1, 68].

To that end an additional factor

$$p_{ij}^{(I)} = \begin{cases} \exp(k_I), & \text{direction of motion changes} \\ 1, & \text{direction of motion remains unchanged} \end{cases}$$

is added to the probabilities in Equation (2.3). The value of the parameter k_I determines the strength of the inertia effect.

- Wall repulsion: An additional factor $p_{ij}^{(W)} = \exp\big(k_W \cdot \min(D_{\max}, d_{ij})\big)$ can be included in Equation (2.3) to describe the interaction between walls and pedestrians [68, 69]. k_W denotes the coupling constant and thus the strength of the interaction, $D_{\max}$ is the range of the wall potential and d_{ij} is the distance of the agent from the nearest wall.

This is by no means a complete list of possible model extensions. There is a multitude of further generalizations and modifications of the floor field cellular automaton model, such as defining an additional vector floor field that describes the force acting on a pedestrian [70, 71] or using a different underlying lattice structure (e.g. a hexagonal lattice [59, 60, 61, 62]).

2.7 Modified matrix of preference

This section proposes a new interpretation of the matrix of preference presented in Section 2.3 which can be used as a tool to locally modify transition probabilities. The modified matrix of preference can be employed to more realistically describe pedestrian movement in a U-turn. This will be discussed in Section 3.3.2.

By linking the matrix of preference to a specific cell, any agent occupying that cell is influenced by the matrix of preference. In principle each cell – instead of each pedestrian – can have its own matrix of preference in addition to the static and dynamic floor field, leading to a lot of freedom to influence the movement of

pedestrians in a given geometry. An interesting choice is using a matrix of preference that has trivial entries[2] for all directions except for one, e.g. downwards,

$$M = \begin{pmatrix} 0 & 1 & 0 \\ 1 & 1 & 1 \\ 0 & \exp(k_S) & 0 \end{pmatrix} \quad . \tag{2.7}$$

The entry $\exp(k_S)$ increases the transition probability for a movement downwards as if the static floor field in the target cell were increased by one: The probability to move downwards is given by

$$p_{1,0} = N \cdot \exp(k_S S_{1,0}) \cdot \exp(k_D D_{1,0}) \cdot M_{1,0} \cdot \xi_{1,0} \tag{2.8}$$

where the indices '1,0' denote the downwards direction of movement according to the definitions in Figure 2.1 and Equation (2.5). $M_{1,0}$ thus corresponds to the nontrivial matrix entry $\exp(k_S)$. Equation (2.8) can then be simplified to

$$p_{10} = N \cdot \exp(k_S S_{10}) \cdot \exp(k_D D_{10}) \cdot \exp(k_S) \cdot \xi_{10} \tag{2.9}$$

$$= N \cdot \exp(k_S (S_{10} + 1)) \cdot \exp(k_D D_{10}) \cdot \xi_{10} \tag{2.10}$$

which is equal to the transition probability without a matrix of preference but with a static floor field that is increased by one in the target cell. It is not possible to directly change the static floor field in a way equivalent to the above change.

[2] A matrix of preference with all entries equal to 1 does not change the transition probabilities.

CHAPTER III

The Hermes project

Figure 3.1: ESPRIT arena [72].

Hermes [5, 6] was an interdisciplinary three-year project funded by the German Federal Ministry of Education and Research in the program 'Research for Civil Security' and successfully finished in 2011. A main goal of the project was to increase the safety of people participating in or attending big events in large buildings like sport stadiums by developing a proof of concept for an evacuation assistant that is capable

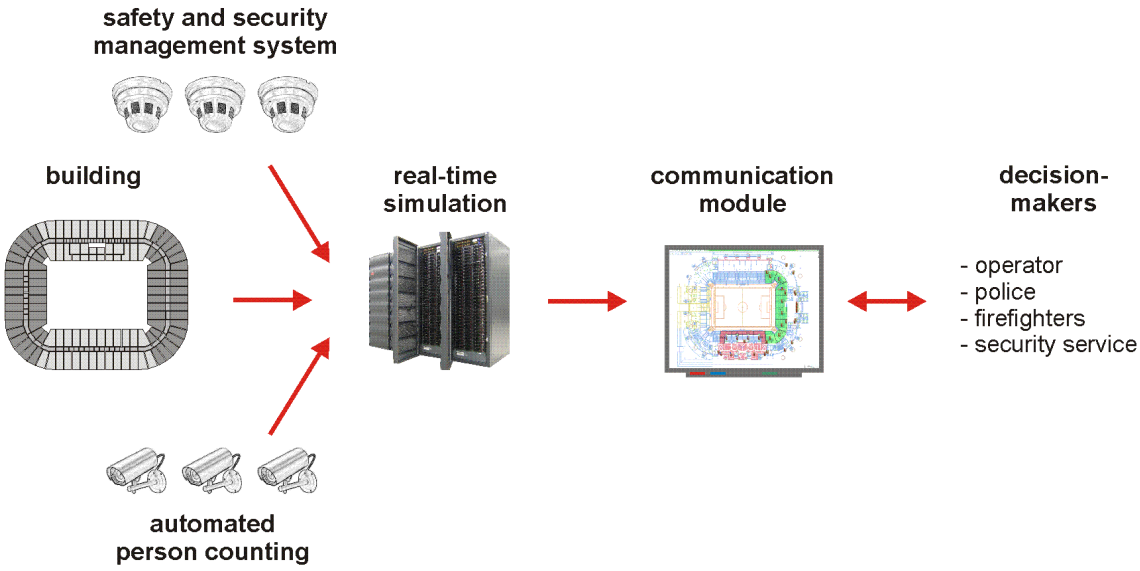

Figure 3.2: Structure of the evacuation assistant. Graphic courtesy of Ulrich Kemloh [73].

of forecasting an evacuation of up to 50,000 pedestrians faster than real-time[1]. The ESPRIT arena (Figure 3.1) in Düsseldorf, Germany has been chosen as the site of the proof of concept.

Figure 3.2 shows the general structure of the evacuation assistant. The geometry of the multifunctional arena as well as the data from automated person counting and the safety and security management system, which tracks the available and unavailable exit routes, are used as input for computer simulations performed on a local computer cluster. These simulations are faster than real-time, meaning that a forecast over 15 minutes can be calculated in one to two minutes, depending on the model. The simulations predict evacuation times as well as high-risk areas, that is areas where high densities and congestion occur. The simulation results are displayed in the user interface, called communication module, which is shown in Figure 3.3. It can be accessed by the decision-makers who can then adapt the positioning of security personnel in order to divert pedestrian flows and avoid high-risk situations. A second

[1]The evacuation assistant can in principle also be used for outdoor events. However, in that case different approaches to some technical aspects of the project are required.

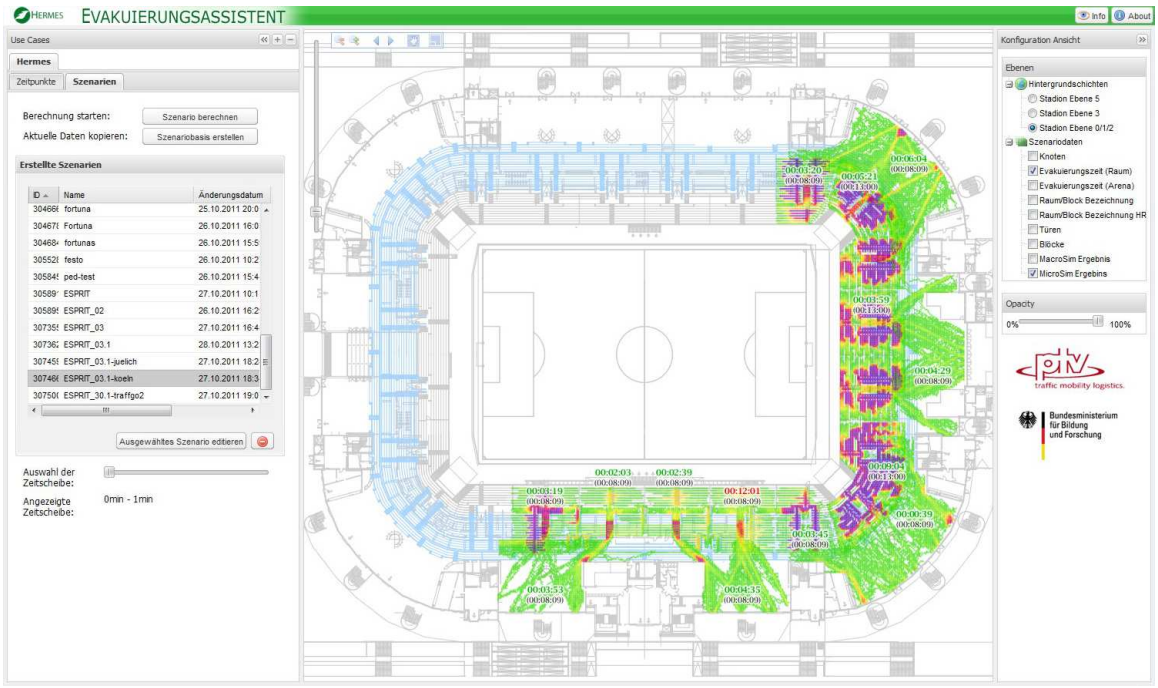

Figure 3.3: User interface of the evacuation assistant.

use case of the evacuation assistant is in the planning phase of an event. The usually automatically gathered input data can be entered or changed manually which allows the creation and detailed analysis of evacuation plans for user-created scenarios.

The evacuation assistant includes several computer models, namely the force-based Generalized Centrifugal Force Model (GCFM) [30], the Network Model Visum [74], the cellular automaton model PedGo [75] and the Floor Field Cellular Automaton (FFCA, see Chapter II) [1, 2, 3]. The geometry input data needs to be provided in two different formats for the continuous and the discrete models and is generated in a semi-automatic fashion. This work focuses on simulations performed with the FFCA.

3.1 Simulation speed

The FFCA simulations use only a small fraction of the available computing power as most of the processors of the Hermes-workstation are reserved for simulation with the GCFM. A big advantage of cellular automaton models such as the FFCA is their computation speed. Due to the discrete nature of the FFCA and its resulting lower spatial and time resolution it is much faster than the continuous GCFM. The area of interest, roughly one quarter of the whole arena, has a size of about $15,000$ m^2, which are approximately $93,000$ cells. A simulation with $12,000$ agents, shown in Figure 3.4, takes 30 s on a standard computer. The simulated time is 15 min and corresponds to the typical time for evacuation. This means that the simulation runs about 30 times faster than real-time. The simulation time of the FFCA could of

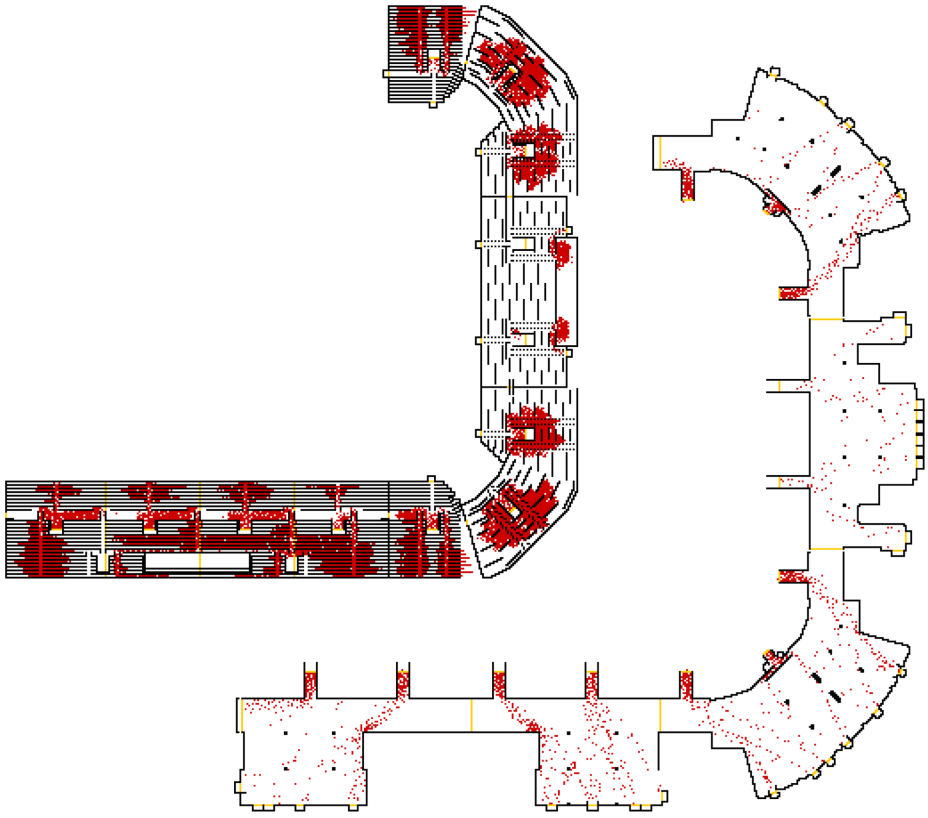

Figure 3.4: Simulation snapshots of the stands (top left) and the promenade (bottom right) of the ESPRIT arena.

course be optimized further, trivially by using a faster computer, but also by runtime optimization of the program code or by parallelization. This is however not necessary as the FFCA is already fast enough, the evacuation assistant only slightly benefits from a further speed-up of the model. A distinct advantage of the FFCA model with regards to applications is that it runs faster than real-time without being reliant on a local computer cluster.

3.2 Different modes of evacuation

The simulations feature two different evacuation modi. Routine egress on the one hand happens regularly after every event when the audience leaves the building. This kind of egress is strongly influenced by unknown factors and diverse pre-movement time[2], varying motivations to leave the arena and hard-to-predict route choices (see Section 3.4) depending on the mood and the preferred method of transportation of the pedestrian. Routine egress is therefore difficult to simulate. Emergency evacuations on the other hand happen very rarely. In the case of an emergency, the evacuation process is much more straightforward and therefore easier to simulate. Each pedestrian has a high motivation to leave the arena, often using the shortest path outside. The distribution of individual pre-movement delay is much narrower and corresponds to the distribution of reaction times – once the stadium announcer asks for evacuation, everybody starts to move as quickly as possible.

Independent of the mode of evacuation there are factors such as the route choice behavior of pedestrians leaving the arena that are not necessarily well-known. This is discussed in further detail in Section 3.4.

[2]Time an individual spends between the end of the event and beginning to leave the building. The influence of the pre-movement time has been analyzed in [76].

3.3 Validation

It is a well-established fact that the FFCA features typical collective phenomena as described in Section 1.1.1. However, a quantitative approach to model calibration allows for more accurate quantitative predictions. This has been discussed in more detail in [77].

The validation of the ESPRIT arena simulations without any data from emergency evacuations was one of the challenges of the project. In addition to the data from routine egress, there is experimental data from simpler geometries with a much lower number of participants but better control over their behavior. This data is also used in the validation process which is performed in various steps.

To get reasonable simulation results for complex geometries such as the ESPRIT arena, one first has to understand the basic geometries, namely corridors, bottlenecks and corners. A comparison of simulation results with experimental data of the one-dimensional fundamental diagram will be used in Section 3.3.1 to perform a basic calibration of the FFCA parameter values. The movement of agents around corners within the framework of the FFCA has been studied in [78] and [79]. The next step is to validate the model for intermediate geometries by comparing simulation results to experiments. To this end a vomitory[3] is considered which connects the stands of the arena to the promenade leading to the exits. A detailed analysis of simulations and experiments using this geometry will be conducted in Section 3.3.2.

3.3.1 Fundamental diagram

The first part of the FFCA calibration is based on the fundamental diagram introduced in Section 1.1.4. The single-file nature of movement in the experiment 'Bergische Kaserne' discussed in Section 1.2.1 justifies using a one-dimensional variant of the floor field model. The corridor has a length of $L = 26$ m which corresponds

[3] in German: 'Mundloch'.

to $\frac{26\ \mathrm{m}}{0.4\ \mathrm{m}} = 65$ cells with periodic boundary conditions. Three different variants of the model are used for simulations: the standard FFCA with $v_{\max} = 1$, a variant with $v_{\max} = 2$, and an improved model which includes a politeness factor as discussed in Section 2.6. Higher speeds in the simulation are defined in the simplest possible way: Each person determines a destination cell at a maximum distance of 2 cells. Conflicts[4] are resolved analogously to the model with $v_{\max} = 1$. Either both agents are denied movement due to friction or one randomly chosen pedestrian is allowed to move.

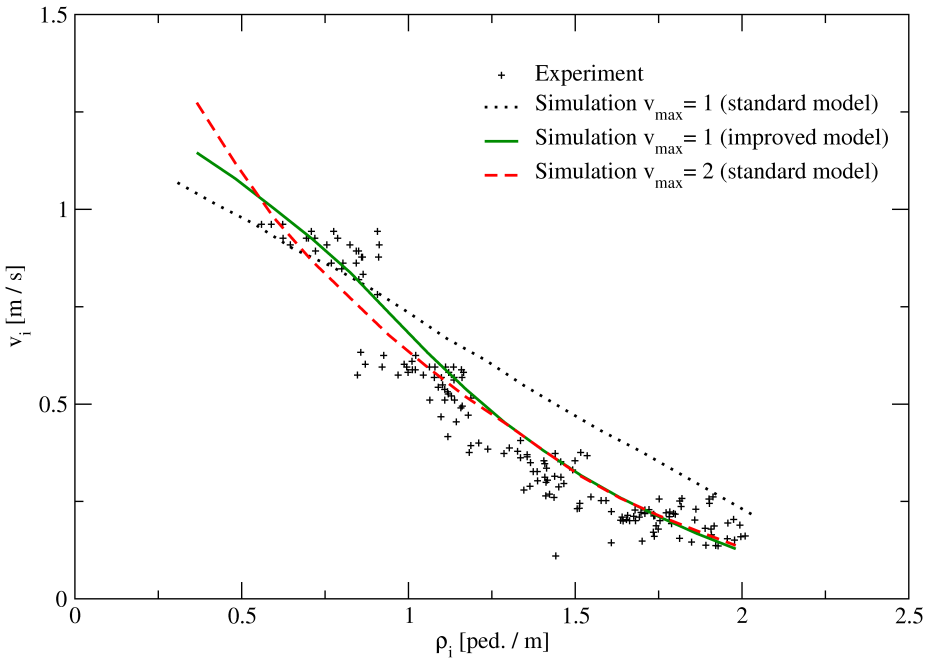

Figure 3.5: Comparison of empirical and simulated fundamental diagrams for three variants of the FFCA. The simulation density is given by the global density $\rho = \frac{N}{L}$.

The first analysis of the simulation results utilizes the global density definition $\rho = \frac{N}{L}$ where N is the number of pedestrians. This is a natural choice for simulations because it allows to treat the density as an easily adjustable parameter. Figure 3.5 shows the comparison of the empirical data with simulation results for the three

[4]Conflicts are possible in the one-dimensional model because a backwards motion is in principle possible. However, they are very unlikely and the influence of friction is thus negligible in a one-dimensional geometry.

parameter	$v_{\max} = 1$ (standard)	$v_{\max} = 1$ (improved)	$v_{\max} = 2$ (standard)
α	0.3	0.2	0.1
δ	0.2	0.2	0.2
k_S	2.5	3	1.8
k_D	3.5	3	4.8
k_P	0	4.5	0
μ	0	0	0

Table 3.1: Parameter values for simulations using the global density.

variants. The parameter values are fitted by eye and given in Table 3.1. The standard model with $v_{\max} = 1$ does not give a good agreement with the experimental data. However, both model extensions lead to a considerable improvement.

To analyze the influence of the measurement method, the local Θ-density definition introduced in Section 1.1.3.2 is utilized in the simulation. Thus both experiment and simulation measure density and flow in the same way. Figure 3.6 shows the simulated fundamental diagrams for the $v_{\max} = 2$ model and for two different parameter sets given in Table 3.2. The simulation with the parameter set optimized for the

parameter	$v_{\max} = 2$ (global)	$v_{\max} = 2$ (local)
α	0.1	0.1
δ	0.2	0.2
k_S	1.8	4
k_D	4.8	4.8
k_P	0	6.5
μ	0	0

Table 3.2: Parameter values for simulations using the Θ-density.

global density measurement does not result in a good agreement with the empirical data. The simulation that uses the parameter set optimized for the local Θ-density measurement on the other hand matches the experimental data well. Using the local density measurement in the simulation, fluctuations become an issue because the length of the measurement section (4 m) corresponds to only 10 cells. In order to reduce the resulting scatter, the size of the simulated system is increased by a factor of 10. The simulation of the original system size shown in the inset of Figure 3.6

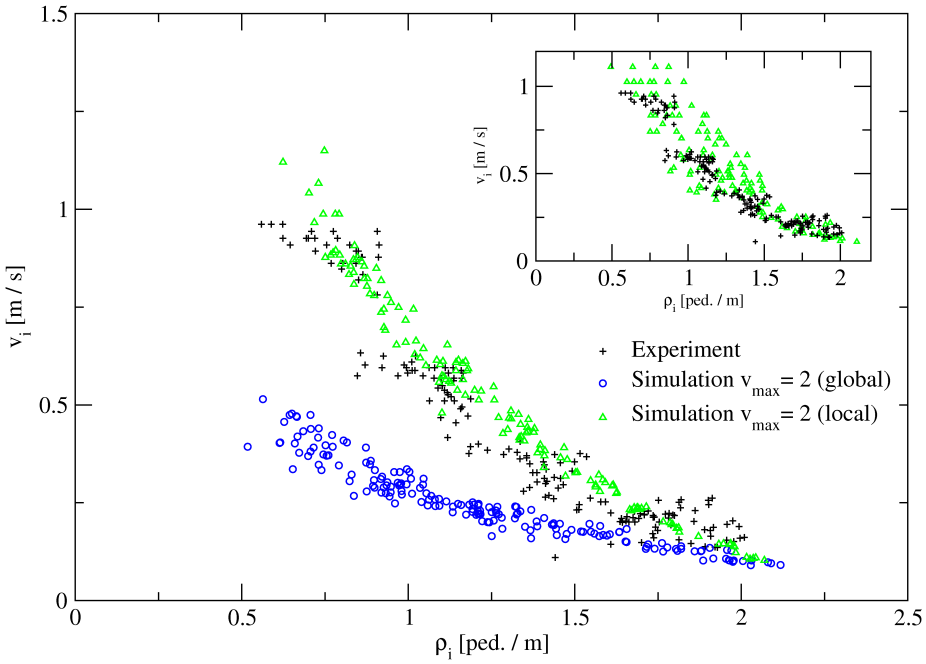

Figure 3.6: Experimental data and simulated fundamental diagrams of the $v_{\max} = 2$ model variant with different parameter sets. The blue circles denote the parameter set which is optimized for the global density definition whereas the parameters of the green triangles are optimized for the local measurement.

features a much larger fluctuation, however the agreement with the empirical data is still good. Simulations with the model variant including politeness factor show similar results.

The measurement method in the simulation has a strong influence on the simulation results. Consequently, one should always aim to use the same measurement methods in simulations as in the experiments that are used to calibrate the corresponding model. This has been discussed in detail in [23].

3.3.2 Entrance to the stands

The stands of the arena are connected to the promenade which in turn leads to the exits. The entrance to the stands is designed in the form of a vomitory, see Figure 3.7. Within the scope of the Hermes project an experiment [80] has been conducted to investigate the pedestrian flow in the proximity of the vomitory. The

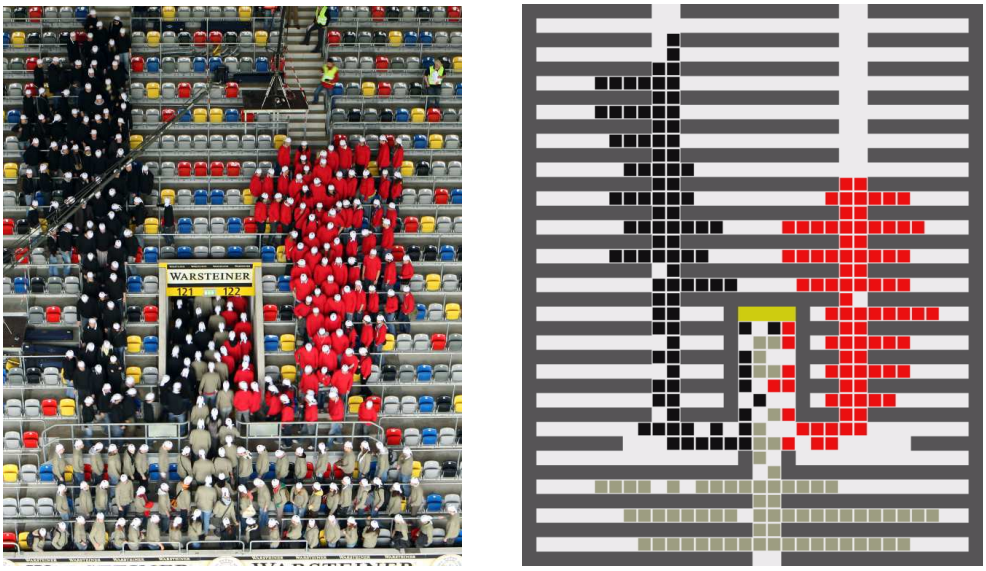

Figure 3.7: Snapshots of the experiment at the entrance to the stands (left) and the corresponding simulation (right) at $t = 20$ s.

pedestrians participating in the experiment shown in Figure 3.7 are instructed to 'walk normally'. No additional motivation for reaching the exit has been given. Depending on their starting position the participants wear differently colored T-shirts in order to allow for a better visual analysis of the experiment. The pedestrians coming from different directions can be distinguished without difficulty and the details of the flow inside the junction are easier to recognize. Each pedestrian wears a white cap with a black marker which is necessary for the automatic extraction of their trajectories [46].

The simulation is performed with the improved FFCA model including the politeness factor with coupling constant $k_I = 2.0$. The other parameter values are given in Table 2.1. The computation time on a standard laptop is only a fraction of a second. A hand-modeled geometry of the entrance as shown in Figure 3.7 is used.

The geometry of the vomitory is more complex than a corner in two major ways:

- In the vomitory a merging of three pedestrian streams occurs.
- The pedestrians coming from the upper part of the stands move through two consecutive corners, thereby performing a U-turn.

By comparing simulation results with video footage from the experiment it turns out that the second point is more important for the validity of the simulation. The merging of pedestrian streams can be described by the model without conceptual changes, the U-turns however require some modification. Using the standard FFCA, the outer corners where pedestrian coming from the top move to the left and right constitute bottlenecks. In contrast to that, the flow in the experiment is determined by the capacity of the vomitory itself. This difference leads to unrealistic pedestrian behavior and higher evacuation times in the simulation.

To better understand the pedestrian behavior in a simulation of the vomitory, it is instructive to first consider the simpler example of a single corner, e.g. from the top to the right. This means that the destination of a pedestrian coming from the top is to the right. The preferred direction of motion of an agent located in the middle of the corner consequently is to the right, following the shortest path to the destination. The agent's probabilities for standing still and for moving downwards are smaller than the probability to move to the right because the first two options do not change the distance to the goal. For the same reason, the probabilities for standing still and for moving downwards are equal. When the motion to the right is blocked by another pedestrian it is therefore likely that the agent will move downwards toward the outer edge of the corner within a few timesteps, especially at relatively high densities when moving back toward the top is likely to be prevented by further pedestrians.

Now consider the left U-turn of the vomitory in contrast. It is composed of two consecutive turns, first from top to right, then from right to top. The shortest path to the destination cells lies in the inner rim of the double corner. The preferred direction of motion of an agent in the middle of the U-turn is to the right, similar to the case of the single corner. However, in the U-turn the transition probability to move downwards is lower than the probability to stand still because moving downwards in the U-turn actually means moving away from the destination. Therefore, even at high

densities only the top area of the U-turn geometry is utilized whereas the bottom is devoid of agents, leading to a jam at the inner border of the U-turn.

To improve the simulation, the modified FFCA model proposed in Section 2.7 is used. The local modification of the model dynamics via the matrix of preference shown in Equation (2.7) is used in the simulation of the entrance to the stands for a few selected cells in the outer corners on the left and right side of the vomitory as shown in Figure 3.8. All other matrices of preference have trivial entries and therefore no influence on the model dynamics.

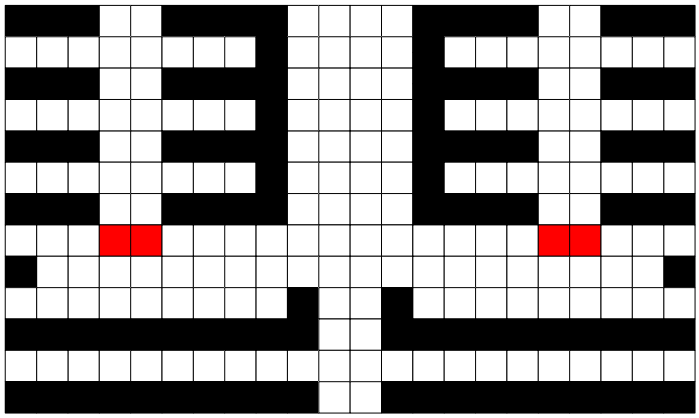

Figure 3.8: Central part of the simulated geometry around the vomitory. Cells with a non-trivial matrix of preference are drawn in red.

Due to the local use of the matrix of preference, the transition probabilities from the highlighted cells in Figure 3.8 to their neighbors directly below are increased as if the static floor field in the target cells were higher by one, making it more likely to move downwards. This change affects the transition probabilities for two possible transitions in each U-turn. It is not possible to directly change the static floor field in a way equivalent to the change described above. This local change of the transition probabilities results in a different pedestrian behavior. It is still more likely for agents in the U-turn to move to the right than it is to move down. But the latter is just as likely as standing still, leading to a more realistic utilization of the lower part of the U-turn geometry.

Due to the discreteness and limited spatial resolution of the FFCA geometry, it is not sensible to do a detailed microscopic comparison of the experimental and the simulated trajectories. However, three other qualitative and quantitative indicators are used to assess the quality of the simulation.

1. The evacuation times of experiment and simulation are about 100 s each, indicating a very similar flow through the entrance - which is the most important characteristic for the evacuation of the ESPRIT arena.

2. The position and shape of the jams as shown in the snapshots in Figure 3.7 feature reasonable qualitative agreement. This holds true not only for the 20 s mark shown here but for the entire duration of the experiment and simulation.

3. The densities in the entrance itself are compared. The densities in the images from the simulation and the experiment shown in Figure 3.7 seem to be quite different. However, e.g. at time $t = 20$ s there are 19 pedestrians inside the vomitory in both simulation and experiment, corresponding to a density of about 3.5 m^{-2}. Comparing the videos of experiment and simulation at other times shows good agreement of the density in the entrance as well.

The optical illusion of different densities is created by the different perspectives of the images. While the simulation is shown in a top view, the experiment is shown from a different angle and thus the density seems to be slightly higher. It is illustrative to consider an isometric image of the simulation as shown in Figure 3.9. Here the overlap of agents and, more importantly, the covering of empty space by agents which leads to a seemingly higher density is obvious.

3.4 Routing

One important aspect of modeling pedestrians in complex geometries is the route choice behavior. This is a very complex issue and object of current research. It has

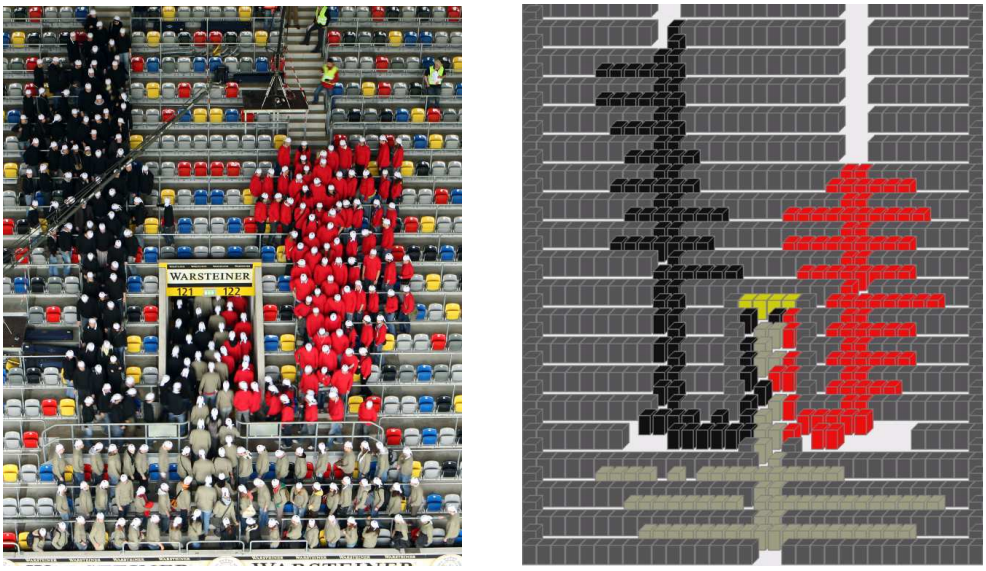

Figure 3.9: Snapshots of the experiment at the entrance to the stands (left) and an isometric view of the simulation (right) at $t = 20$ s.

been discussed extensively in [73]. This section includes a short overview of possible routing strategies and discusses the implementation used for the FFCA model in the Hermes project.

For a pedestrian in a room with several possible exits, the decision to use one of the available routes has to be included into the model. This can be done implicitly e.g. by using a floor field and thereby guiding the pedestrian to the nearest exit. Alternatively, the decision for one of the exits can be modeled explicitly. This distinction is insignificant for simple geometries such as corridors or bottlenecks but highly important for complex geometries such as the ESPRIT arena.

3.4.1 Shortest paths

Typical strategies for route choice behavior are local or global shortest path, schematically shown in Figure 3.10. Both can easily be implemented for cellular automata such as the FFCA.

For simple geometries the agents are coupled to the static floor field[5] which encodes

[5]The construction of the static floor field has been discussed in Section 2.1.

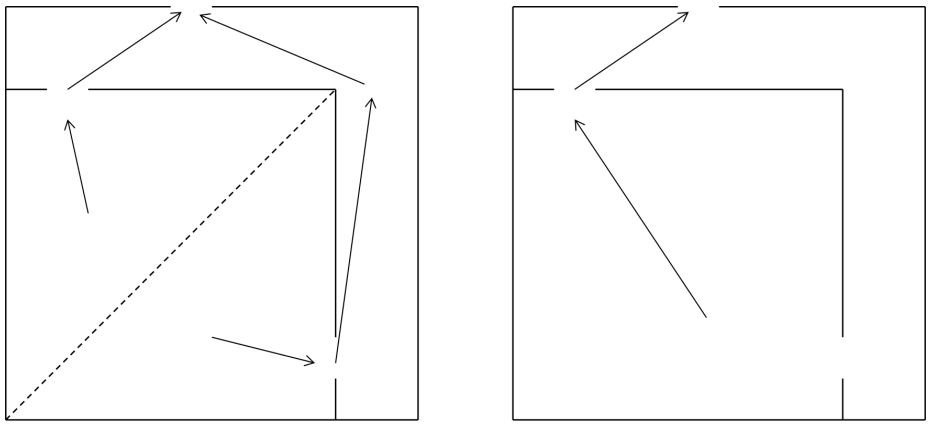

Figure 3.10: Schematic view of local (left) and global (right) shortest path.

the shortest global path to the exit cells. This is also possible for more complex geometries with several rooms which are combined into a global static floor field. Coupling an agent to this global static floor field, however, requires the agent to possess knowledge of the geometry, which is not always given in reality. Alternatively one can use an individual static floor field for each room or for distinct parts of the geometry. Each agent is then coupled to a specific floor field depending on its position and walks to an exit of the room using the shortest path given by the floor field. Upon entering the next room, the agent is coupled to another floor field and led to the nearest exit of this room.

This approach to finding the local shortest path requires an additional component. The nearest exit for an agent who just entered a room is the door it just walked through. To prevent the agent from oscillating between rooms an underlying navigation graph of the rooms is needed. This enforces that agents leave a room only toward neighboring rooms that are closer to an exit. The pedestrians basically follow virtual emergency exit signs.

3.4.2 Quickest paths

An alternative approach is a focus on minimizing travel time instead of travel distance. This is known as shortest time or quickest path strategy and has been

studied in [79, 81, 82, 83].

3.4.3 Stochastic routing

For the simulation of the ESPRIT arena different routing concepts are used for the stands and the promenade (outer hallway). Agents in the stands always use the local shortest path strategy. The stands are divided into several blocks, walking from one block into another one is usually forbidden. Therefore, each block is modeled as a separate room. As agents can only move to neighboring rooms which are closer to the global exit, every agent on the stands leaves its block through the vomitory into the promenade.

On the promenade the agent's route choice behavior is given by a combination of the local shortest path strategy with an additional stochastic aspect for simulations of an emergency evacuation. For the purpose of the simulation the promenade is divided into several 'rooms' in such a way that during an emergency evacuation it is unlikely that a person moves into a neighboring room in the promenade. The room boundaries are highlighted in yellow in Figure 3.11. The navigation graph ensures that each agent walks toward one of the exits of the arena. When there are several exits, the agents choose different exits with different probabilities depending on the distances between themselves and the exits. This is done in such a way that the closest door is the most likely choice; the selection is made when the agent enters the promenade. An agent chooses the i-th exit with probability

$$P_i = \frac{d_i^{-2}}{\sum_j d_j^{-2}} \tag{3.1}$$

where d_j is the distance to the j-th exit. The resulting distribution of travel paths is shown in detail in Figure 3.12 for part of the promenade. It shows that most agents move to the nearest exit and some agents choose an exit farther away. This results in

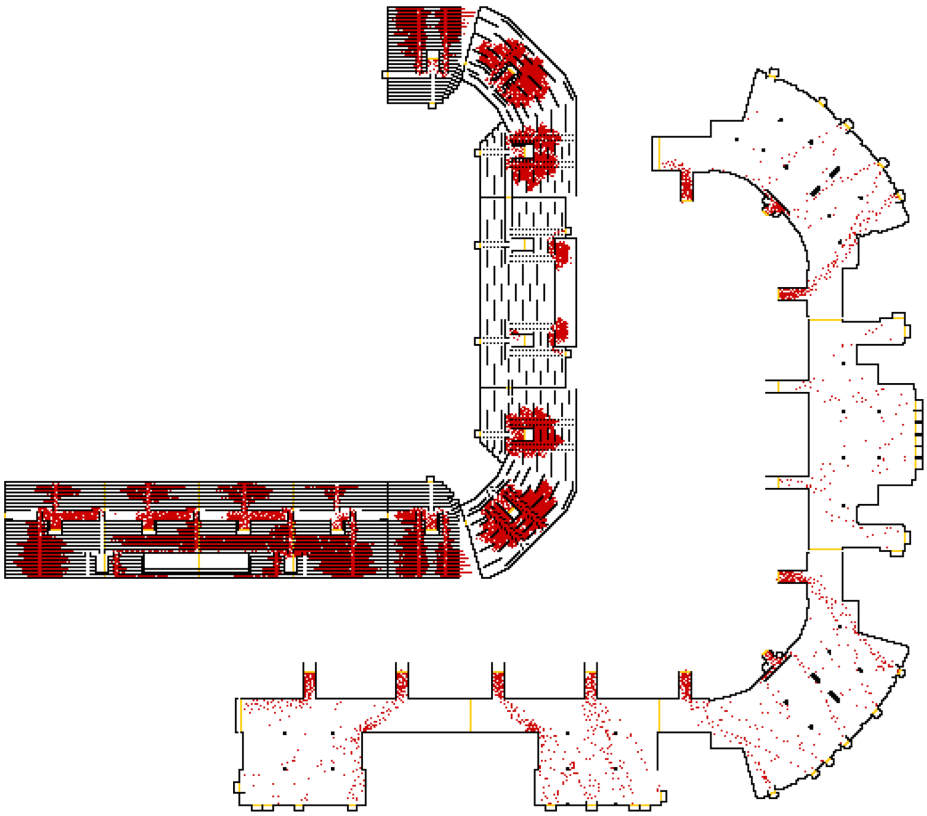

Figure 3.11: Simulation snapshots of the stands (top left) and the promenade (bottom right) of the ESPRIT arena.

a higher utilization of the given space and more realistic behavior than using a strict local shortest path strategy which would lead to unused exits and thus unrealistic behavior.

Simulations of routine egress are more challenging, in particular due to the different and only partially known route choice behavior of the audience. The main goal of a visitor is not to leave the arena as quickly as possible but rather to find a comfortable way to the preferred method of transportation, whether it be cars or public transport. This leads to considerable lateral movement in the promenade from pedestrians moving toward the parking area or the train station. The ideal and, unfortunately, unfeasible way to deal with this behavior is to know the destination of every agent and use that as input for the simulation. The approach taken here only requires knowledge of the approximate percentages of the audience that uses

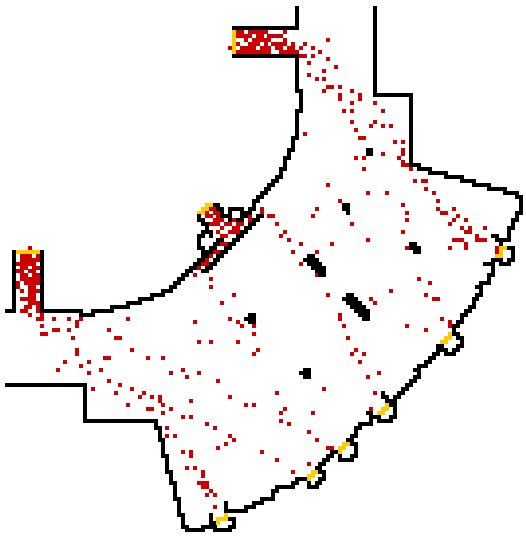

Figure 3.12: Travel paths created by stochastic routing. Pedestrians move from the entrances located at the top left to the exits at the bottom right.

cars and public transport, respectively. At the start of the simulation, each agent is randomly assigned to a destination according to these percentages and coupled to the corresponding navigation graph. An agent with the destination train station will, after leaving the stands, ignore every exit that does not lead to the train station. The fraction of the audience using a specific means of transport varies, depending on the type of event. The typical audience of a concert relies much more on cars than football fans who prefer to use public transportation.

Instead of following one of the strategies discussed above, some people might choose the exit they know from entering the building[6]. Accounting for this can improve the realism of the routing choice behavior and thus the overall accuracy of the simulation. To further improve the route choice behavior in the simulation a dynamic routing might be incorporated in which agents redeem their decisions when necessary, depending on the jamming status of different exits. Additionally, visibility constrains leading to different knowledge and thus diverging behavior of the agents can be included.

[6]This effect is related to the Ellsberg paradox [84]: People generally prefer a known risk to ambiguity.

A comparison of simulated evacuation times and real data is impossible because there was no emergency evacuation during the Hermes project. As discussed in Section 3.2, routine egress times depend on a multitude of uncontrollable factors that cannot be reproduced in the simulation. It is therefore not feasible to compare them to simulated egress times.

3.5 Distribution of evacuation times

The time it takes to make a forecast of the evacuation is very important for the overall usefulness of the evacuation assistant. To be helpful for the decision makers it has to be fast. Its speed is determined by the speed of the simulation kernels on the one hand and the speed of the visualization of the resulting trajectories on the other hand. The latter is mainly a question of software engineering and therefore not part of this work. The (deterministic) GCFM is a computationally expensive model and uses most of the computation power available for microscopic simulations within the Hermes project. Simulations with the stochastic FFCA are fast, but their results vary when several runs are performed. The question therefore is: How may runs need to be analyzed to get meaningful results?

The evacuation time can be defined as the time it takes to evacuate 100 % of the pedestrians. With this natural definition the evacuation time depends strongly on the last stages of the simulation when there are only a few pedestrians remaining in the simulation. For this reason there are other definitions of evacuation times used in the literature [73] that require a smaller percentage of pedestrians to be evacuated and thus reduce the evacuation time variance. Therefore, any interpretation of evacuation times has to be done under careful consideration of the specific definition used.

Figure 3.13 compares evacuation times for the natural evacuation time definition on the right and an alternative definition on the left which requires 90 % of agents to be evacuated. The graphs show a typical scenario with $10,000$ pedestrians as well

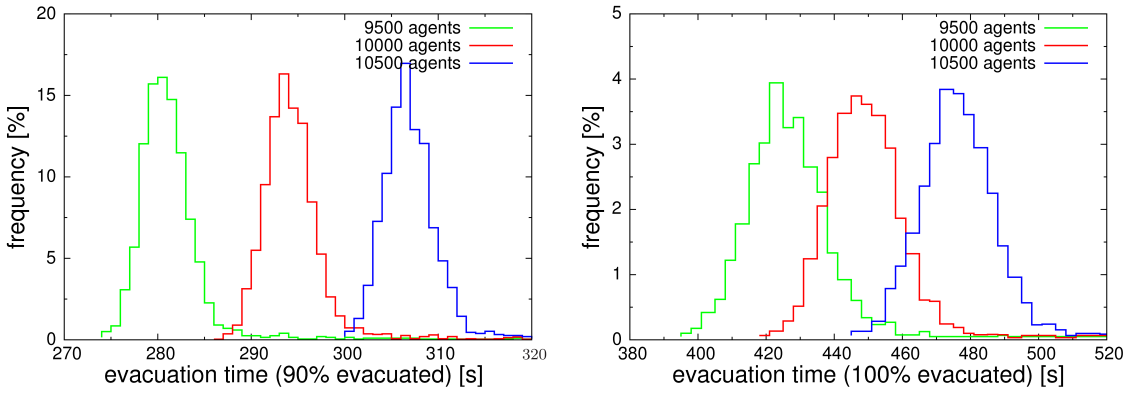

Figure 3.13: Distribution of evacuation times.

as two other scenarios which consider the uncertainty of the pedestrian counting and assume pedestrian numbers 5 % higher and lower, respectively. For both definitions, the variation of the evacuation times over $10,000$ simulation runs is smaller than the uncertainty related to the initial condition, e.g. the exact number of pedestrians in the arena. This effect is expectedly more pronounced for the 90 % - definition. Figure 3.14 shows a comparison of evacuation times for different clearing percentages.

The time series of two typical simulation runs are given in Figure 3.15. At most times they are almost indistinguishable. Even in the last stages of the evacuation, the difference is small. At the time of completion of the first run about 0.6 % of agents remain in the second run. Due to the large number of simulated pedestrians

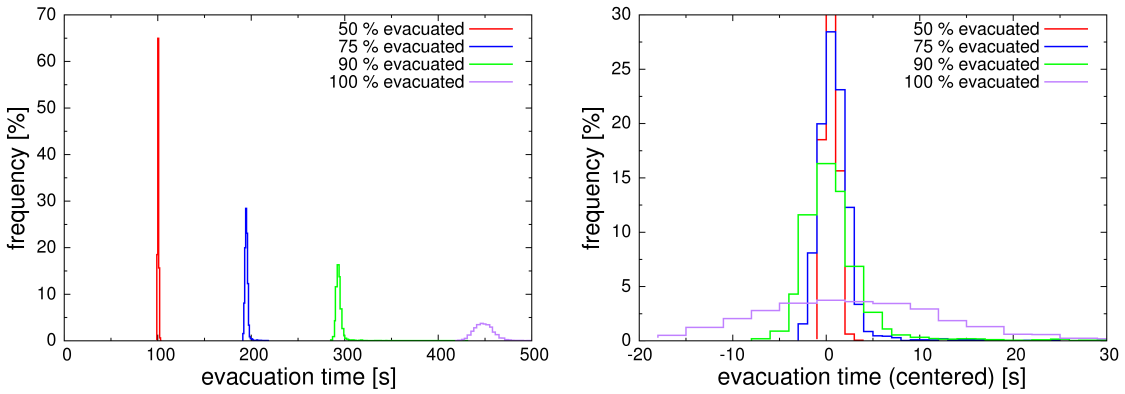

Figure 3.14: Distribution of evacuation times.

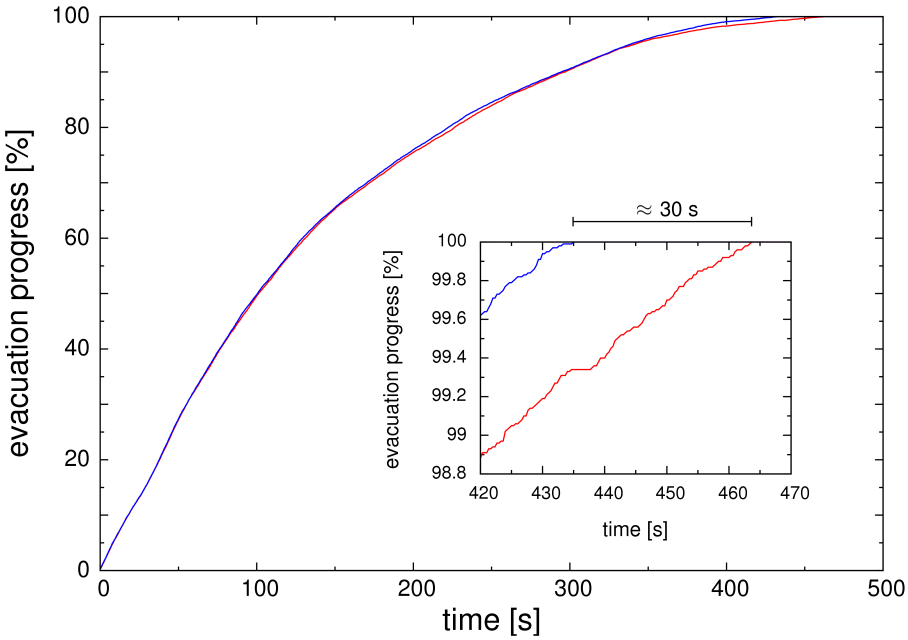

Figure 3.15: Evacuation time series of two typical simulation runs.

and the even larger number of stochastic decisions in the course of the simulation, the standard deviation of the evacuation time is small and the typical result thus very close to the average result. This is related to the law of large numbers and the effect of self averaging. It is therefore sufficient to only perform one simulation run and still get an accurate evacuation time despite the stochastic nature of the model.

3.6 Outlook

The Hermes project as a proof of concept explores the state of the art in evacuation simulation. The FFCA is one of the pedestrian models featured in the project. On a regular computer, an evacuation simulation of the ESPRIT arena is about 30 times faster than real-time. Even though Hermes successfully shows the principal feasibility of an evacuation assistant as a supportive tool for evacuations of large-scale events, there is still a lot of room for improvement. This work focuses on possible advancements of the FFCA simulation within an evacuation assistant.

A more sophisticated calibration of the model is possible and should be pursued

to improve the predictions for a permanent installation of the evacuation assistant. An ongoing refinement of the calibration using the data gathered by the evacuation assistant can further optimize simulation results. The reinterpretation of the matrix of preference can be researched in more detail. In this work, it is used for a few manually selected cells, future work might lead to an automated procedure for defining the matrix of preference of each cell. Additionally, other model improvements can be pursued: The FFCA is limited to 40 cm x 40 cm cells and can only approximate the actual geometry. Smaller cell sizes as discussed in Section 2.6 are subject of current research. The stochastic routing used for the FFCA in the Hermes project could also be improved upon by including more elaborate routing techniques. The details of the pedestrian's route choice behavior actually are one of the most decisive factors of the simulation. Finally, optimizing the runtime of the FFCA implementation was not necessary for the Hermes project but could be of benefit to a permanent evacuation assistant.

Nonetheless, uncertainties outside the scope of the pedestrian models are as important as the model dynamics itself. To reasonably forecast routine egress a lot of additional information is required: relatively exact numbers and positions of all persons in the arena[7] as well as data about the preferred exit (train station, parking ground, neither) of each person. Additionally, the egress time depends on the pre-movement time. Emergency evacuation is in principle easier to simulate than routine egress – it is however difficult to gather appropriate data for calibration beforehand.

[7]The automated person counting only registers how many people are in each room.

CHAPTER IV

Modeling of phase separation in pedestrian dynamics

For evacuation simulations, the high density regime is particularly important. An interesting effect at high densities is the separation of pedestrian traffic into two distinct phases which consist of standing pedestrians and slowly moving pedestrians,

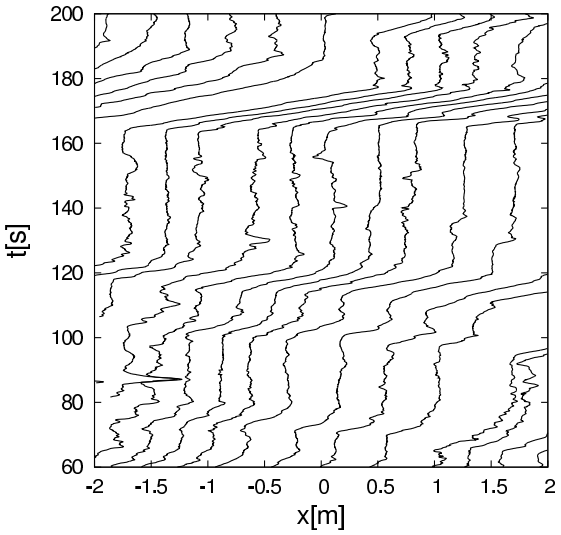

Figure 4.1: Experimental trajectories featuring phase separation.

respectively. The experimental data has been extensively discussed in Section 1.2.1, the trajectories are shown in Figure 4.1. To understand complex phenomena, one typically wants to understand the underlying basic mechanisms first. Therefore, phase

separation in one-dimensional movement without overtaking is considered here, in accordance with the experimental system.

Phase separation is a known feature in simple stochastic transport models such as the asymmetric simple exclusion process (ASEP) [85, 53] and in vehicular traffic [53]. However, the details are quite different from the phase separation observed in pedestrian dynamics. Typical pedestrian models such as force-based models [10, 30] or the Floor Field Cellular Automaton [1, 2, 3] discussed in Chapter II can successfully describe qualitative phenomena like lane formation and are used for quantitative predictions, as outlined in Chapter III. But they do not feature phase separation.

At the start of this chapter, phase separation as observed in pedestrian traffic is compared to phase separation in the ASEP and in vehicular traffic. Several pedestrian models are then briefly introduced and analyzed with regard to the existence and stability of a phase-separated state with the characteristics observed in pedestrian dynamics. The purpose of this chapter is not to perfectly describe the experimental data but rather to find a model that is able to generate the observed phase separation into a jammed and a slowly moving phase at all. For that reason small differences between the experimental setup and the simulated system are of minor importance.

4.1 Phase separation in driven transport models

Typical causes of phase separation in driven systems are (a) the introduction of quenched (time-independent) disorder or (b) the dynamics of the model itself. An example for phase separation caused by quenched disorder can be seen in the ASEP, an example for phase separation caused by the model dynamics is given by the Velocity Dependent Randomization (VDR) model [86]. Both will be discussed briefly in this section.

The ASEP is one of the most common and well-understood models for one-dimensional driven transport processes. Due to its simplicity, many exact results

can be derived (for a detailed discussion, see [53]). Nevertheless, the emerging behavior of the model is remarkably complex. The ASEP is defined on a one-dimensional lattice where each site can be occupied by at most one particle. It is commonly used with several update schemes and can utilize both periodic and open boundary conditions. The update of a particle during an infinitesimal time interval dt consists of two steps. Firstly, a target site is chosen: With probability pdt this is the right neighbor and with probability qdt the left neighbor. Secondly, the particle jumps to the target site if it is empty, otherwise the particle remains on its site. The model variant with backward jump rate $q = 0$ is often called the totally asymmetric simple exclusion process (TASEP)[1].

One typically distinguishes between two kinds of quenched disorder [53, 87]:

- Particlewise disorder: Different particles (agents) can have different jump rates. Agents accumulate behind 'slow' agents that have a smaller forward jump rate p. This leads to phase separation into regions with high density and regions devoid of agents.

- Sitewise disorder: Different lattice sites can cause particles to respect different jump rates. Three subtypes have been discussed in [87]. Boundaries between an upstream region with high density and a downstream region with low density are located at bottlenecks[2] and therefore stationary (non-moving).

These kinds of phase separation can be interpreted as traffic jams due to slow vehicles or road construction, respectively. However, they are quite different from the phase separation observed in pedestrian dynamics discussed in section 1.2.1. Most notably, in the situations discussed here the jam is either stationary or moves forward whereas in pedestrian phase separation the jam moves backward through the system.

[1] There are some inconsistencies in the naming scheme of different ASEP variants [53].

[2] Depending on the distribution of jump rates, several lattice sites may in combination form an effective bottleneck.

Additionally, in the case of particlewise disorder the system contains growing regions devoid of agents.

The phenomenon of phase separation is also a well-understood feature in vehicular traffic [53]. There are two empirically observed, distinct phases: a jammed phase with high density and a free-flow phase with low density where cars move at their desired velocity. This can be reproduced in appropriate models such as the VDR model [86] which is an extension of the well-known Nagel-Schreckenberg model [88] and – as indicated by its name – employs a different randomization (slowdown probability) for moving and non-moving vehicles, respectively. Standing vehicles, e.g. vehicles that are about to leave a jam, have an increased probability to not start moving. Due to this so-called slow-to-start rule, the outflow of the jam is reduced compared to the maximum flow of the system and consequently the average distance between vehicles moving out of the jam is increased. This increased distance leads to a region of non-interacting cars downstream of the jam and thus to the free-flow phase, see Figure 4.2.

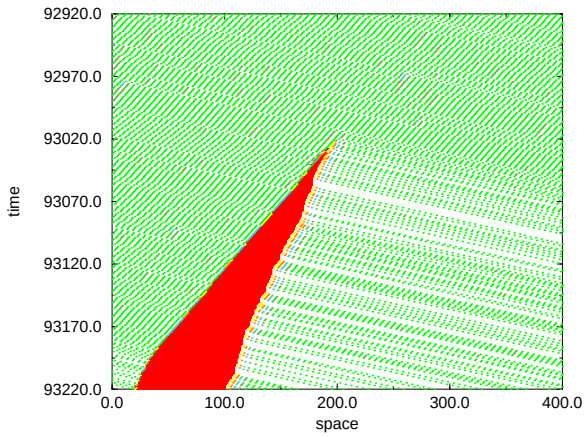

Figure 4.2: Simulated car trajectories in the VDR model [86].

The existence of two distinct phases is connected to the existence of metastable states in the fundamental diagram, see Figure 4.3. For intermediate density values the

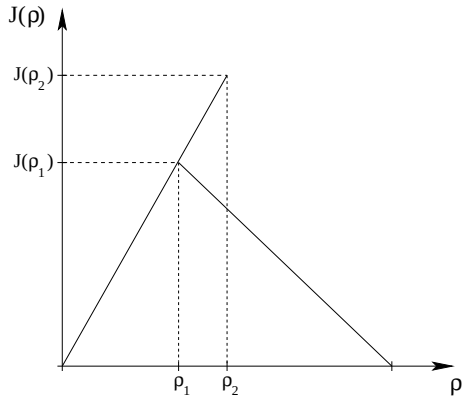

Figure 4.3: Schematic fundamental diagram of the VDR model [53].

flow is not a unique function of the density: The free flow branch can spontaneously break down into a congested state. This is called a capacity drop and leads to a hysteresis loop [89].

Even though the phase separation resulting from the dynamics of the VDR model is relatively similar to the phase separation observed in pedestrian dynamics, the details are different. Vehicular traffic is separated into a jammed phase and a free-flow phase of non-interacting particles; the jam moves backward through the system. In pedestrian traffic, the jam also moves backward through the system. However, both phases consist of interacting particles. The distance between pedestrians in the moving phase is small, not allowing them to move with their desired velocity. The mechanism creating the phase separation in pedestrian dynamics therefore differs from a simple slow-to-start rule.

4.2 Floor Field Cellular Automaton

The first model tested for phase separation is the FFCA [1, 2, 3, 4] introduced in Chapter II. As discussed in Chapter III, the FFCA can realistically describe pedestrian motion in many circumstances and has been used in the Hermes [5, 6] project.

Here, simulations of a periodic one-dimensional system at high densities are per-

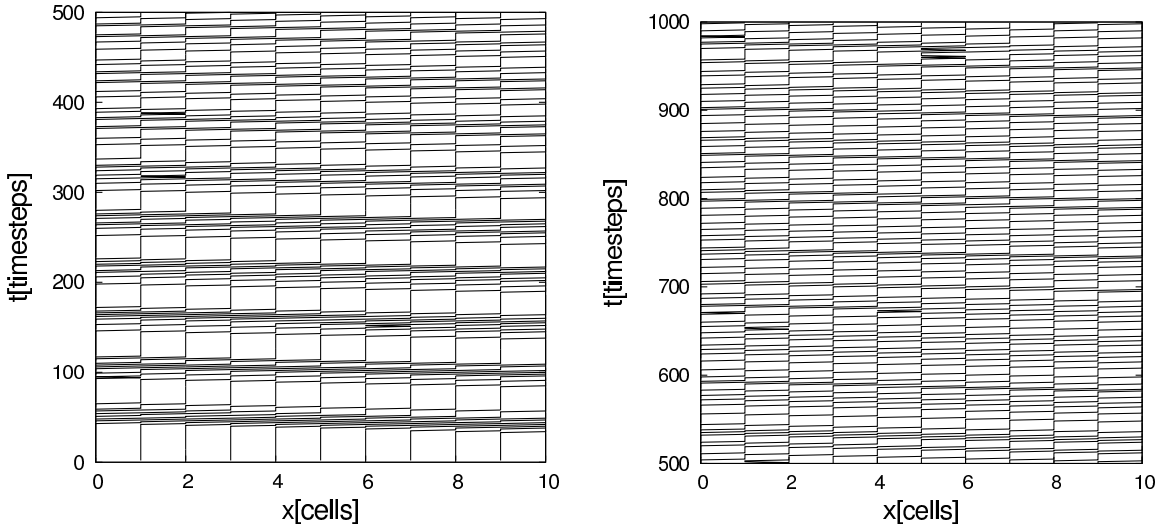

Figure 4.4: Trajectories of the FFCA at the beginning (left) and at a later stage (right) of the simulation. The image is zoomed in to an area equivalent to the measurement section of the experiment.

formed with the FFCA. The parameter values of the model are the same as discussed in Chapter II and given in Table 2.1. Figure 4.4 shows typical trajectories at a high density: 84 % of the cells are occupied, corresponding to an absolute density of $\rho = 2.1$ agents per meter. The same trajectories are also given in Figure 4.5 where every second agent is omitted to generate a clearer image. Note that the density $\rho = 2.7$ pedestrians per meter at which phase separation can be observed in the experimental data shown in Figure 4.1 is beyond the maximum density possible in the FFCA.

The simulation uses the inhomogeneous initial condition. During the first about 300 timesteps of the simulation a separation of moving and standing agents into distinct phases can be observed. However, the initial jam decays quickly and after less than 500 timesteps (150 s) the agents are almost homogeneously distributed. Simulations with different parameter values lead to similar results.

The only observable jam in the one-dimensional system is the initial jam when the simulation starts in an inhomogeneous state. The dynamics of the FFCA cannot generate a phase-separated state.

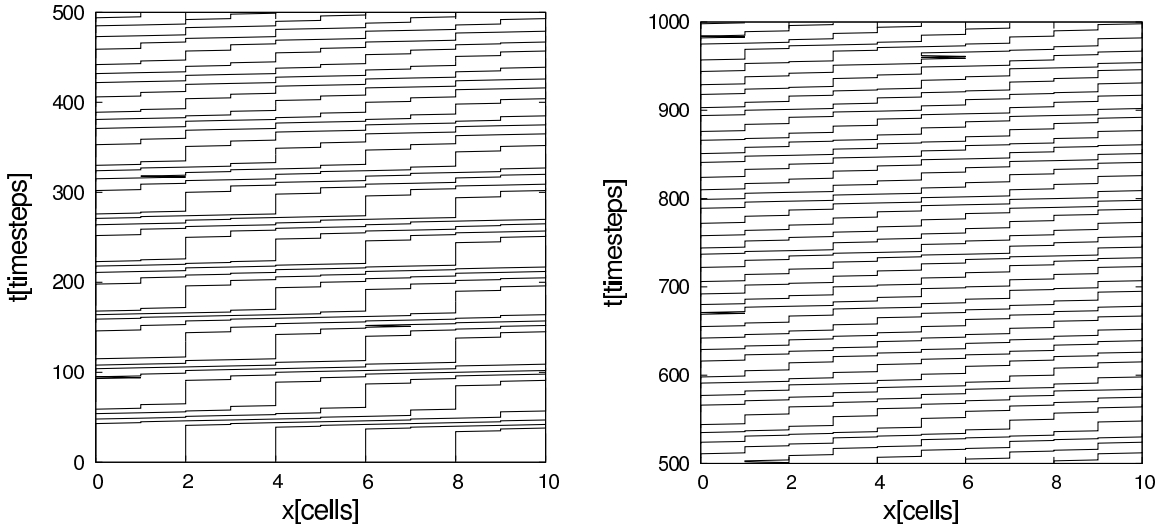

Figure 4.5: FFCA trajectories. For the sake of clarity, only every second agent is shown.

4.3 Generalized Centrifugal Force Model

The second model tested for phase separation is the GCFM [30], which has also been used in the Hermes [5, 6] project, as outlined in Chapter III. The GCFM is a force-based model in which pedestrians are represented by ellipses whose size depends on the current velocity of the pedestrian. The parameter values are given in [30].

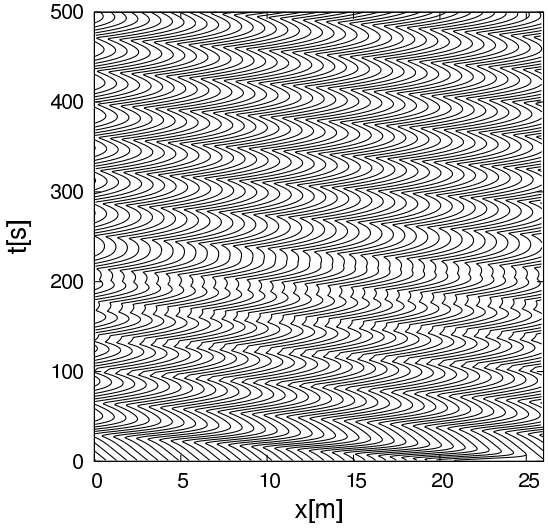

Figure 4.6: GCFM trajectories using an inhomogeneous initial condition. Only every second agent is drawn to avoid cluttering up the plot. Data courtesy of Mohcine Chraibi.

Trajectories of a one-dimensional periodical system with a length of 26 m and a density of 2.7 m^{-1} ($N = 70$) are shown in Figure 4.6. This simulation is performed using an inhomogeneous initial condition. However, there are no standing agents in the system. Instead, all agents except for the first in the initial jam start moving backward and then settle into an oscillating behavior including macroscopic movement in both directions.

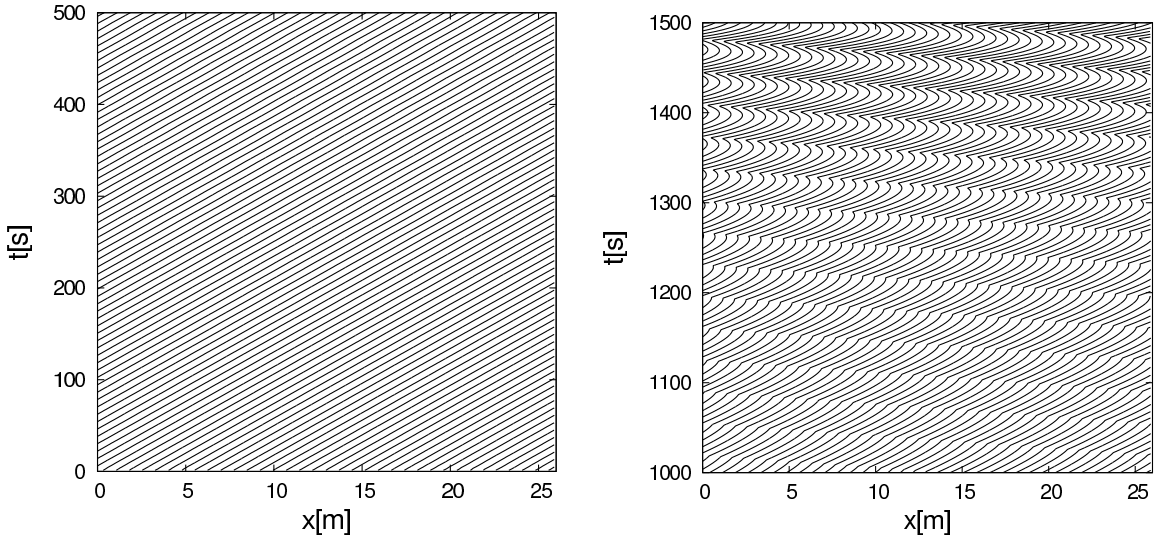

Figure 4.7: GCFM trajectories using the almost homogeneous initial condition at different stages of the simulation. Only every second agent is drawn to avoid cluttering up the plot. Data courtesy of Mohcine Chraibi.

Figure 4.7 shows trajectories of a simulation with a starting configuration similar[3] to the almost homogeneous initial condition discussed in Section 1.3.2.4. At the beginning of the simulation, the system is close to a homogeneous state and all agent move with almost the same velocity. After about 1200 s, the initial perturbations have built up in such a way that this simulation exhibits oscillating behavior as well. For longer simulation times, the observed oscillations grow more extreme and induce very small distances between agents. Because the repulsive force between agents is proportional to the inverse of their distance, it diverges and the simulation

[3]Though the exact implementation is slightly different, the idea is the same: distribute the agents homogeneously and add a small perturbation.

collapses [90].

According to [90], force-based models without additional rules are in general unable to simulate standing agents. The GCFM simulation results do not feature the phase separation observed in the experimental data.

4.4 Adaptive Velocity Model

The adaptive velocity model [25, 91, 92] is an event-driven one-dimensional model designed to reproduce the phase separation observed in pedestrian dynamics. Depending on its headway a pedestrian either accelerates or decelerates. A change between these states is called an event. The parameters defining the pedestrian motion, e.g. the desired velocity, are normally distributed. Each agent has individual parameter values. A detailed definition of the model dynamics as well as parameters values can be found in [25, 91, 92]. The simulated system is a corridor with a length of 26 m with periodic boundary conditions.

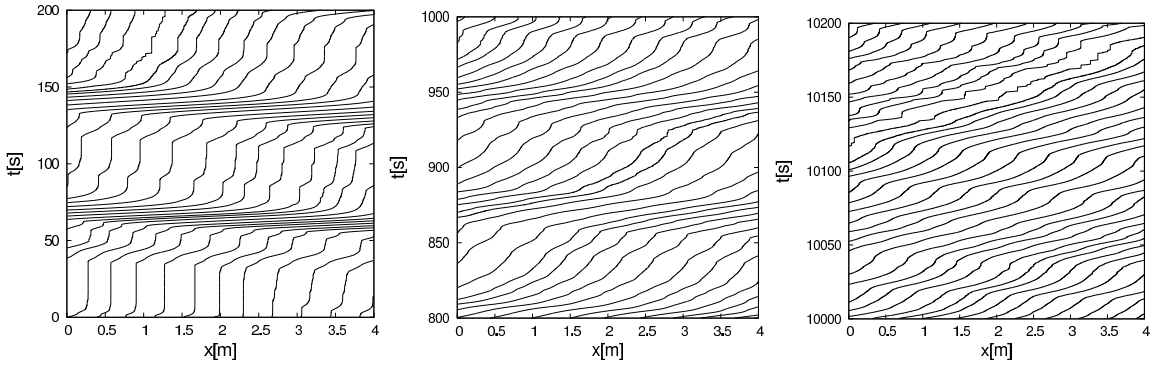

Figure 4.8: Zoomed-in trajectories of the adaptive velocity model with $N = 62$ agents at different stages of the simulation.

Figure 4.8 shows trajectories of the adaptive velocity model at a density of 2.38 agents per meter ($N = 62$), zoomed in to a 4 m interval corresponding to the experimental measurement section. As in [25], the simulation starts in an inhomogeneous state. At the start of the simulation, the agents are separated into distinct moving

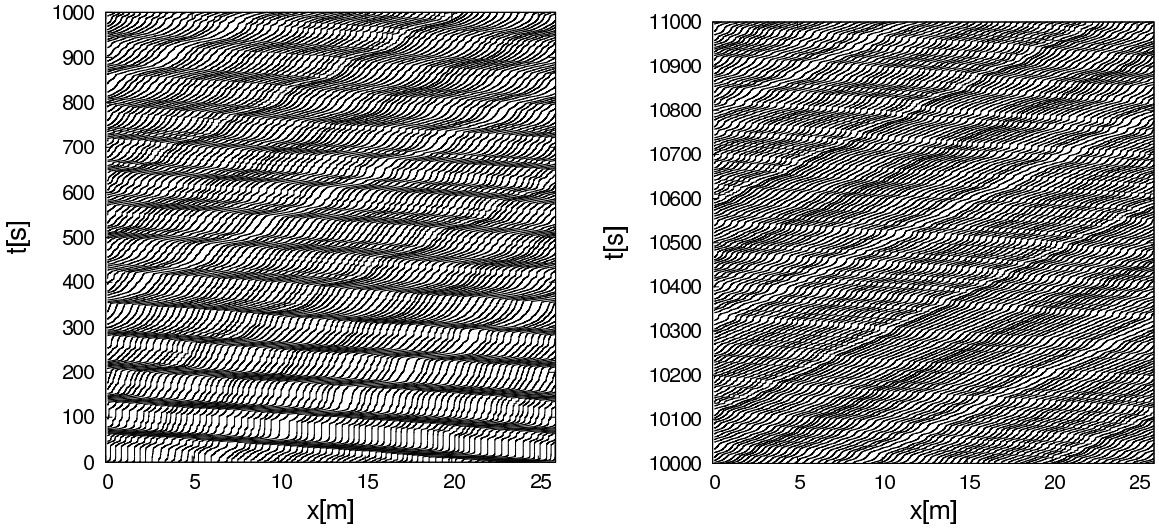

Figure 4.9: Global trajectories of the adaptive velocity model with $N = 62$ agents at different stages of the simulation.

and jammed phases, respectively – as expected due to the initial condition. The initial jam, however, quickly dissolves and at later stages of the simulation the agents are almost homogeneously distributed. The decay of the initial jam can also be seen in the global trajectories shown in Figure 4.9. While there are pronounced inhomogeneities at the beginning of the simulation, later the agents are more evenly distributed. After about 300 timesteps, there are no more standing agents in the simulation.

If the simulation starts with homogeneously distributed agents, the state of the system in later stages of the simulation is unaltered. The slight inhomogeneities introduced by the heterogeneity of the agents prevent the simulation from staying in a completely homogeneous state. However, the simulation never develops a jam, all agents move at all times. The same is true for different parameter values and different densities. Figure 4.10 shows the global trajectories for $N = 70$ with a density of 2.69 agents per meter. Even though the initial jam is larger, the system develops more quickly into an almost homogeneous state without phase separation.

The results presented in this section show that the adaptive velocity model only features phase separation and trajectories similar to the experimental data if the sim-

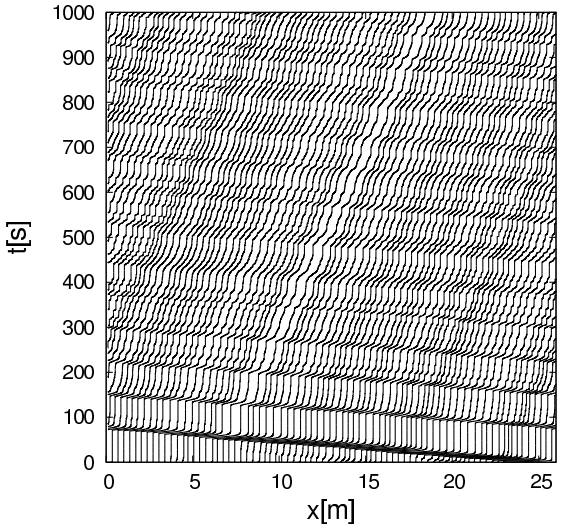

Figure 4.10: Global trajectories of the adaptive velocity model with $N = 70$ agents.

ulation starts with an inhomogeneous initial condition, contrary to the experimental setup. Additionally, the initial jam and thus the phase-separated state decay quickly, leaving the system in an almost homogeneous state where the remaining small inhomogeneities stem from the normal-distributed parameter values.

4.5 Simple CA Model

4.5.1 Model definition

In this section a simple cellular automaton model [93] is analyzed that aims at reproducing the observed phase separation. This model is in principle capable of creating phase separation that is in qualitative agreement with the experimental data, i.e. two coexisting separate phases with slowly moving and not moving particles, respectively. Similar to the adaptive velocity model, the observed phase separation is purely a result of the initial condition and decays over time. The model is defined on a one-dimensional lattice containing $L = 200$ cells. As in the experiments, periodic boundary conditions are used to connect the last cell to the first cell. Each cell can either be occupied by one agent or be empty. Densities are defined relative to

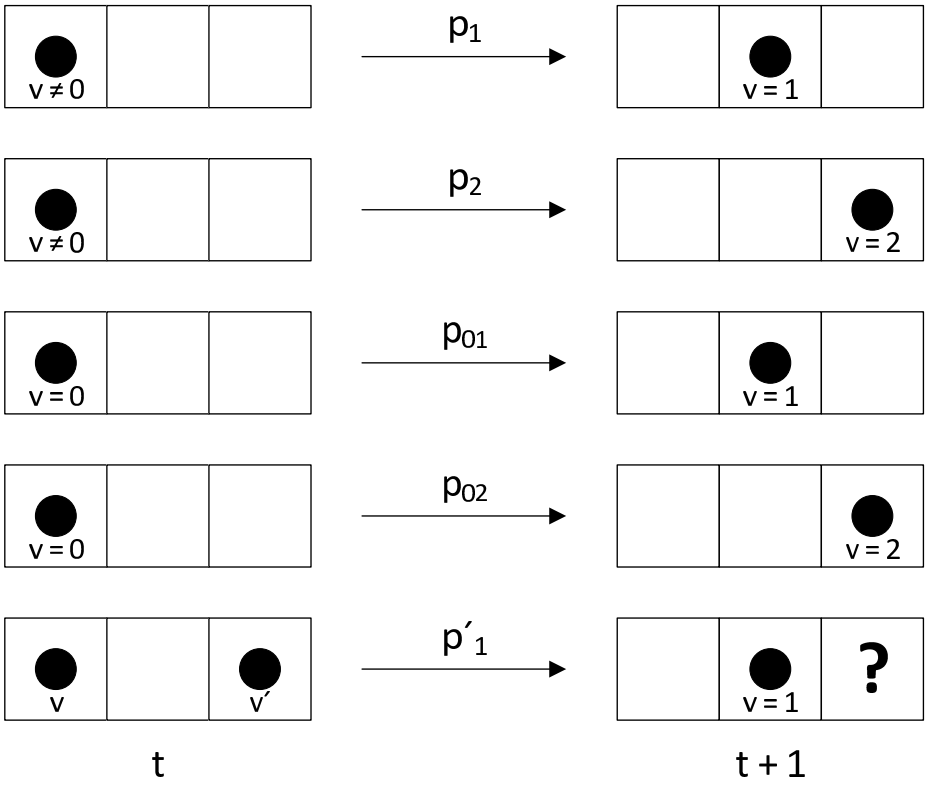

Figure 4.11: Definition of the five transition probabilities used in the model.

the maximum density, $\rho = \frac{N_{\text{occupied}}}{L}$. The current velocity of an agent is defined as the number of cells it moved in the last timestep. In every timestep the agents are updated in parallel according to the following update rules which are also shown in in Figure 4.11. Agents that have a velocity unequal to zero and at least two free cells in front of them move to the cell directly in front of them with probability p_1 and move two cells forward with probability p_2. Agents with a current velocity of zero and two free cells in front of them move to the cell directly in front of them and to the cell two steps in front of them with probabilities p_{01} and p_{02}, respectively. Note that these definitions require both $p_1 + p_2 \leq 1$ and $p_{01} + p_{02} \leq 1$. An agent with only one free cell in front of it moves one cell forward with probability p_1', independent of its velocity and independent of whether the agent two cells in front of it moves as well. The probability not to move is then given by either $1 - p_1 - p_2$, $1 - p_{01} - p_{02}$, or $1 - p_1'$, depending on the velocity and headway of the agent.

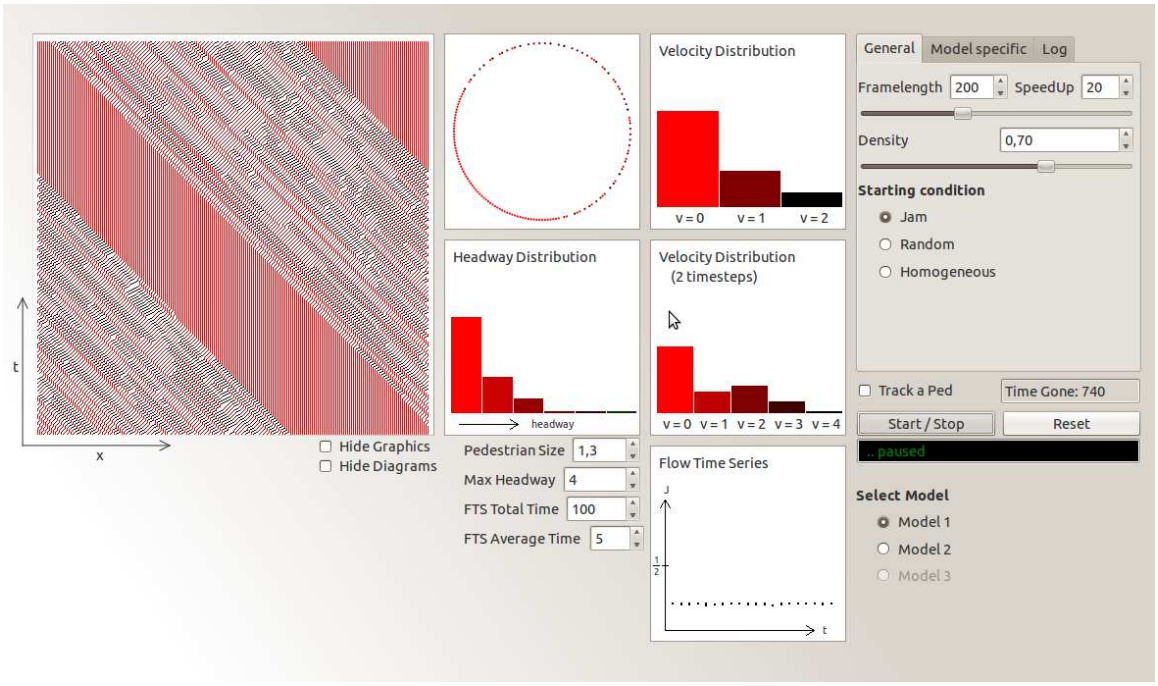

Figure 4.12: Screenshot of the simulation GUI.

The parameter values used here are

$$p_1 = 0.05, \qquad p_2 = 0.9, \qquad p_{01} = 0.01, \qquad p_{02} = 0.99, \qquad p_1' = 0.99\,.$$

They are chosen such that the resulting trajectories resemble the experimental data as much as possible[4]. Small changes of the parameters generally produce small and non-significant changes in the simulation. The resulting free velocity can be approximated by

$$v_{\text{free}} = p_1 + 2 \cdot p_2 = 1.85 \ \frac{\text{cells}}{\text{timestep}} \tag{4.1}$$

because the configurations that require the consideration of p_{01}, p_{02} and p_1' do not occur for free moving agents.

Figure 4.12 shows the graphical user interface (GUI) used to analyze the simulation results of this model in real-time. The GUI project has been abandoned afterward due

[4]The experimental and model trajectories are compared by eye; no formal criterion is employed.

to the disproportionate time and effort required to include additional models into the GUI framework compared to analyzing results by other means after the simulation finished.

The simulation results can be related to the experimental results discussed in Section 1.2.1 by identifying every cell with an area of size 0.4×0.4 m^2. This choice of the cell size is standard for cellular automata models such as the floor field cellular automaton [1, 2, 3] and corresponds to a maximum density of 6.25 agents per square meter or a maximum line density of 2.5 agents per meter. Note that this is a little lower than the maximum density of 2.7 m^{-1} used in the experiment. Identifying each cell with a one-dimensional length of 0.3 m instead leads to a maximum density of 3.33 m^{-1}. The experimental density 2.7 m^{-1} then corresponds to the relative density 0.81. It may not be reasonable to naively extend this to two dimensions because the resulting maximum density of 11.1 m^{-2} is very high. Using this in a one-dimensional simulation is, however, consistent with experimental densities. A timestep corresponds to about 0.35 s. With standard parameter values the free velocity calculated in Equation (4.1) corresponds to

$$v_{\text{free}} = 1.85 \ \frac{\text{cells}}{\text{timestep}} = 1.85 \cdot \frac{0.3 \text{ m}}{0.35 \text{ s}} \approx 1.6 \ \frac{\text{m}}{\text{s}} \tag{4.2}$$

in reasonable accordance with typical experimental values.

4.5.2 Results

The simulated system has a size of $L = 200$ cells. Figure 4.13 shows trajectories from a simulation with inhomogeneous initial conditions at three different densities, zoomed in to a 4 m interval corresponding to the experimental measurement section. The trajectories feature two distinct phases. The size of the slowly-moving and the jammed phase depend on the density and thus on the size of the initial jam. The

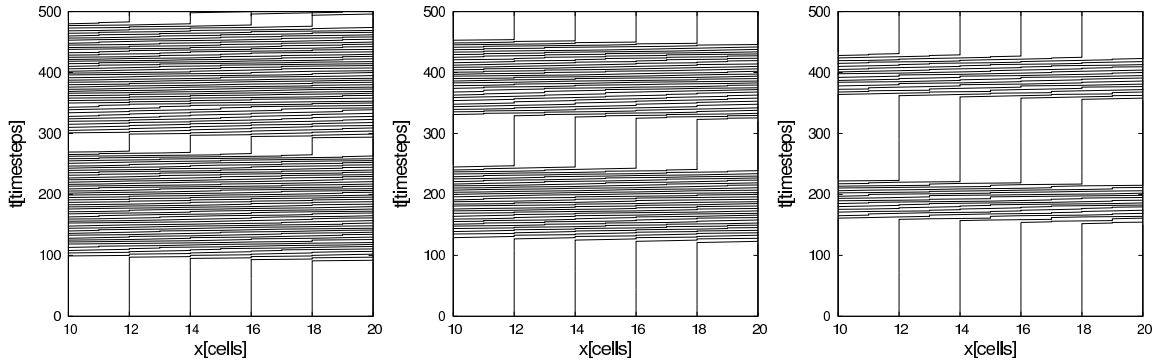

Figure 4.13: Simulated trajectories with inhomogeneous initial conditions and relative densities 0.55 (left), 0.7(middle), and 0.85(right). For the sake of clarity, only every second agent is drawn.

observed phase separation is a direct result of the inhomogeneous initial condition. The velocity in the congested phase is about 0.7 cells per timestep independent of the density and therefore much smaller than the free-flow velocity, in qualitative agreement with the experimental results.

The trajectories at a later stage of the simulation are shown in Figure 4.14. The simulation with $\rho = 0.55$ has developed into an almost homogeneous state whereas the simulation at $\rho = 0.85$ still exhibits phase separation after 2000 timesteps. To

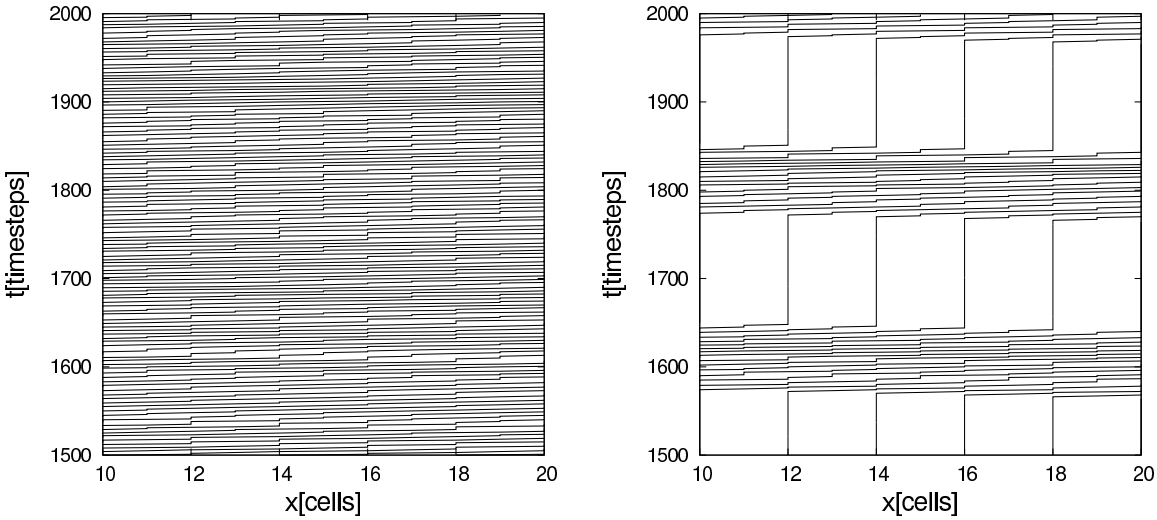

Figure 4.14: Simulated trajectories with inhomogeneous initial conditions and density 0.55 (left) and 0.85 (right) at a later stage of the simulation. For the sake of clarity, only every second agent is drawn.

investigate whether the initial jam is stable or decays at high densities, the jam length as a function of time is analyzed. A jam is defined as a collection of multiple successive cells occupied by non-moving agents, the length of the largest jam in the system is called jam length. For inhomogeneous initial conditions the largest jam typically is the initial jam, at least until the initial jam has decayed such that another randomly emerging jam is larger.

Figure 4.15 shows the jam length during a typical simulation run as a function of the elapsed time for three different densities. For high relative densities such as $\rho = 0.85$ the jam length does not change much over the course of the simulation. Even

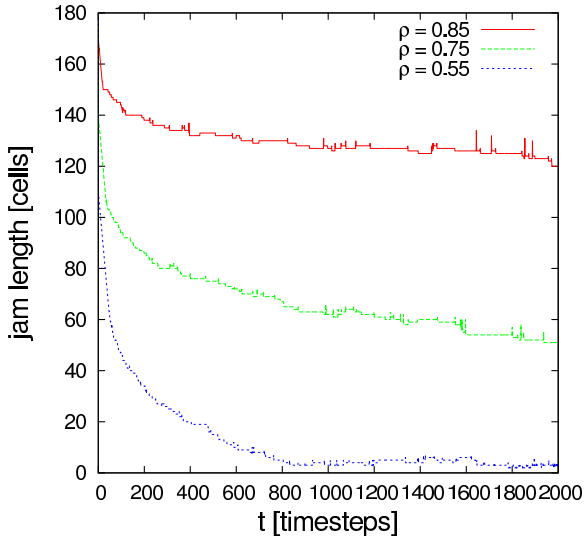

Figure 4.15: Jam length for simulations with inhomogeneous initial conditions as a function of elapsed time.

though the jam length is decreasing, its lifetime is much longer then the duration of the experiment[5] in which phase separation has been observed. At lower densities the decay happens more quickly. The initial jam has decayed completely after about 800 timesteps for $\rho = 0.55$.

Simulations starting with homogeneously or randomly distributed agents typically do not feature a phase-separated state. In simulations with random initial conditions,

[5]With the length of one timestep equal to 0.35 s, the experimental time frame of 140 s corresponds to 400 timesteps.

larger jams decay similar to the initial jam in the case of an inhomogeneous initial condition. Independent of the starting configuration, the system develops into an almost homogeneous high-density state with slowly moving agents and very small jams that dynamically appear and disappear. Several small jams can be in the system at the same time.

Simulations with the simple CA model discussed in this section feature phase separation if the inhomogeneous initial condition is used. However, the initial jam decays and the system develops into an almost homogeneous state. Similar to the results of the adaptive velocity model, the observed phase separation is purely a result of the (unrealistic) inhomogeneous initial condition.

4.6 Distance Based Velocity Model

4.6.1 Model definition

The up to now unpublished Distance Based Velocity Model (DBVM) is a rule-based model continuous in time and space. It is defined on a one-dimensional geometry with periodic boundary conditions, the length of the ring is $L = 26$ m, similar to the experimental setup. The agents are assumed to be point-like. The model does, however, ensure a minimum distance between agents that can be interpreted as the size of a pedestrian. The model includes a slow-to-start rule as well a mechanism for anticipation similar to the politeness factor discussed for the FFCA in Section 2.6 which leads to a slowdown of agents moving into a high-density area.

The velocity of an agent in the DBVM can assume one of three distinct values. It is either 0, $v_{\max}$, or it takes the intermediate value $v_{\text{slow}} = \frac{v_{\max}}{10}$. The reason for this is that the experimentally observed velocity in the moving phase is about 10 % of the maximum velocity, as seen in the velocity distribution discussed in Section 1.2.1. The DBVM does not have to dynamically generate this specific velocity because there is

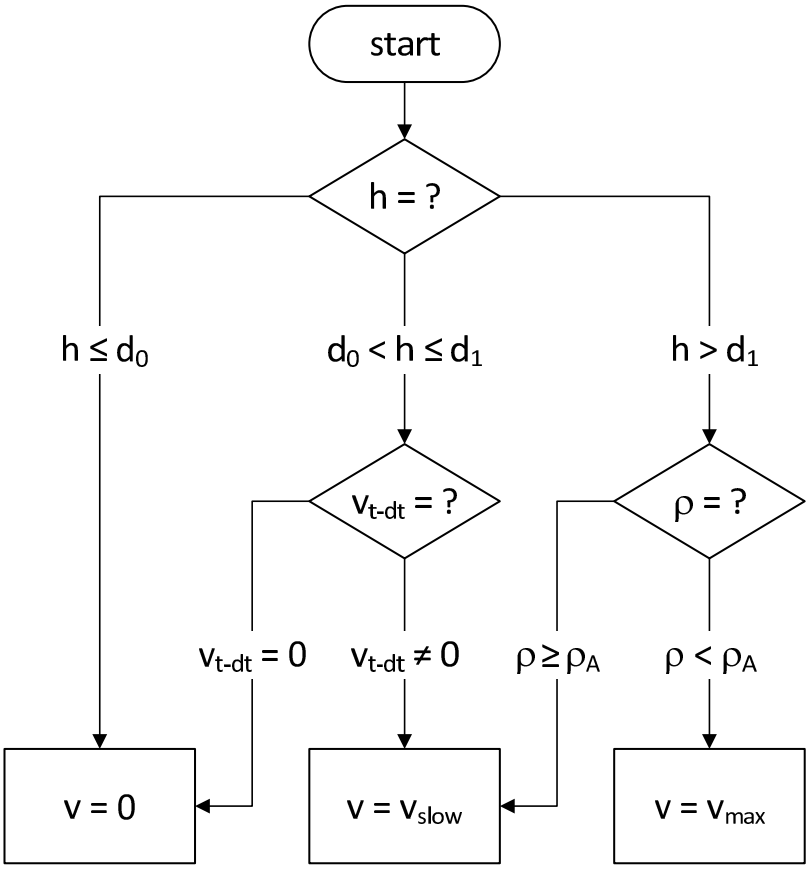

Figure 4.16: Schematic view of the algorithm calculating the new velocity of an updating agent. v_{t-dt} denotes $v_i(d - dt)$; the index i has generally been omitted for better readability.

only one possible velocity between 0 and $v_{\max}$. This makes the simulation results simpler and thus easier to understand. It also allows an event-based [94] implementation of the model. A change of the velocity of any agent is called an event. After the initialization of the simulation, the time of the first event is explicitly calculated. The simulation runs up to that point, changes the velocity of the appropriate agent and then calculates the time of the next event. This can be iterated indefinitely. Because there are only three distinct velocity values, the movement of all agents is uniform between the velocity updates. The event-based nature of the model also ensures that it can be implemented without any approximations in contrast to typical force-based models that require the numerical integration of differential equations.

The anticipation is implemented by defining the anticipation length d_A and anticipation density ρ_A. The density within the distance d_A in front of an agent i is denoted ρ_i. If ρ_i is larger than ρ_A, the velocity of agent i is reduced. The slow-to-start rule is implemented as a kind of hysteresis in the following sense. An agent starts moving as soon as its headway is larger than d_1. A moving agent, however, stops moving when its headway is smaller than $d_0 < d_1$. The velocity of an agent with headway $d_0 < h_i < d_1$ thus depends on the history of the simulation or, equivalently, on its velocity $v_i(t - dt)$ an arbitrarily short time dt ago. The exact definition of the velocity update is given in Equation (4.3) and Figure 4.16.

The velocity v_i of an agent i depends on its headway h_i, the density ρ_i in front of the agent and its velocity $v_i(t - dt)$ just before the update:

$$v_i = \begin{cases} 0 \ \frac{\mathrm{m}}{\mathrm{s}} & , \quad h_i \leq d_0 \quad \text{or} \quad \left(h_i \leq d_1 \text{ and } v_i(t-dt) = 0 \ \frac{\mathrm{m}}{\mathrm{s}}\right) \\ v_{\max} & , \quad h_i > d_1 \text{ and } \rho_i < \rho_A \\ v_{\mathrm{slow}} & , \quad \text{else} \end{cases} \tag{4.3}$$

The model dynamics ensures a minimum distance equal to d_0 between agents. The parameter values used for simulations in this section are $d_0 = 0.35$ m, $d_1 = 0.5$ m, $v_{\max} = 1 \ \frac{\mathrm{m}}{\mathrm{s}}$, $v_{\mathrm{slow}} = \frac{v_{\max}}{10}$, $d_A = 8$ m, and $\rho_A = 1.5 \ m^{-1}$. They are chosen such that d_0 and d_1 have values similar to the cell size in cellular automaton models. $v_{\max}$ is of the same order of magnitude as the empirical free velocity. As discussed above, v_{slow} is enforced to be 10 % of the free velocity in a rough analogy to the experimental velocity distribution. The values of d_A and ρ_A are chosen such that the resulting trajectories resemble the experimental data as much as possible[6].

[6]The experimental and model trajectories are compared by eye; no formal criterion is employed.

4.6.2 Results

All simulations in this section use the almost homogeneous initial condition discussed in Section 1.3.2.4 and are performed with $N = 60$ agents which corresponds to the global density $\rho = 2.3\ m^{-1}$. An extract of the resulting trajectories at the beginning of the simulation and at a much later time are compared with the experimental data in Fig 4.17. Both experimental and model trajectories show a separation into a completely jammed and a slowly-moving phase. The velocity of agents in the latter is – by design – in both cases approximately 10 % of the maximum velocity. The observed phase separation in the DBVM is preserved for at least $10,000$s. A formal analysis of the stability is planned in future work.

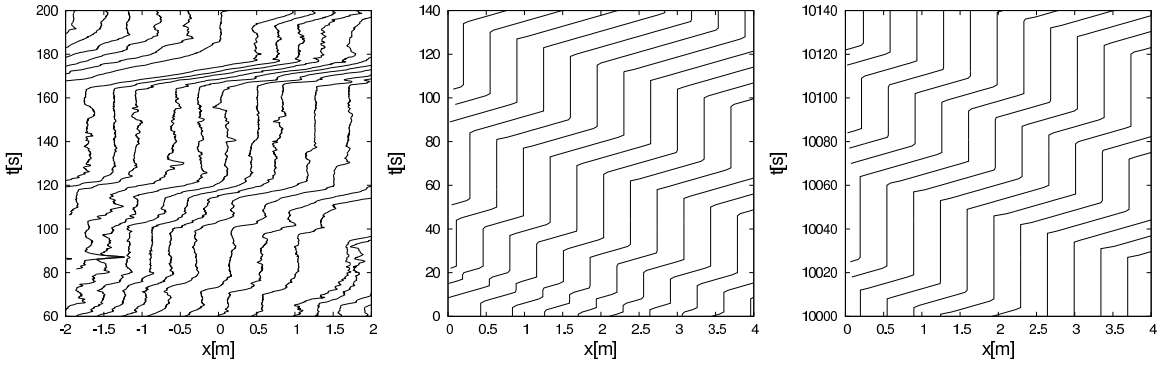

Figure 4.17: Experimental trajectories (left) and trajectories of the DBVM at different stages of the simulation, zoomed in to an area equivalent to the experimental measurement section.

Figure 4.18 shows the global trajectories at the beginning of the simulation and $10,000$s later, confirming the observed stability of the separation into two distinct phases. There are multiple jams in the system at any time. The experimental data discussed in Section 1.2.1 is consistent with both a single large jam in the system and a system containing multiple smaller jams. However, the newest data discussed in Section 1.2.2 suggests that there is only one large jam in the experimental system.

The DBVM can therefore not adequately describe the experimental data. Nevertheless, it is the first model that develops a phase separation into standing and slowly-

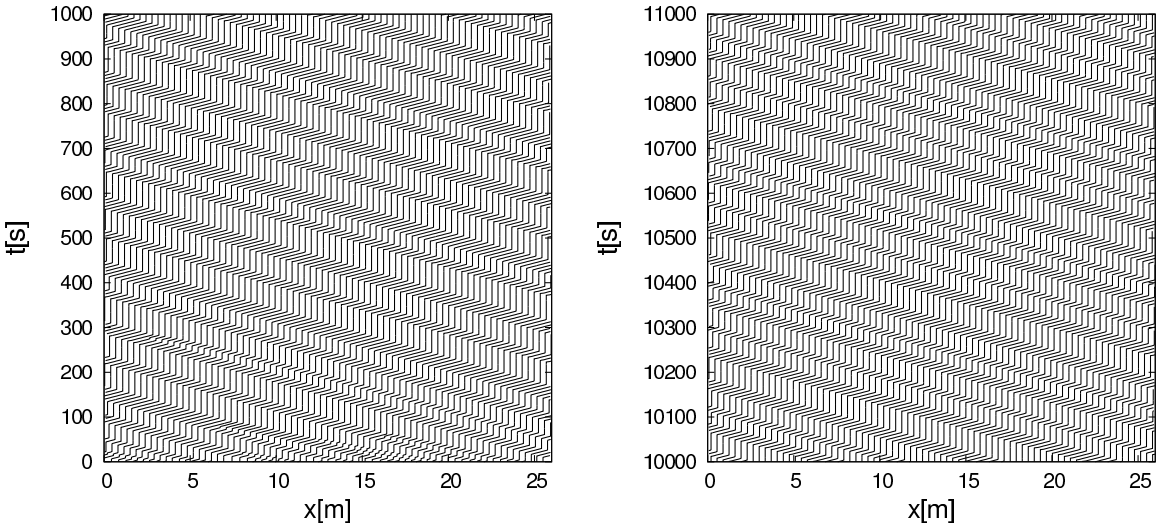

Figure 4.18: Global trajectories of the DBVM at different stages of the simulation.

moving agents without using inhomogeneous initial conditions. A further study of the DBVM can be an interesting topic for future research. The focus of this work, however, is to find a model capable of fully reproducing the characteristics of the experimentally observed phase separation.

CHAPTER V

Stochastic Headway Dependent Velocity Model

5.1 Model definition

The Stochastic Headway Dependent Velocity (SHDV) Model briefly introduced in [95, 96] is a space-continuous model with discrete time in one dimension. It therefore incorporates aspects of both continuous models such as the Generalized Centrifugal Force Model [30] or the Optimal Velocity Model [97, 98] and discrete models, e.g. cellular automata such as [99] or the Floor Field model [1]. Other models with discrete time and continuous space are discussed in [100] and [101]. The SHDV model also includes a variant of a slow-to-start rule used in vehicular traffic models [88, 102, 103].

Time is divided into discrete timesteps which can be identified with the reaction time of a pedestrian. This is equivalent to the time-discreteness in cellular automata models. The length of a timestep is $\Delta t = 0.3$ s. Each pedestrian is represented by an agent and moves through a continuous but finite one-dimensional space. Periodic boundary conditions are used which correspond to the circular course in the experiment discussed in Section 1.2.1. Unless stated otherwise, all simulations in this chapter are performed with a system length of 26 m, equal to the length of the experimental setup.

The initial configuration for the simulations is similar to the one in the experiments and resembles an 'almost homogeneous' state. This is achieved via a two-step process.

The agents are first distributed homogeneously, then each agent's position is shifted slightly according to a Gauss distributed random variable. The Gauss distribution is cut off to prevent overlapping of agents.

For modeling purposes, the agents are assumed to be point-like. However, the model ensures a minimum distance $d_{\min}$ between agents that can be interpreted as the size of an agent, it is calculated in Equation (5.4). In each timestep the velocity is calculated as a function of the headway. Here a piecewise linear form of the velocity function $v(h)$ is chosen, a graphical representation is given in Figure 5.1. The velocity function is characterized by five parameters $v_{\max}$, $v_{\min}$, d, d_c, and α. Four of these are independent, e.g. d_c can be expressed in terms of the other parameters as

$$d_c = d + \frac{1}{\alpha}(v_{\max} - v_{\min})\,. \tag{5.1}$$

Each agent has a maximum velocity $v_{\max}$ and minimum velocity $v_{\min}$. An agent i is allowed to move if its headway h_i exceeds a lower threshold $d = 0.4$ m. Note that this distance includes the space occupied by the pedestrian itself. The minimum distance $d_{\min}$ between agents is slightly smaller than d. Agents that have headways larger than the interaction range d_c move interaction-free with maximum velocity. The final parameter that characterizes the velocity function is its slope α. Additionally a slow-to-start rule is applied. With the probability of $p_0 = 0.5$, the velocity of an agent that did not move in the last timestep remains zero.

The following algorithm describes the update of the SHDV model. In each timestep, a parallel update of all agents is performed by executing the following steps:

1. First the headway h_i of each agent i is calculated.

2. The velocity v_i of each agent i is calculated according to the velocity function

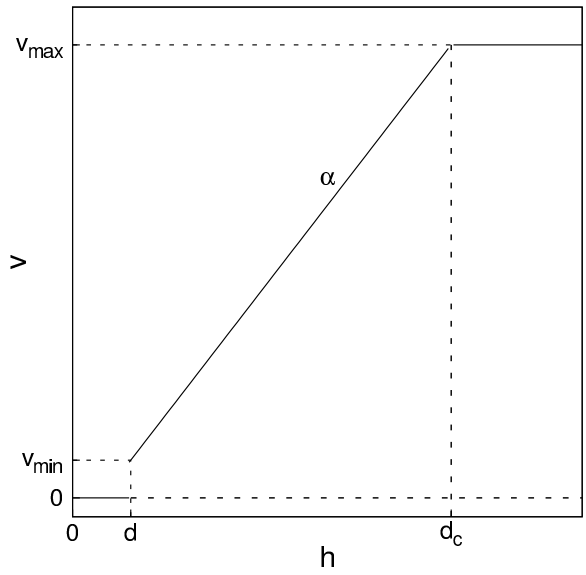

Figure 5.1: Relation between headway and velocity used in the simulations.

$v(h_i)$ depicted in Figure 5.1:

$$v_i = v(h_i), \qquad v(h) = \begin{cases} 0 \ \frac{\mathrm{m}}{\mathrm{s}} & , \quad h \leq d \\ \alpha(h-d) + v_{\min} & , \quad d < h < d_c \\ v_{\max} & , \quad h \geq d_c \end{cases} \tag{5.2}$$

3. If the agent did not move in the last timestep, its velocity remains zero with the stopping probability p_0 and with probability $1 - p_0$ it takes the value given by Equation (5.2).

4. Each agent moves with velocity v_i determined in the previous step and its position changes by $\Delta x = v_i \cdot \Delta t$.

5. Time is advanced by Δt: $t \to t + \Delta t$.

The simulations in this chapter are performed with parameter values $d = 0.4$ m, $v_{\max} = 1.2 \ \frac{\mathrm{m}}{\mathrm{s}}$, $v_{\min} = 0.1 \ \frac{\mathrm{m}}{\mathrm{s}}$, $\alpha = \frac{1}{2} \ s^{-1}$, $p_0 = 0.5$, and $\Delta t = 0.3$ s, resulting in $d_c = 2.6$ m. Thereby $v_{\max}$ takes a value similar to the empirical free velocity and $v_{\min}$ is slightly smaller than the first peak in the velocity distribution of the experimental

data discussed in Section 1.2.1. Both d and Δt are chosen in analogy to the FFCA. The value of the stopping probability p_0 is chosen to be a medium-sized value, its influence is analyzed in detail in Section 5.7.1. The slope $\alpha = \frac{1}{2}\ s^{-1}$ of the velocity function results in a linear approximation[1] of the typical optimal velocity function

$$V(\Delta x) = \tanh(\Delta x - 2) + \tanh(2) \tag{5.3}$$

of the Optimal Velocity Model [98].

Due to the discrete timestep, the actual minimum distance between agents can be smaller than the lower threshold d. Consider an agent i with a headway $h_i = d + \epsilon$ slightly larger than d following an agent $i + 1$ that has a headway smaller than d. In the next timestep agent $i + 1$ does not move whereas agent i moves with velocity $v_i = v(h_i)$. This results in a new headway that is smaller than d. In the limit $h_i \to d$ this is the minimum possible distance in the SHDV model and given by

$$d_{\min} \geq d + \epsilon - v(d + \epsilon) \cdot \Delta t \to d - v_{\min} \cdot \Delta t = 0.37\ \mathrm{m}\,. \tag{5.4}$$

The SHDV model can, in contrast to typical continuous models, be implemented exactly as stated here without the need for approximations such as the discretization of time. This prevents the emergence of artifacts which depend on the implementation such as the details of the time discretization.

5.2 Initial condition

Several possible starting configurations have been discussed in Section 1.3.2. A look at the SHDV model definition shows that in the homogeneous state, all agents

[1] Note that at small and at large velocities the velocity function of the SHDV model differs from the velocity function of the Optimal Velocity Model beyond that; for instance, it implies a minimum velocity.

have the same velocity and there is no source of a perturbation which could cause an agent's velocity to change. The system stays in the homogeneous state that can be explicitly specified. For a simulation with density ρ, the velocity $v_i(\rho, t)$ and position $x_i(\rho, t)$ of the i-th agent at time t are given by

$$v_i(\rho,t) = \begin{cases} 0 \quad , & \rho \geq \frac{1}{d} \\ \alpha(\frac{1}{\rho} - d) + v_{\min} \quad , & \frac{1}{d_c} < \frac{1}{\rho} < \frac{1}{d} \\ v_{\max} \quad , & \rho \leq \frac{1}{d_c} \end{cases} \tag{5.5}$$

and

$$x_i(\rho,t) = x_i^0(\rho,t) + v_i(\rho,t) \cdot t = i \cdot \frac{L}{\rho} + v_i(\rho,t) \cdot t\,. \tag{5.6}$$

This is confirmed in the corresponding simulation runs. The homogeneous state can therefore be interpreted as a fixed point in the state space of the agents consisting of their position and velocity, see also Section 5.8.

With an inhomogeneous initial condition each agent has a headway equal to the minimum distance between agents as calculated in Equation (5.4) except for one agent which has a headway equal to the rest of the system size.

For the reasons given in Section 1.3.2.3, random initial conditions are not used for the SHDV model. Instead, the agents are distributed 'almost homogeneously', as shown in Section 1.3.2.4. The size of an agent or technically speaking the minimum distance $d_{\min}$ between two agents is given by Equation (5.4). Therefore, the distances between agents in the starting configuration cannot be smaller than the minimum distance between agents that can be achieved dynamically. This ensures that the interpretation of this minimum distance as the size of an agent is still valid.

5.3 Fundamental diagram

To obtain the fundamental diagram of the stationary state, the measurement starts after $100,000$ seconds and uses the data from the next 100 seconds (333 timesteps). The resulting fundamental diagram of the SHDV model does not depend on whether the system started in the 'almost homogeneous' state or in the inhomogeneous state. The simulations with inhomogeneous initial conditions, however, take a longer time to converge to the stationary state.

Figure 5.2 shows fundamental diagrams of the SHDV model as well as the fundamental diagram obtained from the experimental data discussed in Section 1.2.1. The global model fundamental diagrams in the top row are obtained by using the averaged velocity and the global density which corresponds to the number of agents in the simulation. For each number of pedestrians, 10 simulation runs are performed. The top row additionally contains the experimental fundamental diagram of the measurement section with density and velocity calculated according to Section 1.1.3.2[2]. The local fundamental diagrams shown in the bottom row on the other hand make use of the individual velocity and density as defined in Section 1.1.3.3.

In each row three different initial conditions of the simulation are shown, from left to right: homogeneous, inhomogeneous and 'almost homogeneous'. The experimental local fundamental diagrams contain a data point for each frame and agent, the local fundamental diagrams of the simulation consist of a data point for each agent and timestep. To improve the clarity of the diagram, only every fifth data point is printed. The global fundamental diagrams of the simulation consist of a data point for each run with a distinct global density. The experimental fundamental diagram has been discussed in Section 1.2.1.

Each model fundamental diagram features three distinct sections. At low densi-

[2]Note that the experimental data only covers the limited measurement area and does not allow the computation of a global FD. Even though the model and experimental data use different density concepts, this allows to approximately compare the form of the FD.

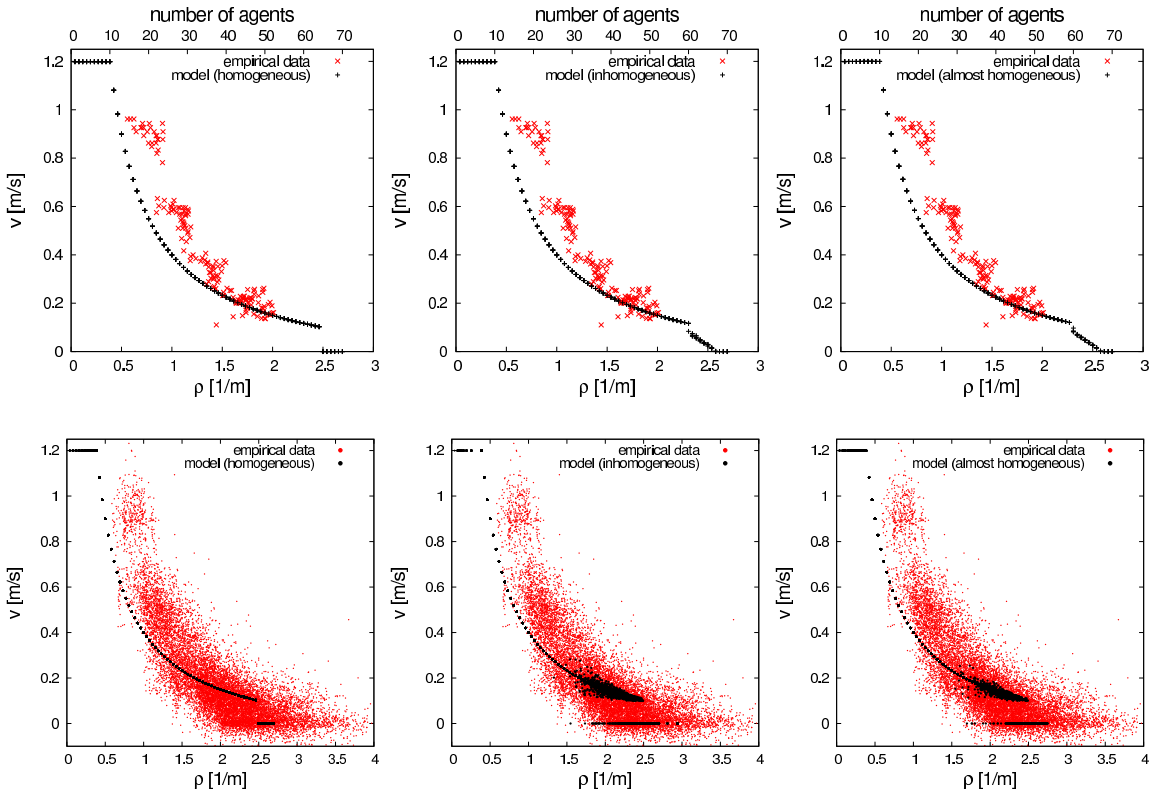

Figure 5.2: Fundamental diagrams of both model and experimental data for different initial conditions in the simulation.

ties up to about 0.5 pedestrians per meter, each agent moves interaction-free with a constant velocity equal to the maximum velocity. In this density regime the distances between agents are large and allow free-flow. The movement is completely deterministic because the stochasticity of the model only contributes to the dynamics when the density is high enough to force agents to stop. The data points of different runs (global FD) or different timesteps and agents (local FD) coincide.

At intermediate (global) densities up to about 2.3 pedestrians per meter, the global model fundamental diagram shows a $1/x$ curve. This can be directly explained by the model dynamics. The density is too big to allow free-flow of all agents, therefore interactions occur. In the stationary state the agents are spaced evenly within the simulation area and the density is equal to the reciprocal of the headway, $\rho = \frac{1}{h}$. The velocity of each agent is proportional to its headway h and therefore proportional

to $\frac{1}{\rho}$. The movement is also deterministic, there are no standing agents in this density regime and the data points of different runs or different timesteps and agents coincide.

At high densities and for non-homogeneous initial conditions there are two branches in the local fundamental diagram. Some agents have a velocity of $v = 0\ \frac{\mathrm{m}}{\mathrm{s}}$ and some agents are moving slowly. The global fundamental diagram on the other hand shows an approximately linear decline due to the averaging of standing and moving agents. At higher densities the fraction of moving agents as well as their velocity decrease. This can be seen in more detail in the velocity distribution in Section 5.4. The gap in the fundamental diagram at the start of the linear decline stems from a reduced average velocity caused by the beginning influence of the stopping probability. The size of this gap depends on the value of p_0, this will be discussed in detail in Section 5.7.1. Stochasticity plays a role for the model dynamics at high densities, leading to a cloud of data points in the local fundamental diagram and a non-unique relation between density and velocity in the global fundamental diagram that cannot be explained by finite-size effects, see Sections 5.7.2 and 5.7.4.

If the agents are homogeneously spaced at the start of the simulation, all distances between successive agents have the same size. Either they are all larger than d and every agent moves with a deterministic velocity or they are all smaller than d and no agent moves. The relation between density and velocity remains unique for all densities and the global and local fundamental diagrams are identical. There is no coexistence of moving and standing agents at any given density for homogeneous initial conditions.

The experimental fundamental diagrams do not show these clearly distinct sections. This is expected due to measurement errors and the resulting scatter of the data points on the one hand and due to the lack of data for very large densities on the other hand.

Simulations with homogeneous initial conditions remain completely homogeneous

and are therefore unrealistic. Inhomogeneous and almost homogeneous initial conditions result in identical fundamental diagrams. Simulations with almost homogeneous initial conditions converge faster to the stationary state and can be compared to the experiment even at early times.

Note that the model is not designed to perfectly reproduce the fundamental diagram but to recreate the observed phenomenon of phase separation in one-dimensional pedestrian flows at high densities. However, there is still a reasonable qualitative agreement between the experimental fundamental diagram and the fundamental diagram of the SHDV model.

5.4 Velocity distribution

In this section, the distribution of different velocities in several density intervals is analyzed for almost homogeneous initial conditions, see Figure 5.3. The velocity distribution uses the local density definition. The size of each velocity bin is 0.005 $\frac{\mathrm{m}}{\mathrm{s}}$. Note that the density bins are different for the experimental and model data. This is

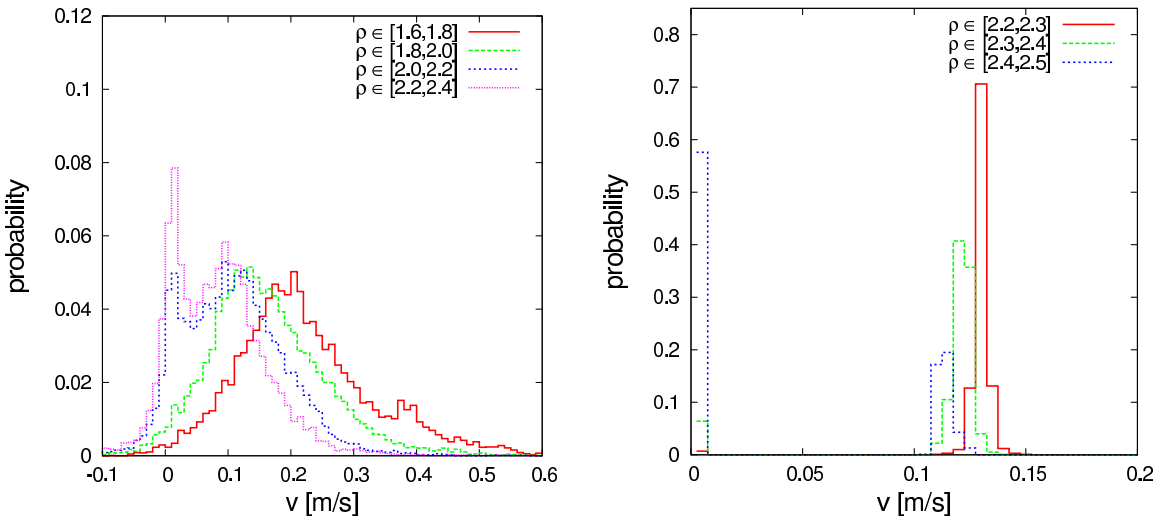

Figure 5.3: Velocity distribution for different density intervals. Experiment (left) and model (right).

necessary because the change from a state that is completely jammed (at a very high density) to a state in which all agents move (at a smaller density) happens in a smaller density interval in the model than in the experiment. The different sizes of the density bins lead to sharper and more pronounced peaks in the model data compared to the broader experimental data. The difference is amplified by the stochasticity related to real pedestrians and the measurement process. For technical reasons, the experiment did not track the center of mass, but the head of each pedestrian. Therefore additional head movement, called swaying, has been tracked as well, leading to a broadening of the measured velocity distribution. This explains the negative velocities in the experimental data. A variation of the stopping probability p_0 to larger values increases the density range in which phase separation happens and thereby results in a broader model velocity distribution than shown here. However, it also leads to more unrealistic pedestrian behavior.

The general structure of the velocity distribution is similar for both model and experimental data. It features two peaks at $v = 0\ \frac{\mathrm{m}}{\mathrm{s}}$ and at about $v = 0.1\ \frac{\mathrm{m}}{\mathrm{s}} - 0.15\ \frac{\mathrm{m}}{\mathrm{s}}$, respectively. The height of the first peak and thus the fraction of standing agents increases with increasing density. A higher local density means on average a smaller headway and thus a lower velocity. The position of the second peak therefore shifts to the left for higher densities.

5.5 Trajectories

A good agreement of fundamental diagram and velocity distribution with the empirical data does not ensure realistic dynamics on a microscopic scale. To achieve a deeper understanding of pedestrian behavior, individual trajectories are considered. The model fundamental diagram as well as the velocity distribution show a coexistence of moving and standing agents at high densities. Whether the moving and standing agents are separated in distinct phases or not, can be analyzed by looking

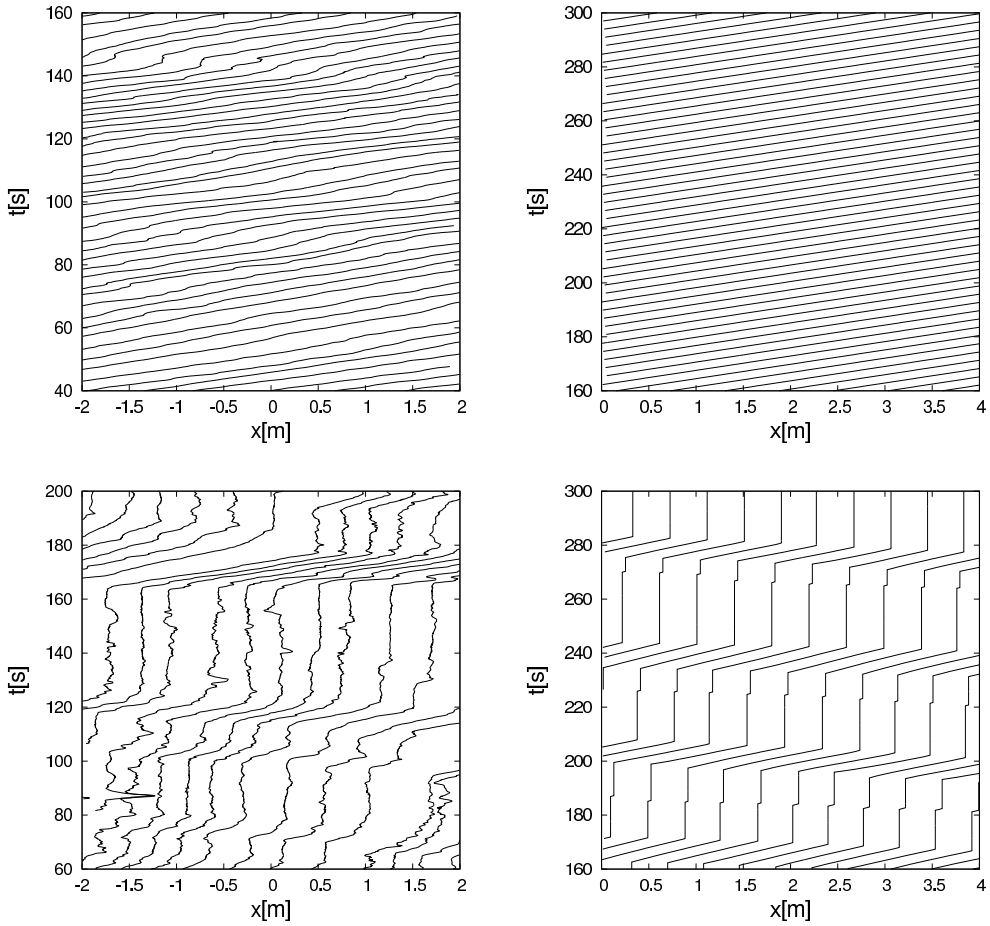

Figure 5.4: Experimental (top left) and model (top right) trajectories for $N = 45$, $\rho = 1.73$ m^{-1}. Experimental trajectories for $N = 70$, $\rho = 2.7$ m^{-1} (bottom left), and model trajectories for $N = 65$, $\rho = 2.5$ m^{-1} (bottom right).

at the trajectories. A state with a lot of small jams and congested areas in the system and a state with one big jam in the system may result in the same fundamental diagram and velocity distributions. Unless specifically stated otherwise, simulations are performed with almost homogeneous initial conditions.

A comparison of experimental and model trajectories is shown in Figure 5.4. The trajectories of the SHDV model are zoomed in to a 4 m long section analogous to the experimental data to allow an easier comparison. For small to intermediate densities both experimental and model trajectories feature relatively evenly spaced pedestrians that move with constant velocity. At high densities model and experimental trajec-

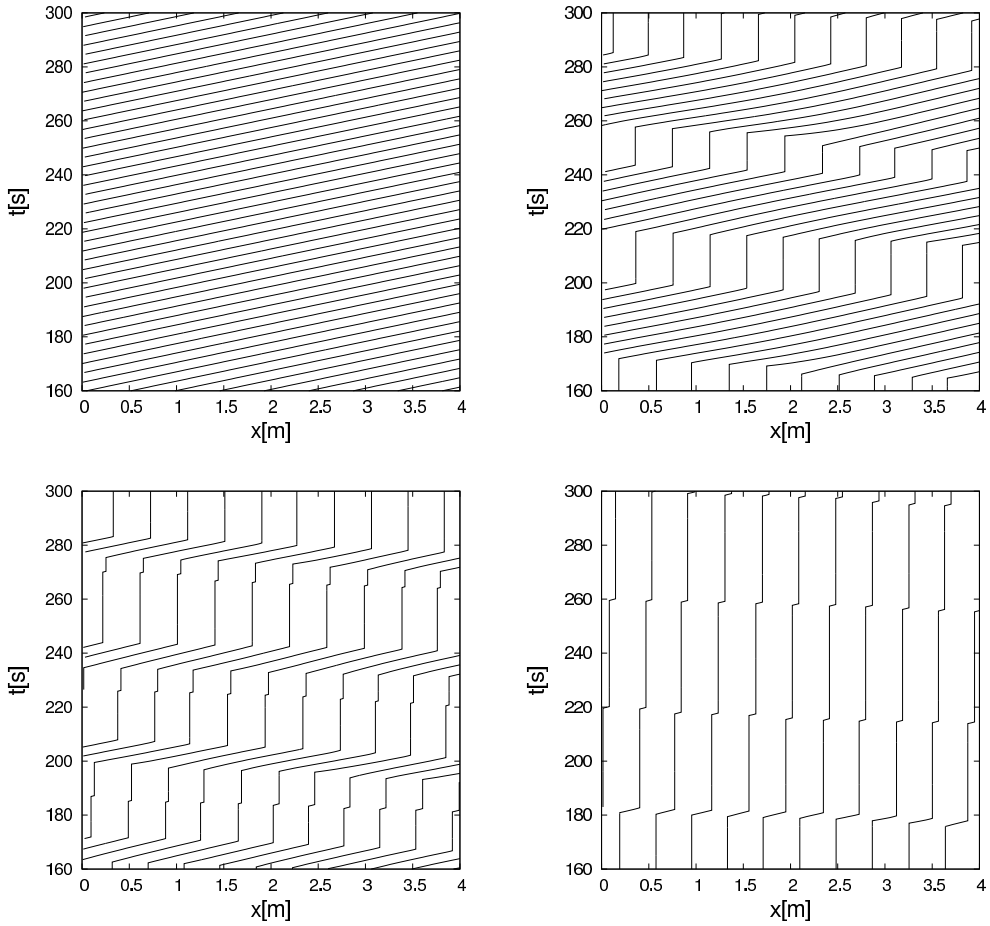

Figure 5.5: Model trajectories for $N = 55$, $\rho = 2.1$ m^{-1} (top left), $N = 60$, $\rho = 2.3$ m^{-1} (top right), $N = 65$, $\rho = 2.5$ m^{-1} (bottom left), and $N = 67$, $\rho = 2.6$ m^{-1} (bottom right).

tories are very similar as well. Both show a separation into two distinct phases, a standing phase and a phase with slowly moving pedestrians. Note the slightly different densities of model and experiment. The model trajectories are shown at a later time because it takes a short time for the phase separation to form, see Figure 5.6 and Appendix A.

Figure 5.5 shows the model trajectories at different global densities, zoomed in to an area equivalent to the measurement section of the experimental data. The details of the observed phase separation in the model depend on the density. Up to densities of about $\rho = 2.2$ m^{-1} the agents are spaced out homogeneously and move with constant velocity. For larger densities phase separation occurs. The size of

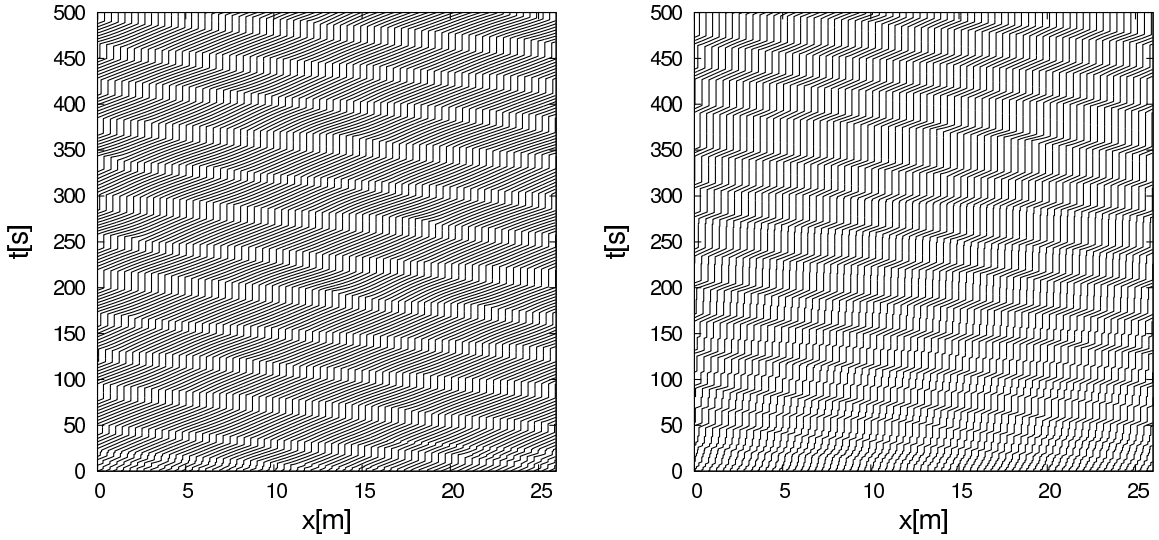

Figure 5.6: Global model trajectories for $N = 60$, $\rho = 2.3$ m^{-1} (left), and $N = 65$, $\rho = 2.5$ m^{-1} (right).

the standing phase increases with increasing density: Both the fraction of standing agents and the number of timesteps they remain standing increases. The velocity in the slow-moving phase slightly decreases with increasing density. At $\rho = 2.6$ m^{-1}, there is almost no moving phase; at even higher densities, the system comes to a complete standstill.

Whether there are multiple standing phases in the system or just one can be distinguished by analyzing the global trajectories, that is trajectories of the whole simulation area. Figure 5.6 shows global model trajectories for two different densities that both feature phase separation. In the first 50 to 100 seconds the system organizes into a phase-separated state. At each point in time after that, there is only one jammed phase and one moving phase in the system. As expected, the moving phase is smaller for the higher density. A larger version of the images in Figure 5.6 as well as the corresponding plot with $\rho = 2.6$ m^{-1} can be found in Appendix A. Both global trajectories and zoomed-in trajectories for $\rho = 2.5$ m^{-1} are given in Figure 5.7 for a much later time. The observed phase-separated state remains virtually unchanged after $100,000$s.

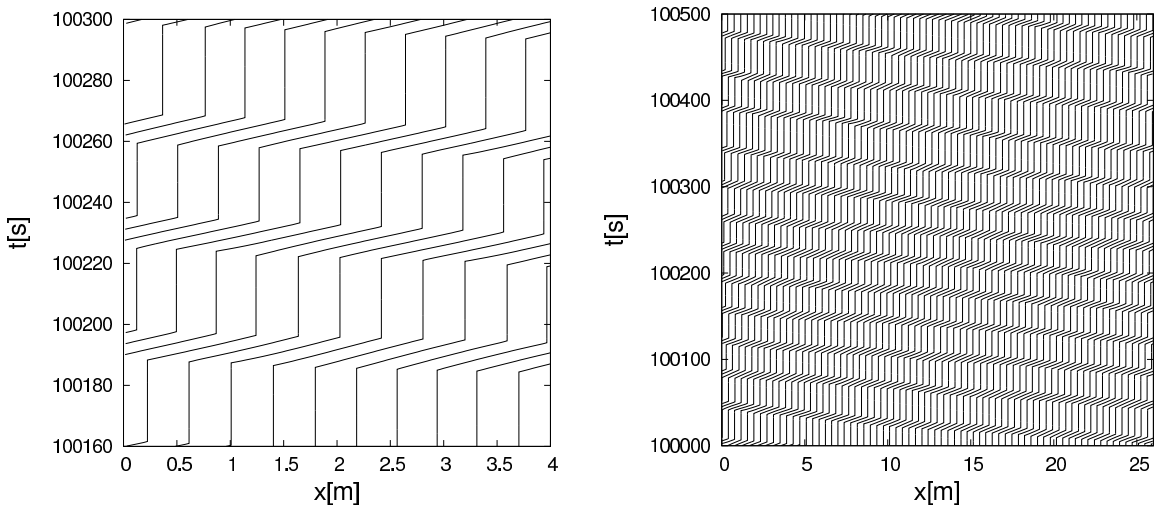

Figure 5.7: Zoomed-in (left) and global (right) trajectories for $N = 65$, $\rho = 2.5$ m^{-1}, after a long simulation time.

The trajectories of the SHDV model at high densities feature phase separation in a relatively small density interval. A more analytical approach to the determination of this density interval can be found in Section 5.8. The movement is homogeneous for smaller densities and the system comes to a complete standstill at larger densities. The separation in two distinct phases happens at a slightly lower density than in the experiment. The phase-separated state is stable, it does not decay in time.

5.6 Order parameter

5.6.1 Definition

As an alternative to explicitly analyzing the individual trajectories in the simulation and looking for phase separation that way, the order parameter δ is introduced. It is designed to describe the inhomogeneity of a given one-dimensional system. The definition of the order parameter is inspired by the order parameter from [104]. The order parameter used here is also used in [105] and [106].

The SHDV model is defined in a one-dimensional geometry with periodic boundary

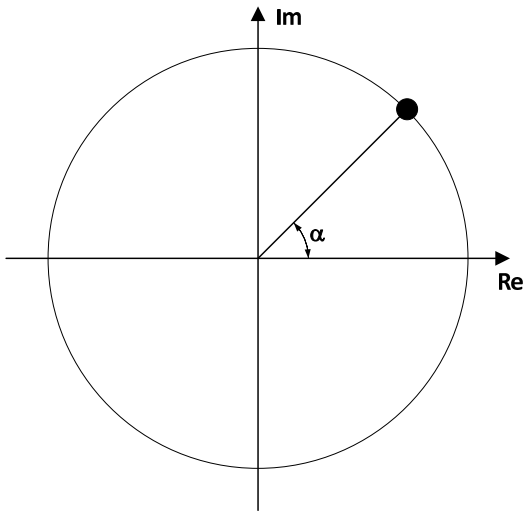

Figure 5.8: Each agent corresponds to a complex number.

conditions. The simulation area can therefore be interpreted as a circle. Each point on the circle corresponds to a specific point in the simulation area. An agent j is represented by a complex number with phase α_j that corresponds to its position, see Figure 5.8. The complex number can also be described by its position vector in the complex plane. The order parameter is defined as

$$\delta = \frac{1}{N_\delta} \cdot \left| \frac{\sum_{j=1}^{N} \exp(i \cdot \alpha_j)}{N} \right| \tag{5.7}$$

where N is the number of agents in the simulation, α_j is the phase corresponding to the position of agent j and N_δ is a normalization factor. The non-normalized order parameter is the average of the position vectors of all agents in the complex plane. When the agents are homogeneously spaced, the contributions from agents on opposite sides of the circle cancel each other out and the order parameter equals zero, see Figure 5.9 (left). This is also true for an odd number of agents. Consider e.g. three evenly spaced agents, the average position vector and thus the order parameter is zero. The order parameter is, however, also equal to zero when there are two jams of the same size on opposite sides of the circle, see Figure 5.9 (right).

Consider a distribution with eight agents and only one jam in the system, see

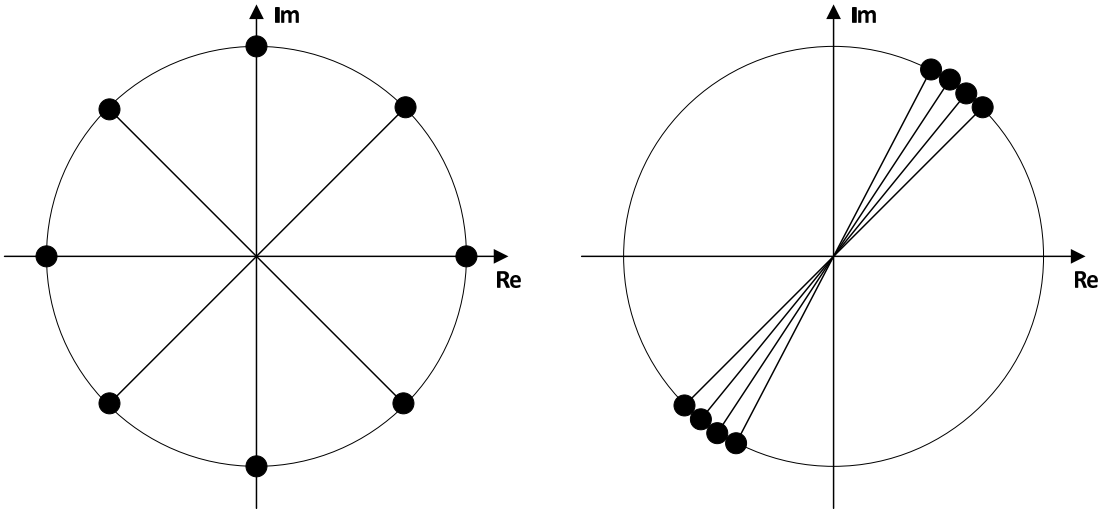

Figure 5.9: Homogeneous distribution of agents (left), two opposing jams (right).

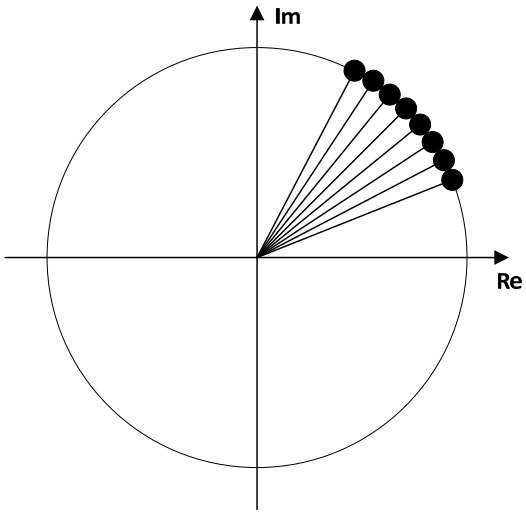

Figure 5.10: Inhomogeneous distribution of agents.

Figure 5.10. Assuming the distances between agents are minimal, which means that the agents cannot be placed closer to each other, the sum of the position vectors and thus the non-normalized order parameter is maximal. There is no distribution of agents that leads to a larger order parameter.

The normalization factor is defined to be equal to the maximum value of the non-normalized order parameter for a given density. This ensures that the normalized order parameter defined in Equation (5.7) is always equal to one for a completely inhomogeneous agent distribution. The maximum possible non-normalized order pa-

rameter depends on the density. As multiple agents cannot occupy the same spot, the average of their position vectors is bound to be smaller than one. The normalization of the order parameter allows meaningful comparisons between different densities. Figure 5.11 shows the normalization factor as a function of the density for the SHDV model, calculated from a system which is in a completely inhomogeneous state, that is in a 'megajam'.

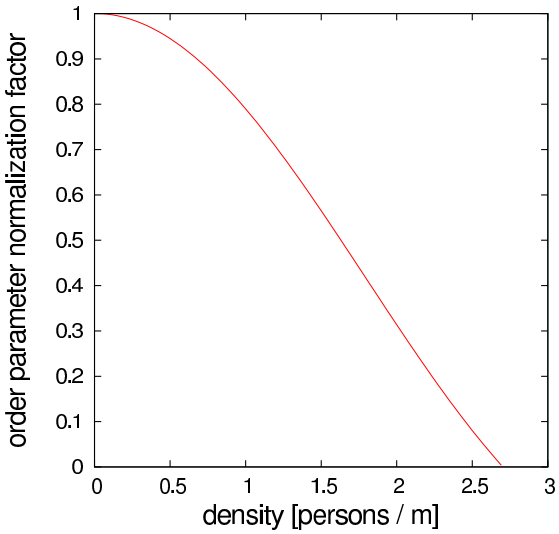

Figure 5.11: Normalization factor for the order parameter.

Note that the normalization factor for space-continuous models or experimental data depends on the minimal distance between agents. While the minimum distance between agents is clearly defined in the SHDV model, other models and of course experimental data might not have an obvious minimum distance. In that case one needs to assume some arbitrary value for the minimum distance in order to calculate the normalization factor of the order parameter. This potentially reduces the usefulness of the instrument for other models or experimental data. Additionally, data from the whole experimental area is needed. The experiment discussed in Section 1.2.1, however, only recorded data from a limited measurement section. The primary application for the order parameter at this time is therefore model data.

The order parameter can be used to distinguish between states with one large jam

in the system on the one hand and states with two or more distinct jams or a random mix of standing and moving agents on the other hand. The order parameter is large in the first case and much smaller in the second case, while the velocity distributions might look similar.

5.6.2 Results

Figure 5.12 shows the normalized order parameter of the SHDV model as a function of the global density for five simulation runs. For $N = 1$, the order parameter is always one. The order parameter at low densities up to about 0.4 pedestrians per

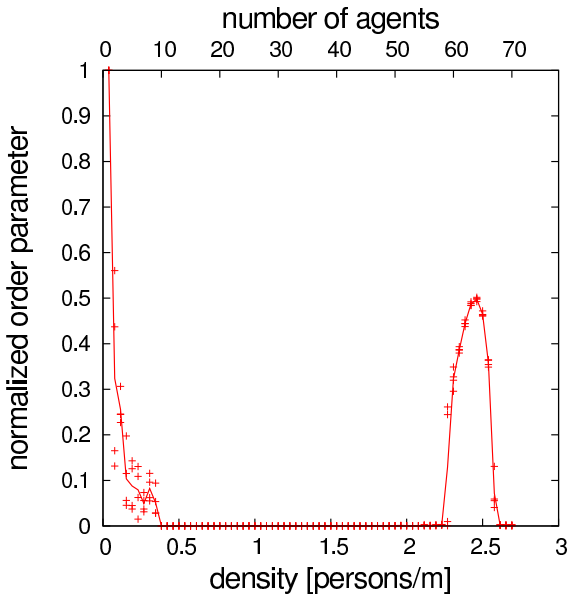

Figure 5.12: Normalized order parameter, averaged from $1000 - 2000$ s of the elapsed simulation time.

meter depends on the stochasticity of the initial condition because the interaction between agents is very limited. For e.g. $N = 2$, the agents might be created at opposite sides of the virtual circle or they might be created relatively close to each other. They can move independently in both cases, the order parameter being small in the first case and large in the second case.

At medium densities up to about 2.3 pedestrians per meter, both systems develop

into a homogeneous state with order parameter zero. There are enough agents in the system to enforce interaction and prevent movement with maximum velocity, but not so many that the phase separation observed earlier occurs.

For high densities between 2.3 and 2.6 pedestrians per meter, the order parameter becomes larger because the systems enters the phase-separated state. The coexistence of jam and slowly-moving phase with lower density leads to a medium-sized order parameter. If the system included only a single megajam and some free space, the order parameter would be of order one.

The order parameter is again of order zero at very high densities beyond 2.6 pedestrians per meter. This is because the density is too large to allow movement as can be seen in the fundamental diagram or in the trajectories. The system starts with an almost homogeneous initial condition and therefore stays in an almost homogeneous state with order parameter slightly larger than zero.

To determine the density region in which phase separation occurs without using the order parameter, one could in principle manually compare trajectories at different densities and check whether the system has developed phase separation or not.

5.7 Model modifications and parameter sensitivity

5.7.1 Stopping probability

In this section the stopping probability p_0 is varied in order to analyze its influence on the model dynamics. The starting configuration for every simulation is given by the almost homogeneous initial condition. Unless otherwise noted, the system is analyzed in the stationary state, that is after a relaxation time of $100,000$ seconds. The data are then averaged over 100 seconds which is equal to 333 timesteps.

Figure 5.13 shows the fundamental diagrams of both the experimental data analyzed in 1.2.1 and the SHDV model in the deterministic case with stopping probability

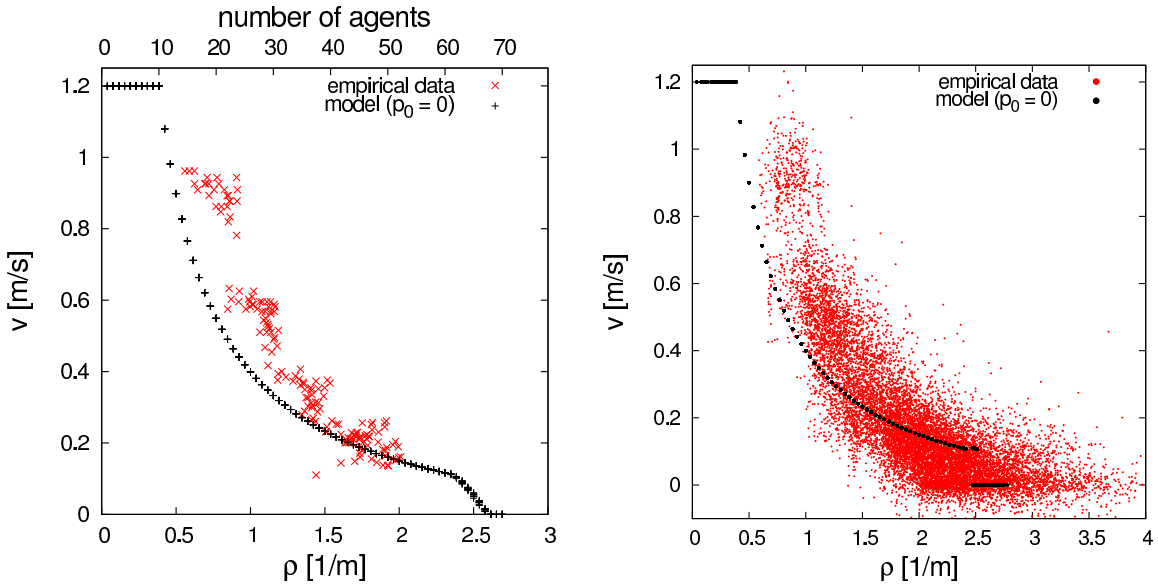

Figure 5.13: Experimental fundamental diagram and model fundamental diagram for stopping probability $p_0 = 0$.

$p_0 = 0$. Some velocity values in the local fundamental diagram at densities slightly below $\rho = 2.5$ m^{-1} are located above the $1/x$ curve. They can be understood as follows: There is no stochastic influence to the model dynamics for $p_0 = 0$. For densities up to about $\rho = 2.4$ m^{-1} the fundamental diagram corresponds to a $1/x$ curve because the interactions between agents lead to a homogeneous distribution of agents despite the almost homogeneous starting condition. At high densities the small initial inhomogeneities persist and lead to fluctuations in the density-velocity-relation. Some agents have a headway a little bit larger than $1/\rho$ and move faster. Other agents have a headway a little bit smaller than $1/\rho$ and move slower. Agents with a headway smaller than $1/\rho$ and also smaller than d stop moving. This is similar to what happens for larger values of p_0, albeit at smaller densities. At a given local density, there is a range of possible nonzero velocities that are cut off at the minimal velocity. For $p_0 = 0$ the cutoff is very close to the $1/x$ curve and there are only a few agents with a smaller but nonzero velocity. It is therefore far more likely that larger velocities occur in a simulation as opposed to smaller (nonzero) velocities. This leads

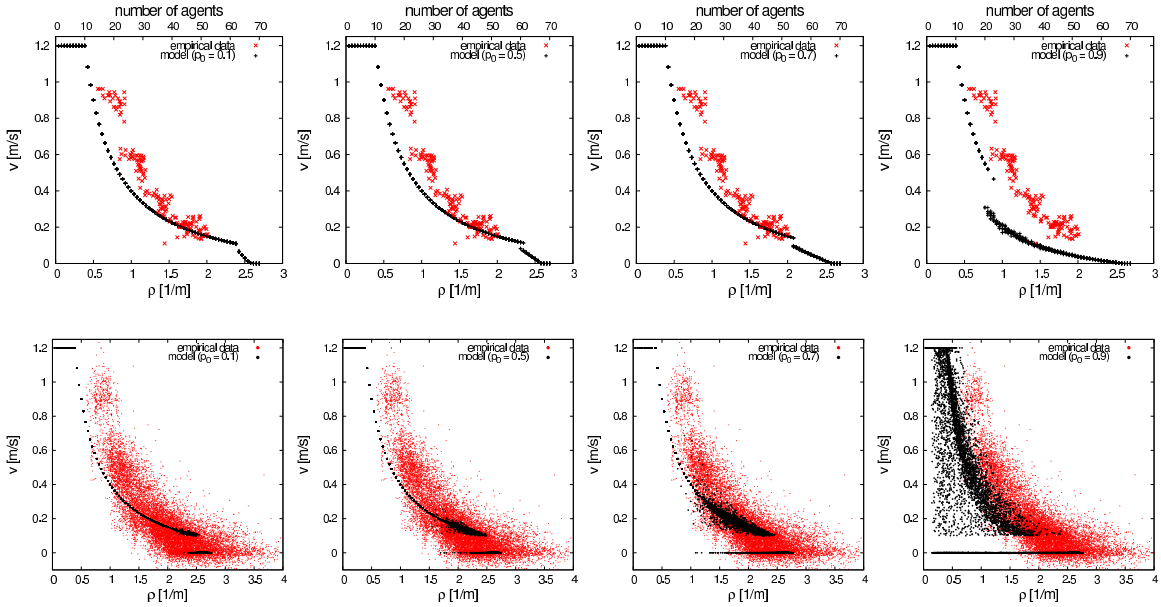

Figure 5.14: Experimental fundamental diagram and model fundamental diagram for different stopping probabilities p_0.

to the data points with velocities above the $1/x$ curve. The exact position of the data points in the fundamental diagram depends on the partially random initial condition.

Figure 5.14 shows the equivalent fundamental diagrams for different nonzero stopping probabilities p_0. The resulting fundamental diagrams fit reasonably well to the experimental data for most values of p_0. The stopping probability p_0 only influences the fundamental diagram at relatively high densities. The position of the boundary between the $1/x$ - shaped part of the fundamental diagram and the high-density part influenced by the stopping probability p_0 shifts to smaller densities for larger values of p_0. The stopping probability p_0 leads to a decreased flow (and thus lower average velocity) at higher densities. The local fundamental diagram shows that the density interval in which there are standing agents in the simulation extends to lower densities for higher values of p_0. For $p_0 = 0.9$ there are standing agents even for very low densities. This does not match the experimental data, simulations with $p_0 = 0.9$ can therefore hardly be interpreted in terms of pedestrian dynamics.

The velocity distributions for different stopping probabilities p_0 can be seen in

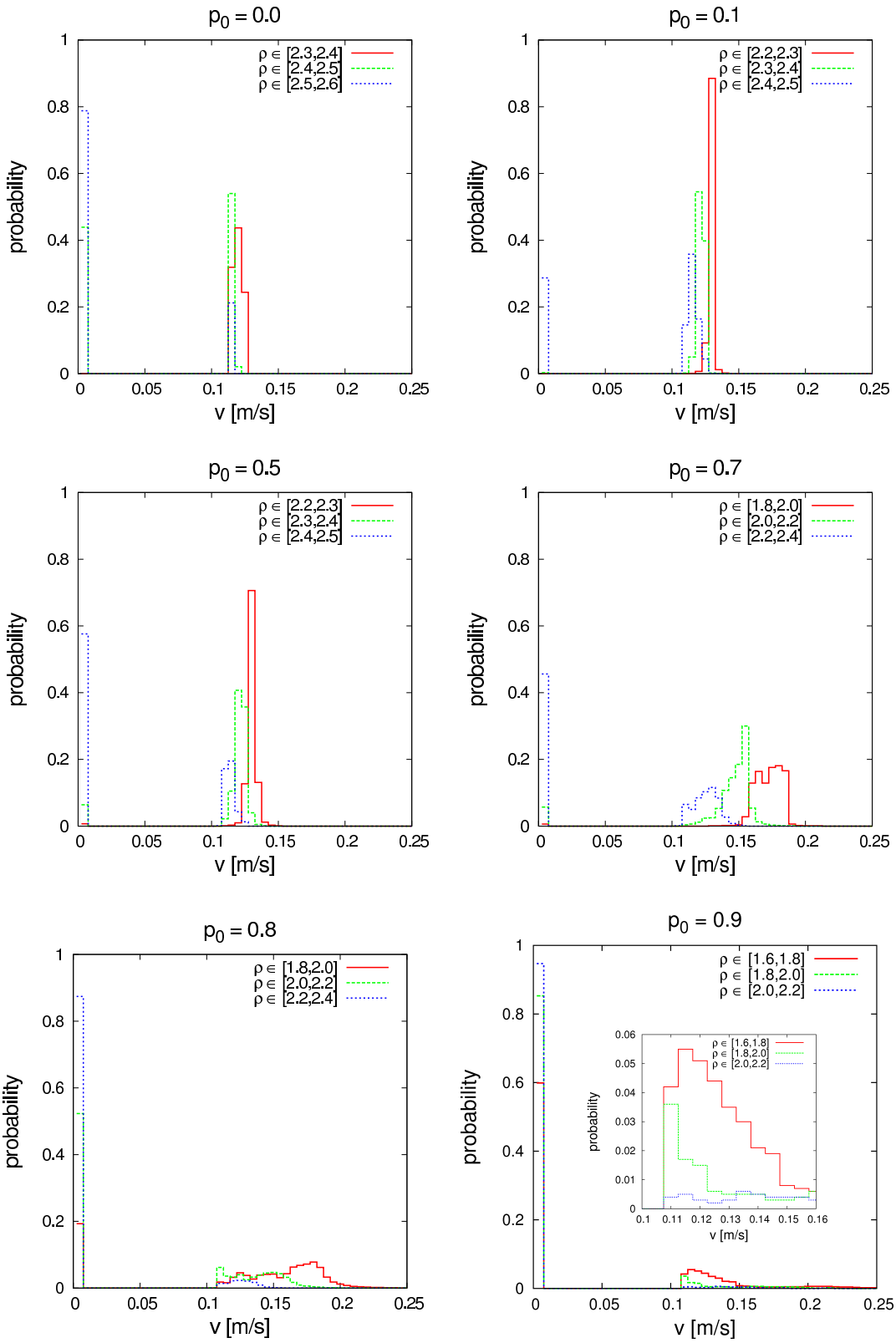

Figure 5.15: Model velocity distribution for different density intervals and different stopping probabilities p_0.

Figure 5.15. Note the different size of the density intervals. The size of each velocity bin is 0.005 $\frac{\mathrm{m}}{\mathrm{s}}$. The general structure of the velocity distribution is independent of p_0, there are two peaks at $v = 0\ \frac{\mathrm{m}}{\mathrm{s}}$ and at about $v = 0.1\ \frac{\mathrm{m}}{\mathrm{s}} - 0.15\ \frac{\mathrm{m}}{\mathrm{s}}$ even for simulations with $p_0 = 0$ and thus without a slow-to-start rule. The position of the second peak depends on the density. The peaks are smaller and higher than the experimental data, especially for a small p_0. The velocity distributions for larger p_0 are broader for two reasons. Firstly, the transition from a completely jammed state to a state without standing agents is stretched out over a larger density interval than for small p_0. Secondly, the density bins are larger. The velocity distribution for large p_0 is, however, also smaller than the experimental distribution. A possible explanation is the heterogeneity of real persons compared to identical agents in the simulation combined with the uncertainty of the velocity- and density measurements. Heterogeneous parameter values for simulation agents might lead to a broader velocity distribution.

Figure 5.16 shows the order parameter for different values of p_0. The stopping probability has a large influence on the order parameter. At small densities the order parameter depends on the partially random initial condition of the agents. The system develops into a homogeneous state with order parameter zero for intermediate densities. The size of this density region strongly depends on p_0. The maximum value of the order parameter and thus the extent of the inhomogeneity at high densities also scales with p_0. Simulations with $p_0 = 0$ result in an order parameter that is slightly above zero, the small inhomogeneity stems from the almost homogeneous initial conditions. Even though there are two branches in the fundamental diagram and the velocity distribution shows the double peak structure that indicates the coexistence of moving and standing agents in the simulation, the agents are spaced out almost homogeneously. The standing agents do not condensate into a single jam.

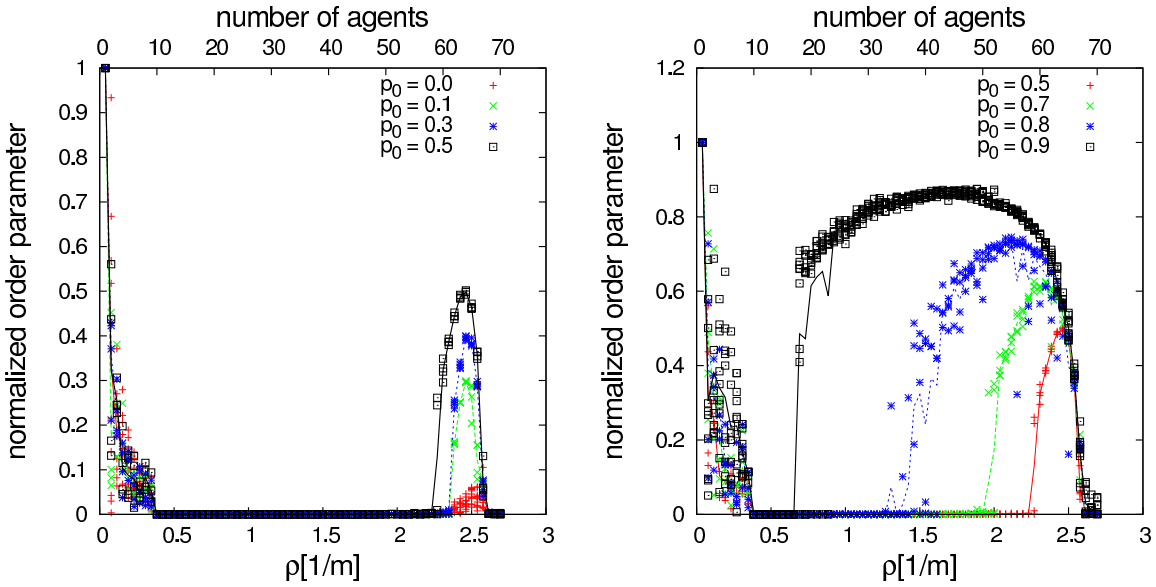

Figure 5.16: Model order parameter as a function of density for different stopping probabilities p_0.

5.7.2 Continuous time limit

In this section a model variant that allows scaling to arbitrarily small timesteps is formulated. It is then used to investigate whether time discreteness is a necessary feature for phase separation.

The stopping probability, that is the probability of a standing agent not to move in a timestep, should not be constant if smaller timescales are considered. Otherwise the probability for an agent to start moving within any given time t can be arbitrary large (close to 1) for sufficiently small timesteps. Therefore, the probability $p_{\text{acc}} = p_{\text{acc}}(\Delta t)$ of a standing agent with a sufficiently large headway to start moving (accelerate) during a single timestep Δt is considered as a function of the size of the timestep.

Let the probability of a standing agent to start moving during the interval $[0, t]$ be denoted $\mathbb{P}(t)$. The model has to meet the following two conditions:

1. $\mathbb{P}(t)$ should be independent of the size of the timestep Δt. This means that however small a timestep Δt is chosen, the probability that an agent does not

start moving during the interval $[0, t]$ stays constant. The alternative to consider smaller timesteps while leaving the stopping probability for each timestep unchanged results in a diverging stopping probability for any finite interval $[0, t]$.

2. $\mathbb{P}(\Delta t_0)$ for the standard-timestep $\Delta t_0 = 0.3$ s should be consistent with the previously used stopping probability p_0, $\mathbb{P}(\Delta t_0) = 1 - p_0$.

In the following, the form required of $p_{\text{acc}} = p_{\text{acc}}(\Delta t)$ to be compatible with these conditions is calculated. The probability of a standing agent not to start moving during a single timestep Δt is given by

$$(1 - p_{\text{acc}}(\Delta t)) \,. \tag{5.8}$$

For a time interval $[0, t]$, with $t = N \cdot \Delta t$ being a multiple of Δt, the probability of a standing agent to still not move afterward is thus given by

$$(1 - p_{\text{acc}}(\Delta t))^N \tag{5.9}$$

and the probability $\mathbb{P}(t)$ to have started to move is

$$\begin{aligned} \mathbb{P}(t) &= 1 - (1 - p_{\text{acc}}(\Delta t))^N \\ &= 1 - (1 - p_{\text{acc}}(\Delta t))^N \\ &= 1 - e^{N \ln(1 - p_{\text{acc}}(\Delta t))} \,. \end{aligned} \tag{5.10}$$

For this to be independent of Δt, the exponent of Equation (5.10) has to be independent of N. With the ansatz

$$p_{\text{acc}}(\Delta t) = 1 - e^{-\lambda \Delta t} \,, \tag{5.11}$$

the exponent of Equation (5.10) becomes

$$\begin{aligned} N \ln(1 - p_{\text{acc}}(\Delta t)) &= N \ln(1 - (1 - e^{-\lambda \Delta t})) \\ &= N \ln(e^{-\lambda \Delta t}) \\ &= N(-\lambda \Delta t) \\ &= -\lambda t \end{aligned} \tag{5.12}$$

which is independent of the timestep Δt. This means that with the ansatz from Equation (5.11), the probability $\mathbb{P}(t)$ of a standing agent to start moving during the interval $[0, t]$ does not depend on the size of the timestep and therefore the first condition is fulfilled.

The second condition requires

$$\begin{aligned} \mathbb{P}(\Delta t_0) &= 1 - e^{-\lambda \Delta t_0} \\ &= 1 - p_0 \,, \end{aligned} \tag{5.13}$$

or equivalently,

$$e^{-\lambda \Delta t_0} = p_0 \qquad \Leftrightarrow \qquad \lambda = -\frac{\ln(p_0)}{\Delta t_0} = -\frac{\ln(0.5)}{0.3\ s} \approx 2.3\ s^{-1} \,. \tag{5.14}$$

The resulting form of the acceleration probability p_{acc} using the ansatz from Equation (5.11) is

$$p_{\text{acc}}(\Delta t) = 1 - e^{\frac{\ln(p_0)}{\Delta t_0} \Delta t} \quad . \tag{5.15}$$

The acceleration probability has to be between zero and one, $0 < p_{\text{acc}}(\Delta t) < 1$. This limits the values Δt can assume to $\Delta t \in \,]0, \infty[$.

Using $p_{\text{acc}}(\Delta t)$ as given in Equation (5.15) ensures that the model is consistent with the two conditions formulated above and thus a reasonable extension to arbi-

trarily small timesteps. The stopping probability for a given timestep is equal to $1 - p_{\mathrm{acc}}(\Delta t)$, smaller timesteps therefore directly correspond to larger stopping probabilities. According to Equation (5.4), a smaller timestep also leads to a smaller minimum distance d_{min}. This relation is depicted in Figure 5.17.

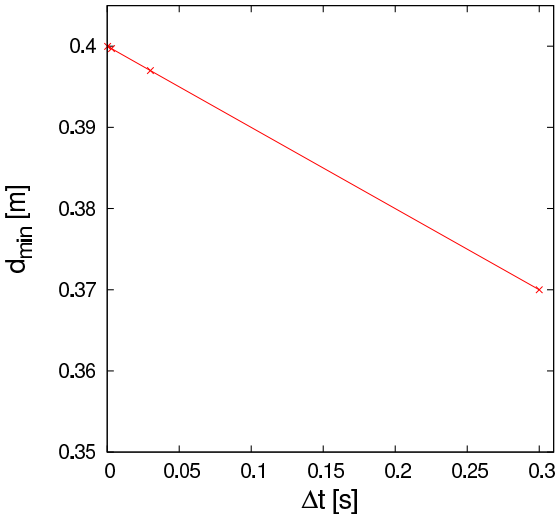

Figure 5.17: Minimum distance between agents as a function of the timestep.

The continuous time limit of the SHDV model is analyzed for two different update schemes: firstly for the parallel update that is part of the model definition, secondly for the random sequential update typically used to approximate continuous time dynamics [53].

5.7.2.1 Parallel update

Figure 5.18 shows the fundamental diagrams of the SHDV model with parallel update for different timesteps and corresponding stopping probabilities according to Equation (5.15).

It can be seen in Figure 5.17 that for $\Delta t = 0.03$ s or smaller timesteps, the minimum distance is close to the lower threshold $d = 0.4$ m. The average headway in the simulation cannot be smaller than the minimum distance between agents. This limits the maximum number of agents to $N = 65$ because an additional agent would

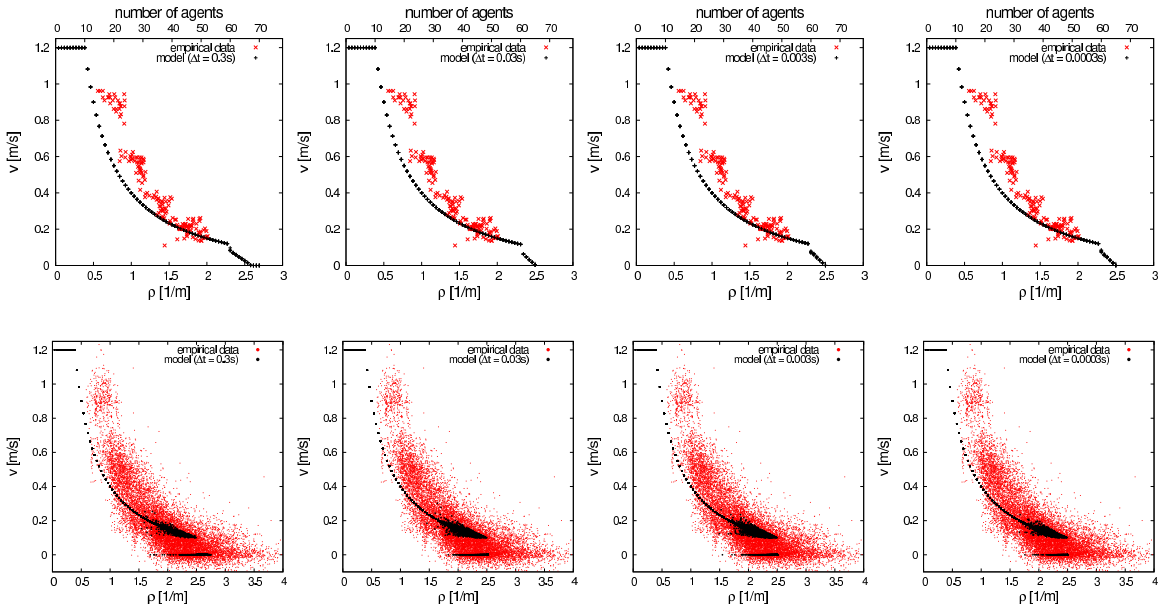

Figure 5.18: Parallel update: experimental and model fundamental diagrams for different timesteps and appropriate stopping probabilities.

decrease the average headway to $0.\overline{39}$ m which is slightly lower than the minimum distance $d_{\min} = 0.397$ m for $\Delta t = 0.03$ s. $N = 65$ corresponds to an average headway $h = 0.4$ m and global density $\rho = 2.5$ m^{-1}. This explains the lack of data points for density values beyond that at small timesteps as well as the different slope of the almost linear section in the global fundamental diagram. The almost homogeneous initial conditions cannot generate distances smaller than the minimum distance. For $\Delta t \leq 0.03$ s this means that the initial agent configuration can therefore not contain distances smaller than $d_{\min} = 0.397$ m. Consider the case $\rho = 2.5$ m^{-1} ($N = 65$) and $\Delta t = 0.3$ s, some headways might be equal to 0.375 m and others equal to 0.425 m, which allows some agents to move and leads to a nonzero velocity value in the global fundamental diagram at $\rho = 2.5$ m^{-1}. For $N = 65$ and $\Delta t = 0.03$ s, on the other hand, all agents have a headway that is almost equal to $d = 0.4$ m, resulting in an average velocity in the global fundamental diagram that is slightly above zero. The local fundamental diagrams are virtually identical except for the absence of data points at very high densities.

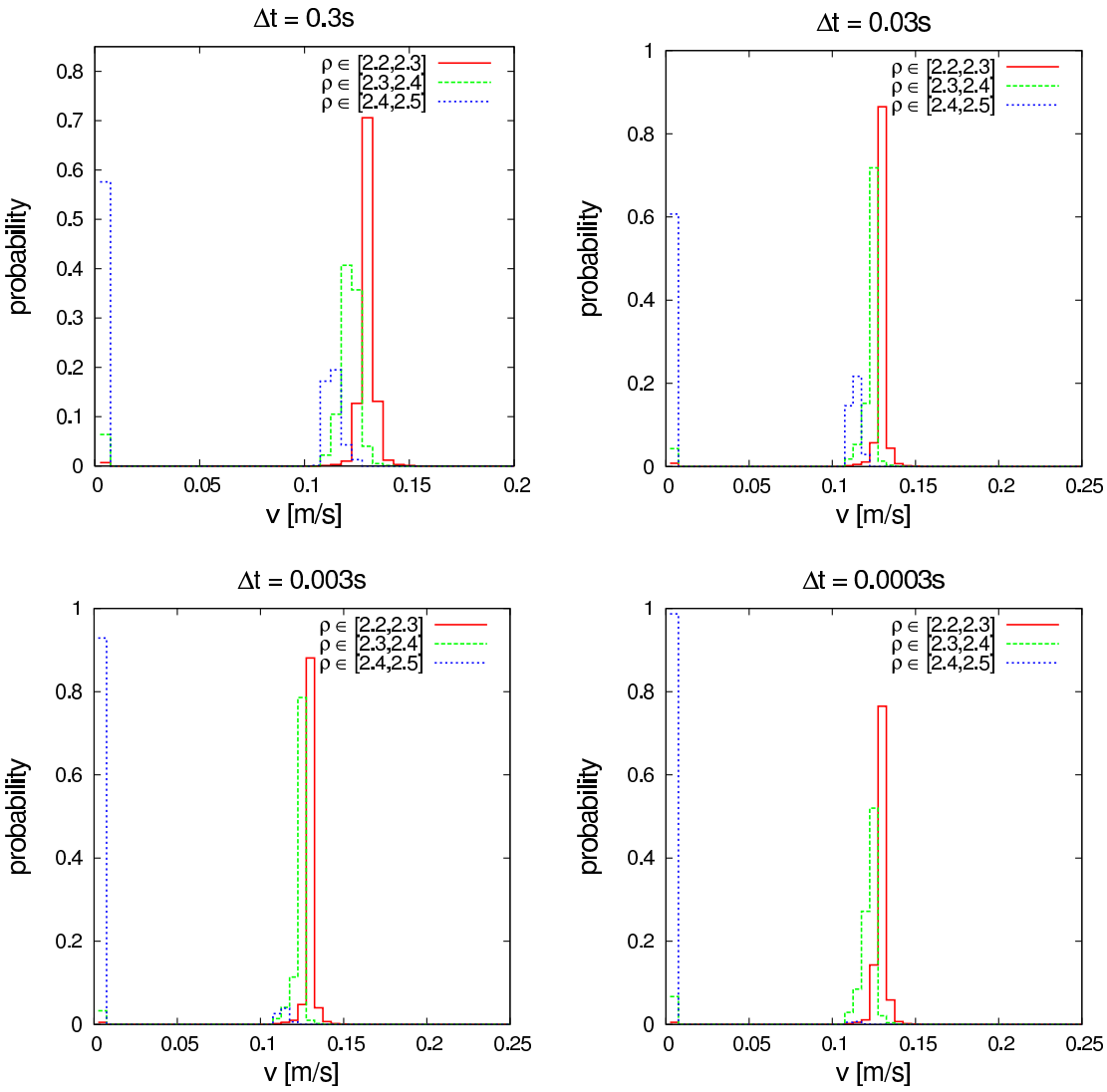

Figure 5.19: Parallel update: model velocity distributions for different timesteps and appropriate stopping probabilities.

The velocity distributions for different timesteps and corresponding stopping probabilities are depicted in Figure 5.19. There are only minor differences at different timesteps. The peak at $v \approx 0.11 \frac{\mathrm{m}}{\mathrm{s}}$ for the density interval $\rho \in [2.4, 2.5]$ disappears almost completely for smaller timesteps. The reason is the same as for the fundamental diagram. In this high density regime the average headway is only a little bit below $d = 0.4$ m. Moving agents must have a headway larger than d and consequently their distance to the next agent behind them is most likely smaller than d, ensuring that their local density is in the given density interval.

In simulations with $\Delta t = 0.3$ s, there is a larger difference between d and $d_{\min}$ and it is therefore more likely for agents to have a headway that allows them to move compared to smaller timesteps. This means that for $\Delta t = 0.3$ s and $d_{\min} = 0.37$ m, there may be agents with a local density of $\rho \in [2.4, 2.5]$ whose headway is larger than d and whose distance to the next agent behind them is correspondingly smaller than d, allowing them to move. For $\Delta t = 0.03$ s or smaller timesteps this is increasingly unlikely, which leads to the decrease of the corresponding peak in the velocity distribution.

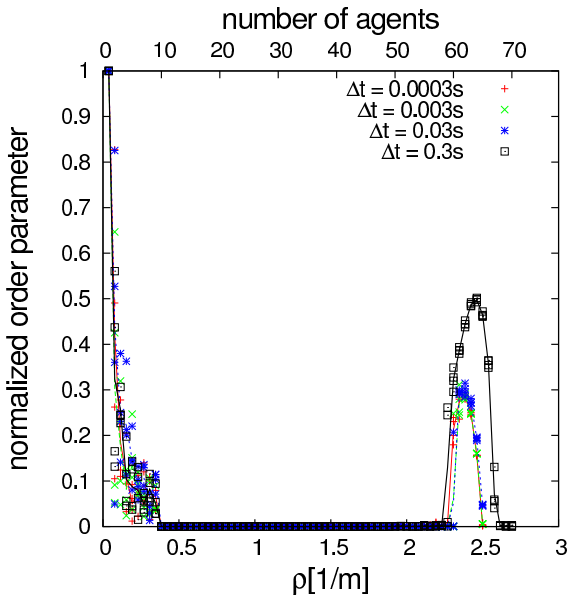

Figure 5.20: Parallel update: model order parameter as a function of density for different timesteps and respective stopping probabilities.

The order parameter is shown in Figure 5.20 for different timesteps and corresponding stopping probabilities. The inhomogeneity at high densities decreases a little bit for timesteps smaller than $\Delta t = 0.3$ s. The reason is the absence of agent headways that are notably smaller than d. For $0.0003 \text{ s} \leq \Delta t \leq 0.03$ s, the order parameter curves are almost indistinguishable.

Fundamental diagram, velocity distribution, and order parameter all slightly differ at densities $\rho \approx 2.5$ m^{-1} for $\Delta t = 0.3$ s, compared the analyzed smaller timesteps,

because the adjusted minimum distance $d_{\min}$ is almost equal to the lower threshold d. Whether the timestep is $\Delta t = 0.03$ s, $\Delta t = 0.003$ s, or $\Delta t = 0.0003$ s is, however, basically irrelevant. A reasonable extrapolation to even smaller timesteps suggests that pedestrian phase separation can be observed in the SHDV model with parallel update at arbitrarily small timesteps.

5.7.2.2 Random sequential update

To tackle the limit to continuous time from another point of view, a random sequential update procedure is considered instead of the parallel update. To be more specific, the standard timestep Δt is divided into N sub-timesteps of length $\frac{\Delta t}{N}$. In each sub-timestep a random agent is chosen and individually updated. It is possible, though unlikely, that the same agent is chosen twice in a row. The designated agent is updated by first calculating its headway h_i and subsequently its velocity v_i according to the velocity function defined in Equation (5.2). If appropriate, this velocity is modified according to the stopping probability p_0. Secondly, the agent moves with the resulting velocity v_i and its position changes by $\Delta x = v_i \cdot \Delta t$. Thirdly, the time is advanced by $\frac{\Delta t}{N}$. This concludes one sub-timestep and the next agent to update is chosen.

Note that the time is advanced by the length of a sub-timestep $\frac{\Delta t}{N}$, even though the formula calculating the agent's movement includes the full timestep Δt. Using the random sequential update, the step length of an agent in one sub-timestep is the same as the step length of an agent in a simulation with parallel update in a normal timestep. This is consistent with the situation in a cellular automaton: An agent that would move one cell in one parallel-update timestep moves one cell in one sub-timestep when a random-sequential update is used. When using a random-sequential update, each agent is updated on average every N-th sub-timestep or, equivalently, once every timestep. The average velocity of an agent is therefore consistent for both

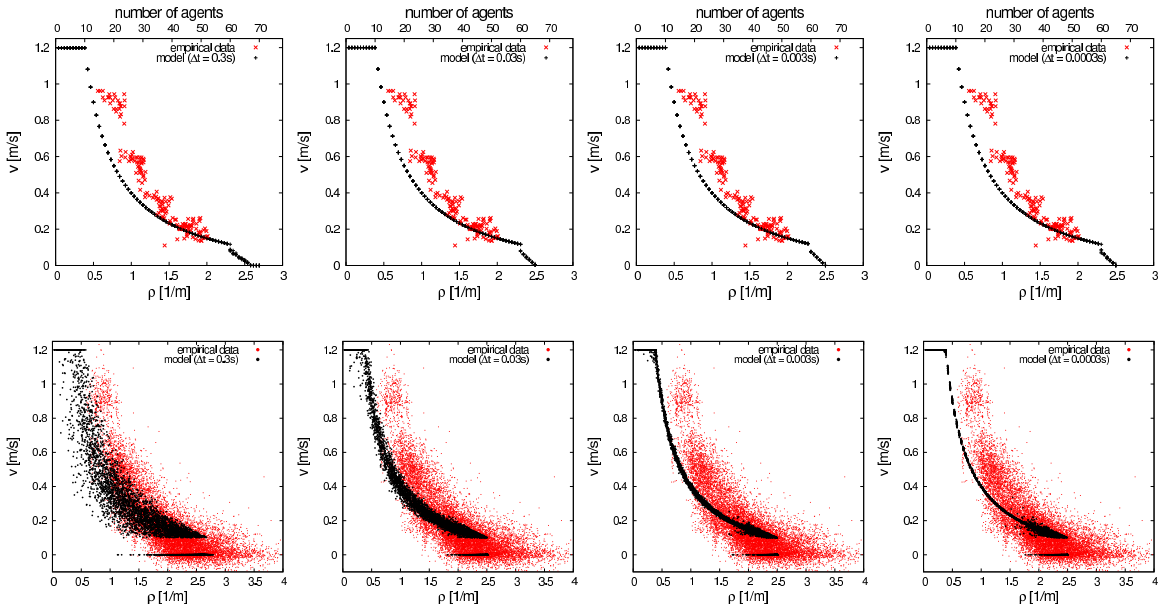

Figure 5.21: Random sequential update: experimental and model fundamental diagrams for different timesteps and appropriate stopping probabilities.

update methods.

Figure 5.21 shows the fundamental diagram of the SHDV model variant with random sequential update. While the global fundamental diagram is very similar to the behavior of the model with parallel update, the local fundamental diagram is different. For timesteps $\Delta t = 0.3$ s and $\Delta t = 0.03$ s and to a smaller extent also for $\Delta t = 0.003$ s, there is a lot of scatter in the local fundamental diagram. This stochasticity is induced by the intrinsically random nature of the random-sequential update. It is much more pronounced at large timesteps, which is to be expected because the agents move farther in an individual timestep and the sequential movement of agents therefore plays a bigger role. At small timesteps of about $\Delta t = 0.0003$ s or smaller, the difference between the resulting fundamental diagrams of parallel update and random-sequential update are minimal.

The velocity distribution shown in Figure 5.22 features the same behavior as the local fundamental diagram. For timesteps larger than $\Delta t = 0.003$ s the distribution is broader than the corresponding velocity distribution of the model with parallel

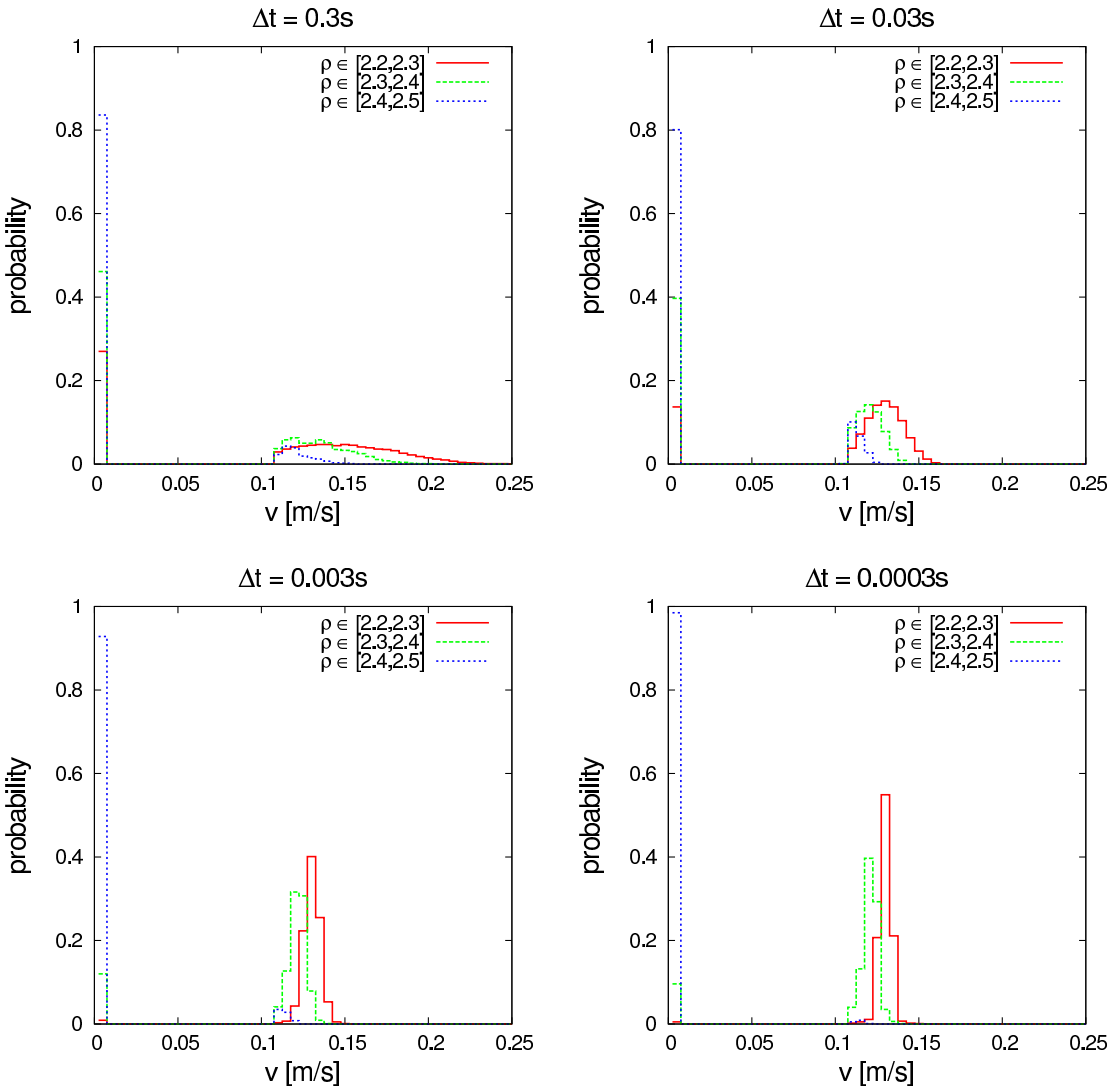

Figure 5.22: Random sequential update: model velocity distributions for different timesteps and appropriate stopping probabilities.

update. For small timesteps such as $\Delta t = 0.0003$ s the velocity distribution strongly resembles the parallel-update analog.

The order parameter shown in Figure 5.23 paints a similar picture. At the larger timesteps $\Delta t = 0.3$ s and $\Delta t = 0.03$ s there is a lot of scatter. Disregarding the densities below $\rho \approx 0.5$ m^{-1}, there is no clear trend for $\Delta t = 0.3$ s. The order parameter is only slightly higher at densities above $\rho \approx 2$ m^{-1} compared to smaller densities, which indicates that most of the inhomogeneity in the system is generated by the stochasticity of the random sequential update in combination with the large

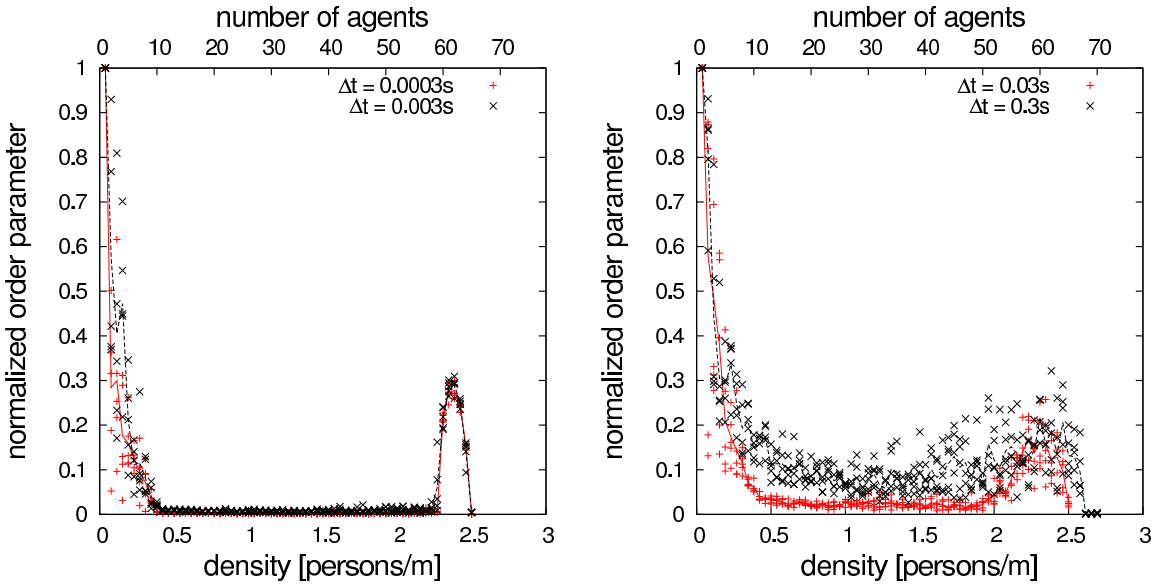

Figure 5.23: Random sequential update: model order parameter as a function of density for different timesteps and respective stopping probabilities.

timestep. For $\Delta t = 0.03$ s the order parameter peaks at about $\rho \approx 2.3$ m^{-1}. In comparison to the order parameter of simulations with smaller timesteps or parallel update, the peak is broader and lower. The lower amount of inhomogeneity suggests that multiple jams exist in the system. For the smaller timesteps $\Delta t = 0.003$ s and $\Delta t = 0.0003$ s the order parameter is almost identical to the corresponding data with parallel update. There is a clear maximum at about $\rho \approx 2.3$ m^{-1} which corresponds to the phase-separated state. At intermediate densities with 0.4 m$^{-1} \lesssim \rho \lesssim 2.2$ m^{-1}, there are small deviations from the completely homogeneous steady state with order parameter zero that can be observed with parallel update. This is a result of the intrinsic stochasticity of the random-sequential update. Because not all agents move at the same time, it is very unlikely to arrive at a completely homogeneous state. Additionally, it is impossible to maintain the homogeneous state. This is true for arbitrarily small timesteps. The deviation from the homogeneous state increases with the size of the timestep.

At small timesteps, the simulation results of the SHDV model variant with ran-

dom sequential update are consistent with results of the model with parallel update. The random-sequential update constitutes a source of additional noise that is largely irrelevant at small timesteps. At larger timesteps, the amplitude of the noise increases and the simulation results differ.

For both parallel and random-sequential updates, the simulation results depend on the size of the timestep. Note that this change of behavior is different to cellular automata models with random-sequential update. In that case the random-sequential update does not imply a specific timescale and is often used to approximate continuous time. In the SHDV model with random-sequential update, however, the distance an agent travels in one timestep explicitly depends on the size of the timestep and the model dynamics change accordingly. Therefore, the random sequential update can only approximate continuous time in the limit $\Delta t \to 0$.

Cellular automata models with parallel update whose dynamics is independent of the size of the timestep also show the same behavior for different timesteps. In general, their parameter values do not depend on the size of the timestep. The model dynamics is often heavily influenced by the existence of a specific timescale which is usually interpreted as some kind of reaction time. Consequently, the parallel update is not typically used to approximate continuous time. In the SHDV model on the other hand, the parameter values implicitly depend on the size of the timestep. The distance an agent travels in one timestep and thus the model dynamics change for varying timesteps. To approximate continuous time using the parallel update, the limit $\Delta t \to 0$ has to be studied.

The simulation results for timesteps below $\Delta t = 0.0003$ s are basically identical for parallel and random-sequential update schemes. The agreement of the order parameter and other simulation data is a strong indication that a continuous model with otherwise the same characteristics as the SHDV model exists. The actual dynamics of the SHDV model, namely the intrinsic stochasticity in form of the stopping

probability, has no clear counterpart in continuous time. This makes it difficult to find an explicit formulation for the corresponding continuous model. It is, however, a reasonable assumption that a model does not generally need discrete time in order to develop phase separation.

5.7.3 Minimum velocity

The minimum velocity $v_{\min}$ is a distinct feature of the velocity function defined in Section 5.1. This section investigates whether the observed phase separation with a slow-moving phase is dependent on a nonzero minimum velocity. Every simulation in this section utilizes the almost homogeneous initial condition.

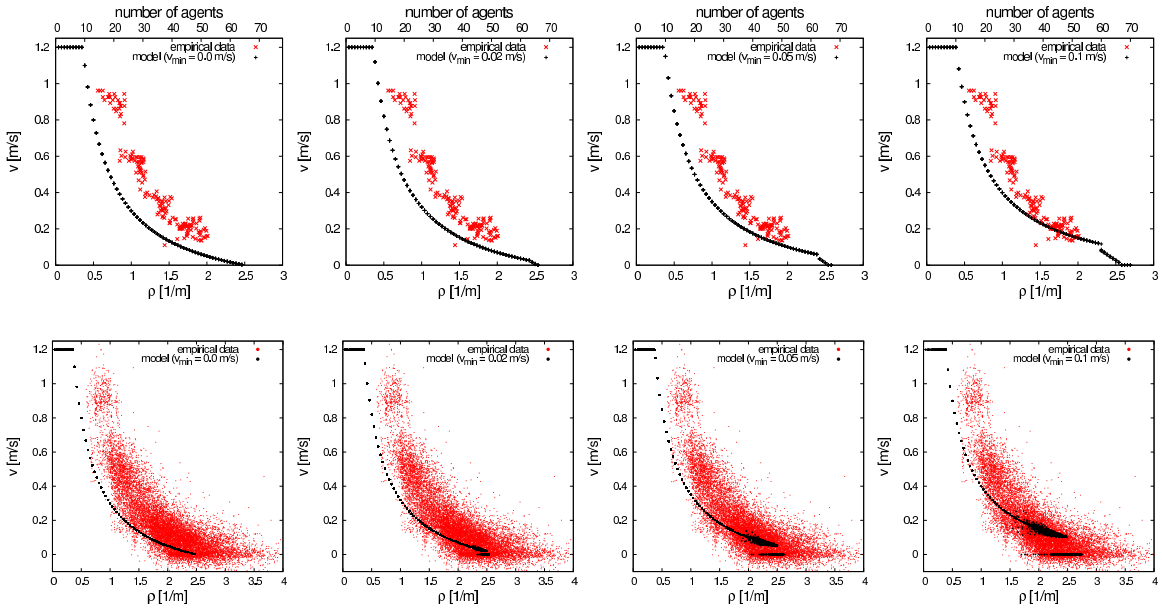

Figure 5.24: Experimental and model fundamental diagrams for different minimum velocities.

Figure 5.24 shows the fundamental diagrams for different values of the minimum velocity $v_{\min}$. The rightmost column shows the result for the standard value $v_{\min} = 0.1\ \frac{\mathrm{m}}{\mathrm{s}}$. Note that a smaller minimum velocity leads to a larger minimum distance according to Equation (5.4) and therefore to a smaller maximum density. The maximum local density in the local fundamental diagram is equal to the reciprocal of

the minimum distance. The maximum global density in the global fundamental diagram can, however, only assume discrete values and thus is typically slightly smaller than the local maximum density.

The high density regime, in which the global fundamental diagram declines linearly, starts at a higher density for smaller minimum velocities and disappears completely for $v_{\min} = 0\ \frac{\mathrm{m}}{\mathrm{s}}$. The local fundamental diagram shows two changes depending on $v_{\min}$. Firstly, no agent has a velocity between zero and the minimum velocity. As the latter decreases, the velocity interval free of data points diminishes as well. At $v_{\min} = 0\ \frac{\mathrm{m}}{\mathrm{s}}$ agents can assume arbitrarily small velocities. Secondly, the density interval in which the fundamental diagram is non-deterministic and exhibits scatter becomes smaller at smaller minimum velocities and vanishes at $v_{\min} = 0\ \frac{\mathrm{m}}{\mathrm{s}}$.

To understand why there are no standing agents at a minimum velocity of zero, consider an agent that closes in on a jam. As the agent moves nearer to the end of the jam, its headway decreases and it slows down. Its velocity is given by $v_i = \alpha(h_i - d)$ according to Equation (5.4), which results in a standstill when the agent reaches the headway $h_i = d$. With $v_{\min} = 0\ \frac{\mathrm{m}}{\mathrm{s}}$, the velocity can reach arbitrarily small values. This means that in each timestep, the agent moves a constant fraction, which is given by $\alpha \cdot \Delta t$, of the distance $h_i - d$ to the end of the jam, that is to the position where the agent is forced to stand still in the next timestep. It takes an infinite number of timesteps until the agent reaches the end of the jam, which corresponds to the headway $h_i = d$. The agent will therefore never come to a complete standstill and its headway will never be equal to the lower threshold d. Consequently, any jam will dissolve before the first agent closing in on it stops and there are no standing agents in the stationary state of the simulation.

The behavior with a small but nonzero minimum velocity is qualitatively different: An agent closing in on a jam slows down according to the velocity function. Due to the nonzero minimum velocity, its velocity $v_i = \alpha(h_i - d) + v_{\min}$ at a given headway h_i is

larger than in the previous example by the constant value $v_{\min}$. The agent therefore comes to a standstill after a finite number of timesteps and is a part of the jam afterward. Consider a system with a completely inhomogeneous agent configuration for different nonzero minimum velocities. The first agent of the jam starts moving and, after some time, approaches the end of the jam. Once its headway is smaller than d_c, its velocity is smaller than $v_{\max}$. Note that d_c depends on the minimum velocity according to the model definition and for a given headway $h_i < d_c$, the velocity v_i is lower at smaller values of $v_{\min}$. Consequently, the time until the agent reaches the end of the jam and stops moving is higher for smaller values of $v_{\min}$. This means that at smaller minimum velocities more agents at the front of the jam start moving before the first agent queues up again. The jam can therefore completely dissolve in a wider density regime and up to higher densities. The same argument can be made for an almost homogeneous configuration and explains the behavior of the fundamental diagram for different minimum velocities.

The velocity distributions shown in Figure 5.25 feature the typical double peak structure for all nonzero values of the minimum velocity. The density regime in which a coexistence of moving and standing agents exits and consequently the extent of the double peak decrease with decreasing $v_{\min}$. In addition, the position of the peak corresponding to moving agents shifts according to the minimum velocity. At $v_{\min} = 0\ \frac{\mathrm{m}}{\mathrm{s}}$, there are two cases. Either the density is equal to 2.5 m^{-1}, corresponding to an average headway of 0.4 m which is exactly equal to the minimum distance d or the density is smaller. In the first case, there is only one possible agent configuration and no agent is allowed to move. In the second case, there are no standing agents. Note that the size of each velocity bin is 0.005 $\frac{\mathrm{m}}{\mathrm{s}}$ and agents with a nonzero velocity smaller than that are included in the leftmost bar.

Figure 5.26 shows the order parameter for simulations with different minimum velocities. The size of the high-density regime with nonzero order parameter shrinks

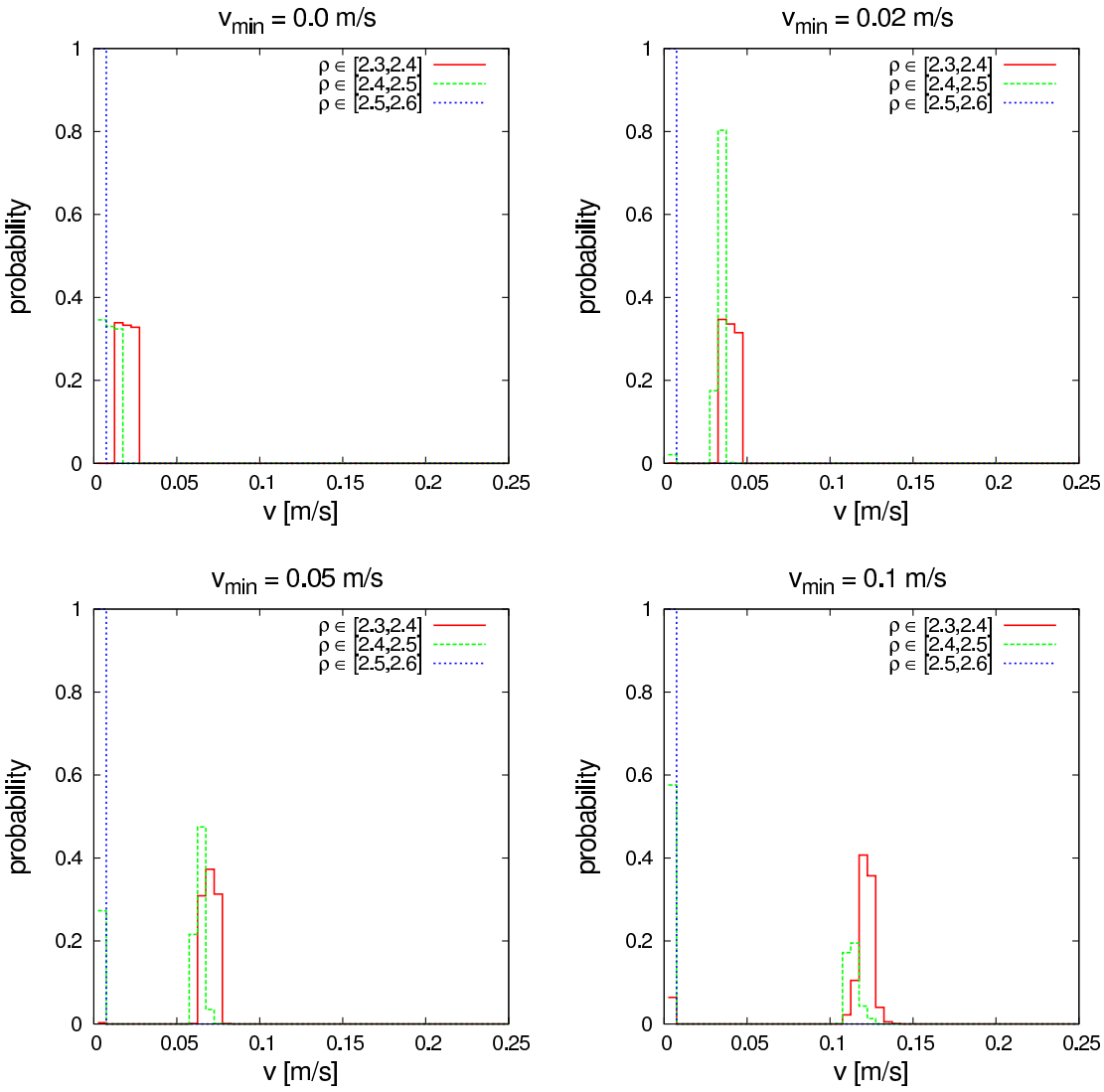

Figure 5.25: Model velocity distributions for different minimum velocities.

for smaller minimum velocities. This is completely analogous to the fundamental diagram. At smaller minimum velocities, agents close to the end of the jam move slower and thus stop moving later. The jam has more time until it is extended by new agents and is therefore more likely to dissolve completely. At $v_{\min} = 0 \frac{\mathrm{m}}{\mathrm{s}}$, moving agents can slow down to arbitrarily small velocities but as a consequence do not stop moving. Therefore any jam dissolves and the system evolves into a homogeneous state with order parameter zero.

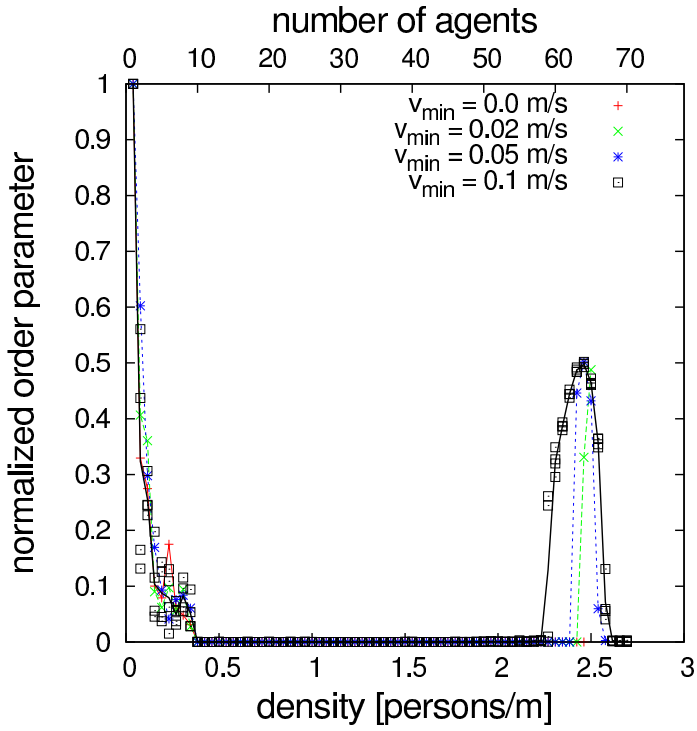

Figure 5.26: Model order parameter as a function of density for different minimum velocities.

5.7.4 System size

Up to now, relatively small system sizes have been considered, in accordance with the experimental data. To achieve a deeper understanding of the phenomenon 'phase separation into a slow-moving and a jammed phase', especially in the thermodynamic limit, larger systems are analyzed. The characteristics or even the existence of phase separation might depend on the system size. A particularly interesting question is whether there are multiple jams or only one jam in a larger system. Figure 5.27 shows the fundamental diagrams as well as the velocity distribution for a tenfold increase in system size to $L = 260$ m. They exhibit the same qualitative behavior as for $L = 26$ m.

The order parameter is shown in Figure 5.28 as a function of the density. At high densities, the order parameter mirrors the results for the system size $L = 26$ m which are shown in Figure 5.12. The system also develops into a homogeneous state with

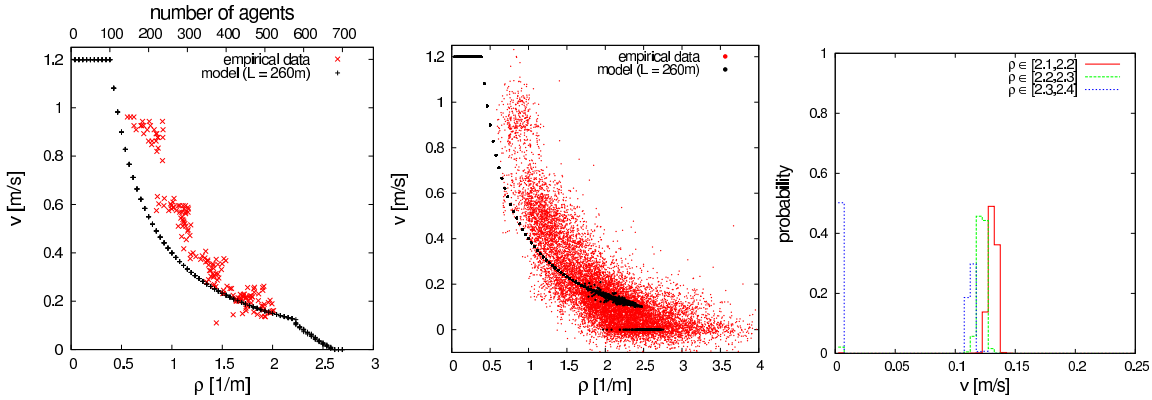

Figure 5.27: Global and local fundamental diagrams and velocity distribution at system size $L = 260$ m.

the order parameter being equal to zero at intermediate densities. The behavior at small densities seems to be different: The order parameter in the larger system with $L = 260$ m is smaller than in the original system with $L = 26$ m at corresponding densities. This difference can be explained as follows. The size of the order parameter at low densities is determined by the initial distribution of agents because the agents move mostly independent of each other. Simulations of the larger system include ten times the number of agents that are simulated in the original system at the same

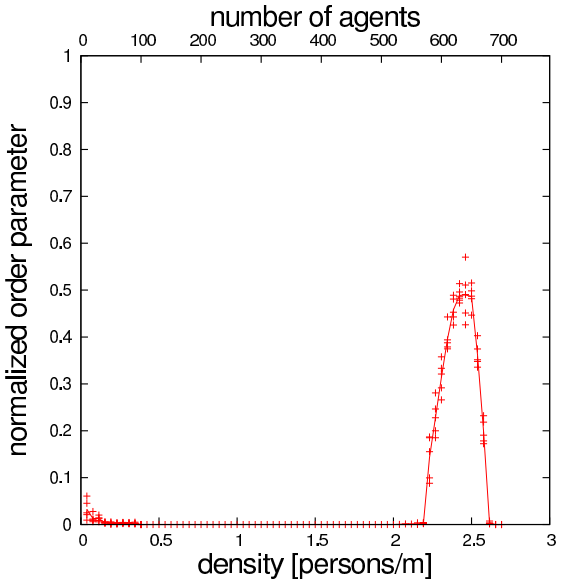

Figure 5.28: Order parameter at system size $L = 260$ m.

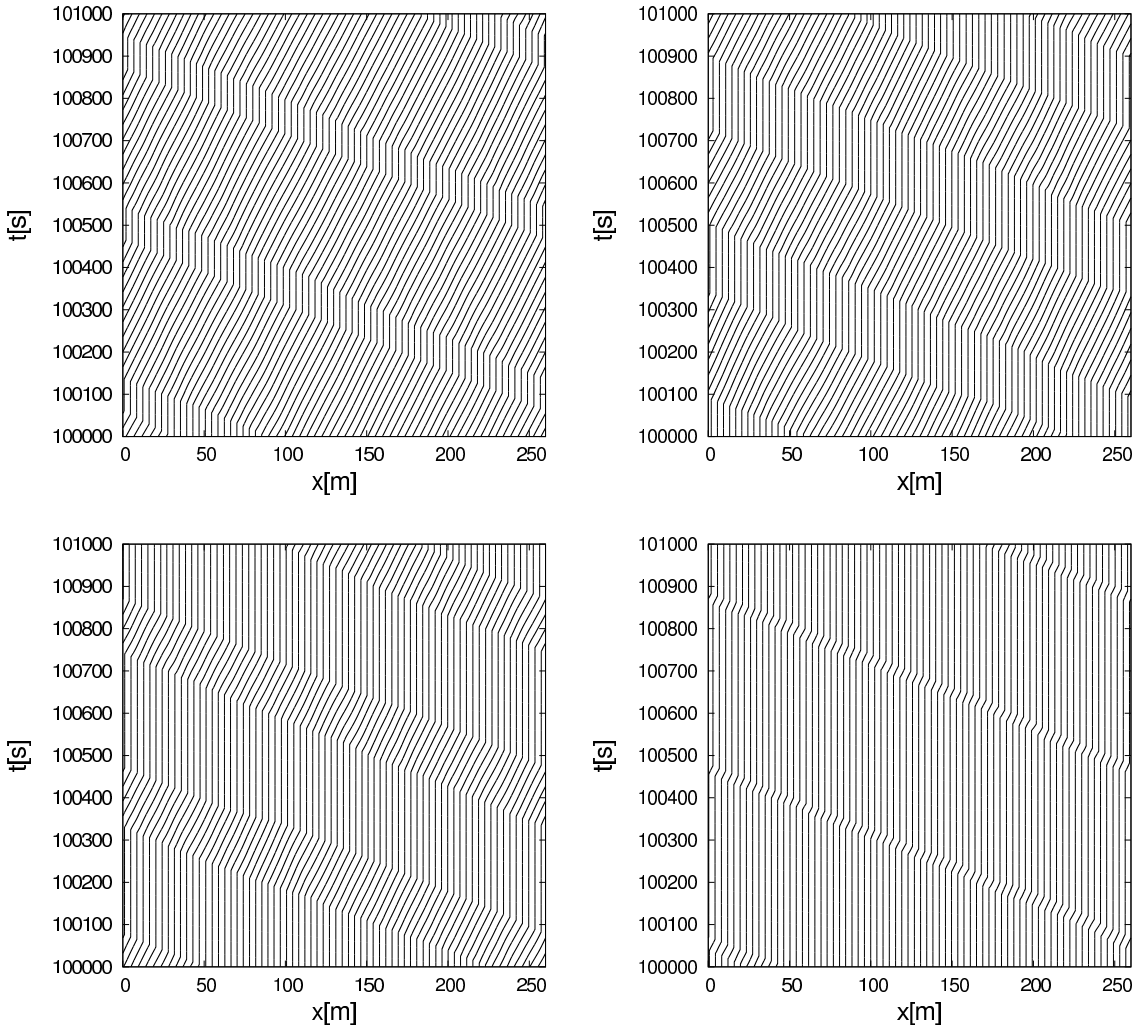

Figure 5.29: Trajectories at system size $L = 260$ m with densities $\rho = 2,23$ m^{-1}, $\rho = 2,35$ m^{-1}, $\rho = 2,46$ m^{-1}, $\rho = 2,58$ m^{-1} and agent numbers $N = 580$, $N = 610$, $N = 640$, $N = 670$, respectively (first top, then bottom row from left to right).

density. This leads to a more homogeneous initial distribution of the agents and consequently to a smaller order parameter. Additionally, the minimum density that is simulated corresponds to a single agent in the smaller system and to $N = 10$ agents in the larger system.

Selected global trajectories of the system with $L = 260$ m and densities chosen from the regime with nonzero order parameter are shown in Figure 5.29. As suggested by the nonzero order parameter, the system is always in a phase-separated state. For

large simulation times, the system evolves into a state with only one jam. With increasing density the size of the jammed phase increases while the size of the slowly moving phase decreases.

Simulations with even larger system sizes feature the same qualitative behavior. A quantitative analysis of the order parameter at a given density for different system sizes is given in Figure 5.30. The density $\rho \approx 2.42\ \mathrm{m}^{-1}$ corresponding to $N = 63$ in the canonical system with $L_0 = 26$ m is chosen because the order parameter is maximal at that density. Because the density can only take discrete values corresponding to the number of agents in the simulation, the density at which the order parameter is maximal might shift slightly in larger systems and assume a value that is not accessible at $L_0 = 26$ m.

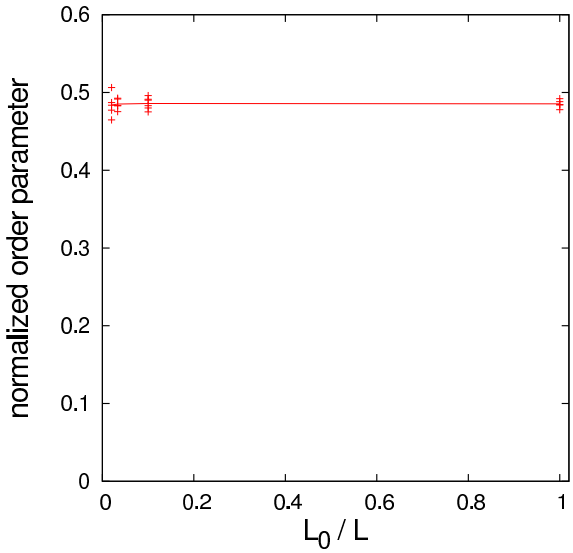

Figure 5.30: Order parameter as a function of the normalized inverse system size $\frac{L_0}{L}$ at $N = 63 \cdot \frac{L}{L_0}$ with $L_0 = 26$ m.

Five simulation runs each are performed for several systems with equal density but different sizes and thus different numbers of agents. The flat trend of the resulting order parameter illustrates that the existence of phase separation is indeed independent of system size. Additionally, it indicates that after a sufficiently long simulation time there is only one jam in the system, since a system with multiple jams would

have a smaller order parameter.

Extrapolating the order parameter shown in Figure 5.30 to arbitrarily large systems and thus $\frac{L_0}{L} \to 0$ suggests that the SHDV model exhibits phase separation in the thermodynamic limit.

5.8 Phase separation density regime

In general, a simulation of the SHDV model can be in one of three stable states: Either all agents are distributed homogeneously and move with identical velocities, or the system exhibits phase separation, or the density is too high to allow movement which results in a complete standstill. In this section, the density regimes of these states are estimated by determining the density interval in which phase separation occurs. Both the lower and upper bound of the phase separation density regime depend on the initial condition of the simulation. As a first step, consider homogeneous initial conditions. The stopping probability p_0 is irrelevant: At densities smaller than d^{-1} all agents move, at densities larger than d^{-1} all agents are in a system-wide jam.

The case of almost homogeneous or inhomogeneous initial conditions is more interesting because the stopping probability p_0 becomes relevant. Firstly, the upper density boundary of phase separation is considered, that is the density at which the jammed phase occupies the whole system and there are no more moving agents. It is determined by the density ρ_{jam} of the jammed phase. If the global density is equal to or larger than ρ_{jam}, there are only standing agents in the system. At global densities smaller than ρ_{jam} (and larger than the lower boundary discussed below), the system develops phase separation.

To calculate ρ_{jam}, or rather the average distance of agents in the jam, $d_{\text{jam}} = \rho_{\text{jam}}^{-1}$, an agent who is about to move into the jam is considered. Its headway h is equal to its distance from the end of the jam; h has to be larger than or equal to d, otherwise the agent would not be allowed to move, it would already be part of the jam. On the

other hand, there is a maximum headway $h_{\max}$ at which the agent barely reaches the end of jam. It is assumed that all possible headways h that lead to the agent being part of the jam after its movement are equally likely. The minimum possible headway is d, and the maximum possible headway $h_{\max}$ is defined by

$$h_{\max} - v(h_{\max}) \cdot \Delta t = d - \epsilon \,, \tag{5.16}$$

ensuring that the headway after the agent's movement in the next timestep is infinitesimally smaller than d and thus too small to allow further movement. The velocity function defined in Equation (5.2) is inserted into Equation (5.16),

$$h_{\max} = \big(\alpha(h_{\max} - d) + v_{\min}\big)\Delta t + d - \epsilon \,, \tag{5.17}$$

which can be simplified to

$$v_{\min}\Delta t = (1 - \alpha\Delta t)(h_{\max} - d) \tag{5.18}$$

with $\epsilon \to 0$. The maximum possible headway $h_{\max}$ is then given by

$$h_{\max} = \frac{v_{\min}\Delta t}{1 - \alpha\Delta t} + d \approx 0.453 \text{ m} \,. \tag{5.19}$$

The expected headway after the next timestep and thus d_{jam} is given by the normalized integral over all possible headways minus their corresponding movement during one timestep,

$$d_{\text{jam}} = \frac{1}{h_{\max} - d} \int_{d}^{h_{\max}} dh \big(h - v(h)\Delta t\big) \,. \tag{5.20}$$

Because the velocity function is linear between the bounds of the integration, this

integral can be simplified by using the mean value of the possible headways and the corresponding velocity:

$$\begin{aligned} d_{\text{jam}} &= \frac{h_{\max}+d}{2} - v\Big(\frac{h_{\max}+d}{2}\Big)\cdot\Delta t \\ &= \frac{h_{\max}+d}{2} - \Big[\alpha\Big(\frac{h_{\max}+d}{2}-d\Big)+v_{\min}\Big]\Delta t \\ &= \frac{h_{\max}+d}{2}(1-\alpha\Delta t)+\alpha d\Delta t - v_{\min}\Delta t \\ &= \Big[\frac{1}{2}\cdot\frac{v_{\min}\Delta t}{1-\alpha\Delta t}+d\Big](1-\alpha\Delta t)+\alpha d\Delta t - v_{\min}\Delta t \\ &= \frac{1}{2}v_{\min}\Delta t + d(1-\alpha\Delta t)+\alpha d\Delta t - v_{\min}\Delta t \\ &= d - \frac{1}{2}v_{\min}\Delta t\,. \end{aligned} \tag{5.21}$$

Inserting the definition of the minimum velocity results in

$$d_{\text{jam}} = \frac{d+d_{\min}}{2} = 0.385\ \text{m}\,. \tag{5.22}$$

This corresponds to a density in the jam of

$$\rho_{\text{jam}} = \frac{2}{d+d_{\min}} \approx 2.6\ \text{m}^{-1}\,, \tag{5.23}$$

which is in good agreement with the values obtained manually in Sections 5.5 and 5.6.2.

In the following, the lower density boundary of phase separation, that is the density at which the system changes from a homogeneous distribution of agents to phase separation, is investigated. Let ρ_{moving} denote the density in the moving phase in case of phase separation. If the global density is smaller than or equal to ρ_{moving}, the agents distribute homogeneously in the system and all agents move. If the global density is larger than ρ_{moving} and smaller than the upper boundary discussed above, there has to be a jam somewhere in the system and thus phase separation occurs.

The average distance between agents in the moving phase is $d_{\text{moving}} = \rho_{\text{moving}}^{-1}$

and can be estimated as follows: The distance between agents in a jam has been approximated as $\frac{d+d_{\min}}{2}$ in Equation (5.22). The velocity of an agent leaving the jam is assumed to be equal to the velocity v_{moving} in the moving phase. As can be observed in the various velocity distributions discussed in this chapter, see. e.g. Figure 5.3, v_{moving} is slightly larger than the minimum velocity and could be approximated by $v_{\text{moving}} \approx v_{\min} + \epsilon$. A more accurate approach is to instead calculate $v_{\text{moving}} = v(d_{\text{moving}})$ using the velocity function. When the first agent moves out of the jam, the headway h of the following agent in the next timestep is given by the previous headway $\frac{d+d_{\min}}{2}$ plus the movement of the leading agent, resulting in

$$\begin{aligned} h &= \frac{d + d_{\min}}{2} + v_{\text{moving}}\Delta t \\ &= d - \frac{v_{\min}\Delta t}{2} + v_{\text{moving}}\Delta t \\ &= d + \Delta t\Big(v_{\text{moving}} - \frac{v_{\min}}{2}\Big) \\ &> d\,, \end{aligned} \tag{5.24}$$

using the formula for the minimum distance. Because the second agent's headway is larger than the lower threshold, it is allowed to move in the next timestep with a probability of $1 - p_0$. The temporal distance between agents moving out of the jam depends on the stopping probability p_0 and the size of a timestep Δt. An agent starts to move with probability $1 - p_0$, it thus takes an average of $(1 - p_0)^{-1}$ timesteps until the agents starts moving, which results in the average temporal distance

$$T = \frac{\Delta t}{1 - p_0}\,. \tag{5.25}$$

The spatial distance between agents moving out of the jam and thus the spatial

distance between agents in the moving phase is then given by

$$\begin{aligned} d_{\text{moving}} &= d_{\text{jam}} + T \cdot v_{\text{moving}} \\ &= d - \frac{v_{\min}\Delta t}{2} + \frac{\Delta t}{1-p_0} \cdot v(d_{\text{moving}}) \\ &= d - \frac{v_{\min}\Delta t}{2} + \frac{\Delta t}{1-p_0} \cdot \big(\alpha(d_{\text{moving}} - d) + v_{\min}\big) \\ &= d + v_{\min}\Delta t\Big(\frac{1}{1-p_0} - \frac{1}{2}\Big) + \frac{\alpha\Delta t}{1-p_0}(d_{\text{moving}} - d) \\ &= d + \frac{1}{2}v_{\min}\Delta t\frac{1+p_0}{1-p_0} + \frac{\alpha\Delta t}{1-p_0}(d_{\text{moving}} - d) \end{aligned} \tag{5.26}$$

which can be written as

$$(d_{\text{moving}} - d) \cdot \Big(1 - \frac{\alpha\Delta t}{1-p_0}\Big) = \frac{1}{2}v_{\min}\Delta t\frac{1+p_0}{1-p_0} \tag{5.27}$$

$$\Leftrightarrow \quad (d_{\text{moving}} - d) \cdot \Big(\frac{1-p_0-\alpha\Delta t}{1-p_0}\Big) = \frac{1}{2}v_{\min}\Delta t\frac{1+p_0}{1-p_0} \tag{5.28}$$

$$\Leftrightarrow \quad (d_{\text{moving}} - d) = \frac{1}{2}v_{\min}\Delta t\frac{1+p_0}{1-p_0} \cdot \Big(\frac{1-p_0}{1-p_0-\alpha\Delta t}\Big) \tag{5.29}$$

$$\Leftrightarrow \quad (d_{\text{moving}} - d) = \frac{v_{\min}\Delta t(1+p_0)}{2(1-p_0-\alpha\Delta t)} \tag{5.30}$$

and finally

$$d_{\text{moving}} = d + \frac{v_{\min}\Delta t(1+p_0)}{2(1-p_0-\alpha\Delta t)} \approx 0.42 \text{ m}\,. \tag{5.31}$$

It follows that

$$\rho_{\text{moving}} = \frac{1}{d_{\text{moving}}} = \frac{2(1-p_0-\alpha\Delta t)}{2d(1-p_0-\alpha\Delta t) + v_{\min}\Delta t(1+p_0)} \approx 2.37 \text{ m}^{-1}\,, \tag{5.32}$$

which reasonably agrees with the values obtained manually in Sections 5.5 and 5.6.2.

5.9 Phase separation mechanism

The main difference between phase separation in vehicular traffic and phase separation in pedestrian dynamics is the small velocity of agents in the moving phase. To understand this behavior, consider the movement of agents leaving a jam in a simulation with an inhomogeneous initial condition. The first agent moves with its maximum velocity because its headway is larger than the interaction range d_c. The second agent leaving the jam starts moving as soon as its headway is larger than the lower threshold d. Assuming that the first agent starts moving with $v_1 = v_{\max}$, one timestep later the headway of the second agent is $h_2 = d_{\min} + v_{\max} \cdot \Delta t = 0.37 \text{ m} + 1.2 \frac{\text{m}}{\text{s}} \cdot 0.3 \text{ m} = 0.73 \text{ m}$ and its velocity thus $v_2 \approx 0.27 \frac{\text{m}}{\text{s}}$, according to the velocity function given in Equation (5.2)[3]. If the second agent starts moving one or a few timesteps later because of the stopping probability, its velocity is still small compared to the velocity of the first agent. The third agent leaving the jam starts with an even lower velocity. If, for the sake of simplicity, it is again assumed that the agent starts moving despite p_0, its velocity is $v_3 \approx 0.13 \frac{\text{m}}{\text{s}}$. Each consecutive agent leaving the jam starts moving with a smaller velocity than the last one. After a few iterations, the next agent leaves the jam with a velocity almost equal to the minimum velocity.

The influence of the stopping probability p_0 does not change much. The velocity of the agent leaving the jam in its first timestep still decreases with the number of agents that have left the jam beforehand. The stopping probability does, however, explain why the velocity of agents in the moving phase is not equal to the minimum velocity. Due to the stopping probability, an agent might not move even though its headway is large enough. When the agent leaves the jam after one or more timesteps, its headway is slightly larger and its velocity thus slightly higher than the minimum velocity. Additionally, the first agent moving into a jam decreases its velocity as soon as its headway becomes smaller than the interaction range. This slows down all

[3]This is only exactly true if the agent starts moving despite the stopping probability.

agents behind the first one. The combination of these two effects is responsible for the low velocity in the slow-moving phase.

The reason for the differences between vehicular traffic models and the SHDV model described above seems to be twofold. Firstly, agents moving out of the jam in e.g. the VDR model cannot interact. The interaction range of a standing agent, which is one cell[4], is equal to the distance an agent at the front of the jam moves in one timestep[5]. In the SHDV model in contrast, the interaction range $d_c = 2.6$ m of a standing agent – of any agent – is large compared to the maximum distance $v_{\max} \cdot \Delta t = 0.36$ m an agent can move in one timestep. Therefore, it is much larger than the typical distance $v_{\text{moving}} \cdot \Delta t \approx 0.03$ m an agent in the moving phase covers in one timestep. This leads to interaction in the start wave. Secondly, an agent in the VDR model moving toward a jam moves with free-flow velocity until it reaches the jam and then stops. In the SHDV model an agent moving toward a jam starts to slow down beforehand, namely when its headway is smaller than the interaction range. Both reasons therefore come down to one: The interaction range of the SHDV model is large in comparison to the typical step length.

5.10 Requirements for phase separation

Up to now, there is no model other than the SHDV model that exhibits phase separation into a slow-moving and a jammed phase similar to the experimental data. This section discusses requirements for this kind of phase separation within the context of the SHDV model. There might be a way to construct a completely unrelated model that is also able to reproduce the experimentally observed phase separation. However, it is likely that the requirements outlined below will be helpful in designing

[4]The interaction range in the VDR model is defined by collision-avoidance only and thus depends on the velocity. It has an upper bound that depends on $v_{\max}$.

[5]Due to the slow-to-start rule the first agent in the jam only starts to move with a certain probability, the distance it travels in one timestep is, however, independent thereof.

pedestrian models that realistically describe the experimental results with regard to one-dimensional movement at high densities.

As discussed in Section 5.9, the largeness of the interaction range compared to the typical step length plays an important part in the creation of a phase-separated state. The slow-to-start rule implemented in the form of the stopping probability and discussed in Section 5.7.1 stabilizes the jam, similar to the case of vehicular traffic. Even though at $p_0 = 0$, standing agents and slowly moving agents coexist, they do not condensate into macroscopic phases. Being allowed to reach arbitrarily small velocities prevents an agent from being able to stop moving. Consequently, the stopping probability becomes meaningless and jams in the system disappear. The minimum velocity is therefore an integral part of the SHDV model.

The time-discreteness of the SHDV model is not required for phase separation. In Section 5.7.2 it has been shown that the simulation results are essentially independent of the size of the timestep. At small timesteps the type of update – parallel or random-sequential – does not matter, either. This suggests that a time-continuous analog to the SHDV model exists. For the SHDV model with parallel update, the finite timestep can be interpreted as an explicit reaction time. However, the model variant with random-sequential update does not include an explicit reaction time, neither does the standard SHDV model in the limit $\Delta t \to 0$. Then again, the slow-to-start rule can be interpreted as an implicit reaction time even in a continuous model variant.

The SHDV model is defined in continuous space. A discrete version of the model with similar minimum velocity and timestep requires a cell size of about $v_{\min} \cdot \Delta t = 0.03$ m which is much smaller than typically used in pedestrian dynamics. Whether a space-discrete SHDV model develops phase separation could be explored in future work.

A recent paper [107] developed a criterion for condensation in one-dimensional

traffic models with a kinetic constraint[6], using a distinction between active (free-flowing) and inactive (kinetically constrained) agents. The requirements for condensation are twofold. Firstly, inactive clusters must not split up; secondly, they must grow or at least not shrink. The criterion is not directly applicable to the SHDV model because in the case of high densities, which is relevant to the effect of phase separation, all agents are interacting agents and thus kinetically constrained. However, a similar argument can be made for the SHDV model with a redefinition of active and inactive agents as moving and not moving agents, respectively.

The first requirement is trivially fulfilled due to the new definition of inactive agents. In order to split up an inactive cluster, an agent within the cluster has to start moving. However, any standing agent has a headway of $h \leq d$. As long as the agent in front of it does not move, the headway cannot change and the agent in question remains standing. The second requirement is formulated in terms of inflow and outflow rates and can be connected to the creation of new inactive clusters [107]. To create a new inactive cluster, a moving agent has to stop moving while the agent in front of it still moves. However, this is per definition impossible within the SHDV model, which can be shown by considering two successive agents with velocities v_1 and v_2. The agent in front moves with velocity $v_1 \geq v_{\min}$ and the agent behind it with velocity v_2. The smallest possible distance h_2 between the two moving agents occurs if $h_2(t-1) = d+\epsilon$ one timestep earlier, the distance at time t is then given by

$$\begin{aligned} h_2(t) &= d + \epsilon - v_2(d+\epsilon) \cdot \Delta t + v_1 \cdot \Delta t \\ &= d + \epsilon - (\alpha\epsilon + v_{\min}) \cdot \Delta t + v_1 \cdot \Delta t \\ &= d + \epsilon \cdot (1 - \alpha\Delta t) + \Delta t \cdot (v_1 - v_{\min}) > d\,, \end{aligned} \tag{5.33}$$

[6]The kinetic constraint forces an agent that closely approaches another agent to reduce its velocity in order to avoid a collision; agents whose headway is smaller than the interaction range are thus called kinetically constrained.

preventing the agent from stopping. The modified criterion for condensation is therefore consistent with the phase separation observed in the SHDV model.

5.11 Outlook

There are two main directions to expand upon this work. The first is trying to further improve the understanding of phase separation into a jammed and a slow-moving phase. To that end, the formulation of a time-continuous variant of the SHDV model as well as a variant discrete in space will be instructive. Furthermore, using different forms of the velocity function consistent with the characteristics discussed in Section 5.10 might lead to further insights. The comprehension of phase separation can also be improved by developing additional models that meet the requirements outlined in Section 5.10 and thus probably feature phase separation into a jammed and a slow-moving phase.

The second approach is to work on a better replication of the experimental data. A straightforward way to achieve a larger variance of e.g. the velocity distribution is to introduce heterogeneous agents with gauss-distributed parameter values. This additional noise is likely to increase the realism of the simulation because it leads to a broadening of the fundamental diagram and the velocity distribution. Additionally, an expansion of the SHDV model to two dimensions can be a worthwhile task. Alternatively, the modification of established two-dimensional pedestrian models such as the FFCA or GCFM according to the findings of this work might be pursued.

An alternative method to identify a phase-separated state can probably be obtained by studying headway correlations, leading to a complementary technique to the order parameter.

CHAPTER VI

Conclusion

Pedestrian dynamics is a broad field of research, therefore any single contribution is necessarily limited to studying a small part thereof. Advancing the understanding of pedestrian crowds has the potential to improve the design of airports, shopping centers, train stations, soccer stadiums, and other areas that regularly exhibit high densities. It leads to an improvement of the safety of pedestrians during evacuations. For mass events, especially the high-density regime is important. Computer simulations of models that describe pedestrian motion are an important approach to studying pedestrian dynamics.

Chapters II and III outlined the successful application of the Floor Field Cellular Automaton (FFCA) within the framework of an evacuation assistant performing faster than real-time simulations of a large multi-purpose arena. A variation of the FCCA has been proposed by reinterpreting the matrix of preference as a characteristic of individual cells, whereas in the original model the matrix of preference is a property of individual agents. A detailed summary and ideas for future work related to the FFCA have been given at the end of Chapter III.

The high-density effect of phase separation into a single slow-moving and jammed phase each has been discussed in Chapters IV and V. None of the models examined in Chapter IV is able to accurately reproduce the observed phase separation, including

the FFCA, the Generalized Centrifugal Force Model, the Adaptive Velocity Model, and the simple cellular automaton model introduced in [93]. The Distance Based Velocity Model (DBVM) which has been proposed in this work features a separation of slow-moving and standing agents. However, it exhibits multiple jams in the system as opposed to a single jam in the experimental data. Nevertheless, the DBVM is an interesting model deserving further attention.

Finally the Stochastic Headway Dependent Velocity (SHDV) Model has been introduced and extensively analyzed in Chapter V. It is able to reproduce the experimentally observed phase separation using initial conditions similar to the experimental setup. A detailed investigation of the model parameters has been performed to examine their necessity for creating phase separation. Important aspects of the model are the slow-to-start rule which stabilizes the jam, the minimum velocity that ensures that agents indeed stop moving instead of slowing down indefinitely, and the large interaction range which causes agents in both the start wave and the stop wave to slow down. The discrete timestep utilized in the SHDV model is, however, not required. Whether a space-discrete variant of the SHDV model develops phase separation as well could be explored in further work.

Additional ideas and suggestions regarding further research related to phase separation in pedestrian dynamics and the SHDV model have been discussed in detail at the end of Chapter V.

APPENDICES

APPENDIX A

Additional plots from the SHDV model

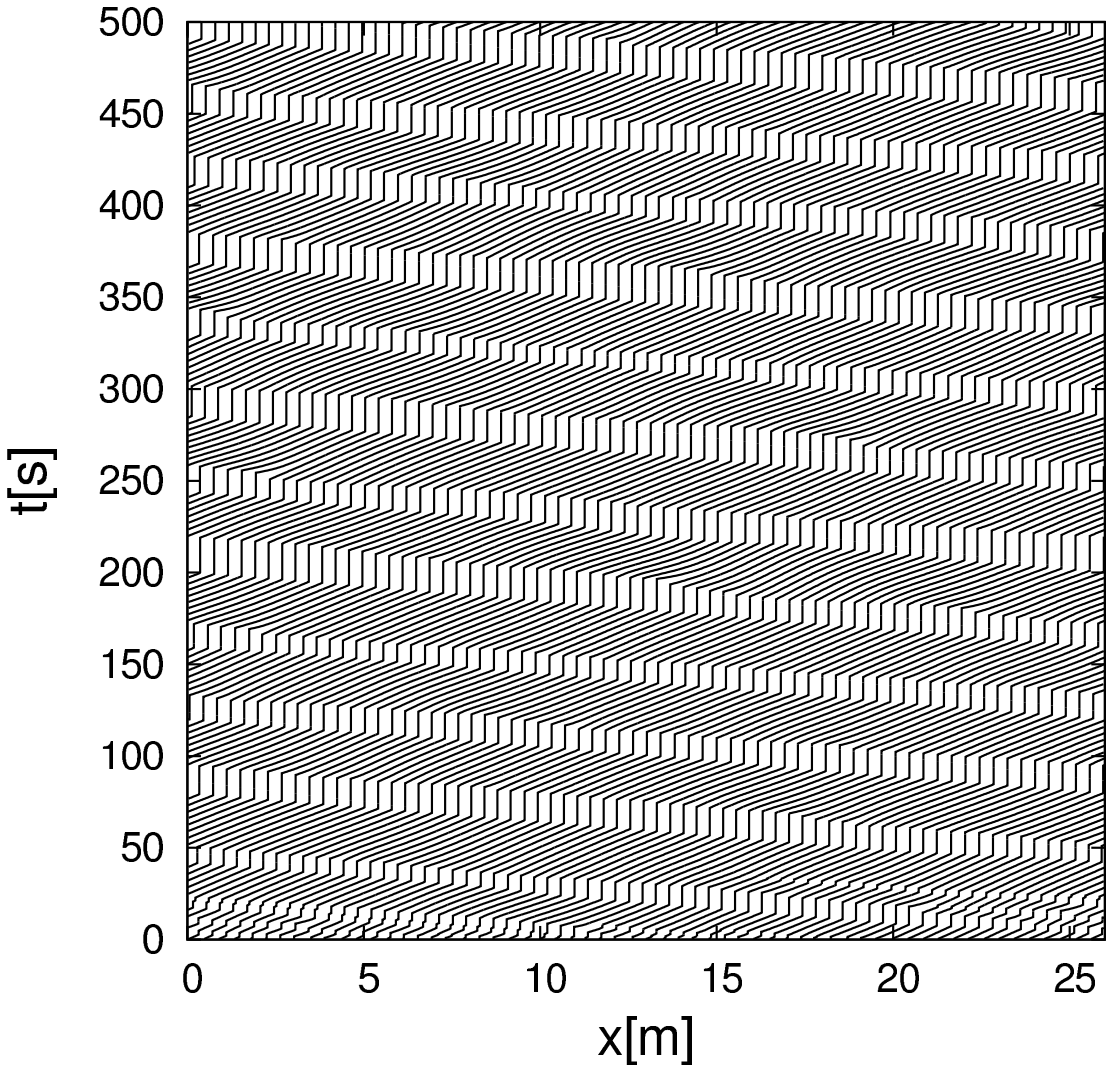

Figure A.1: Global trajectories of the SHDV model for $N = 60$, $\rho = 2.3$ m^{-1}.

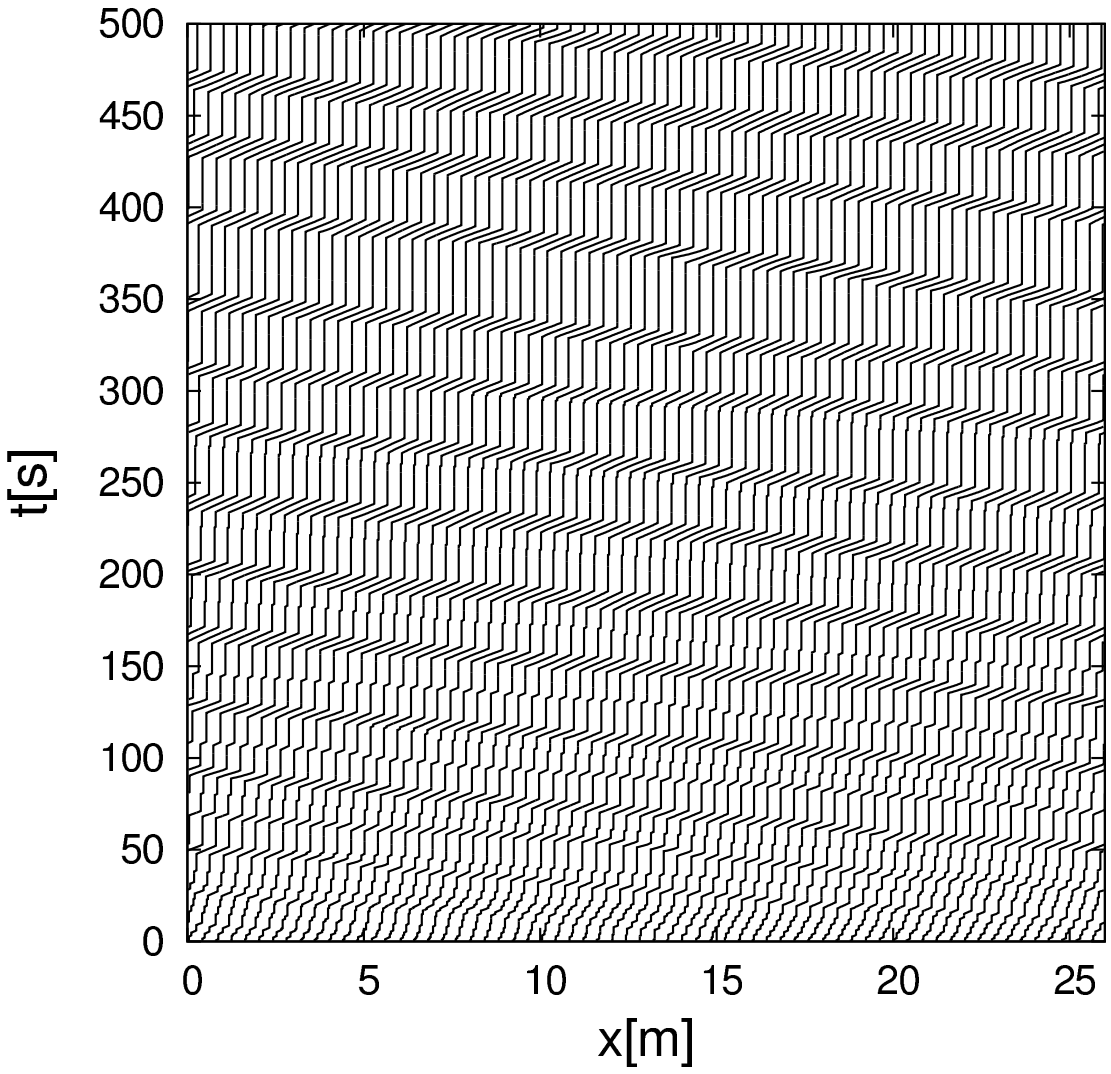

Figure A.2: Global trajectories of the SHDV model for $N = 65$, $\rho = 2.5$ m^{-1}.

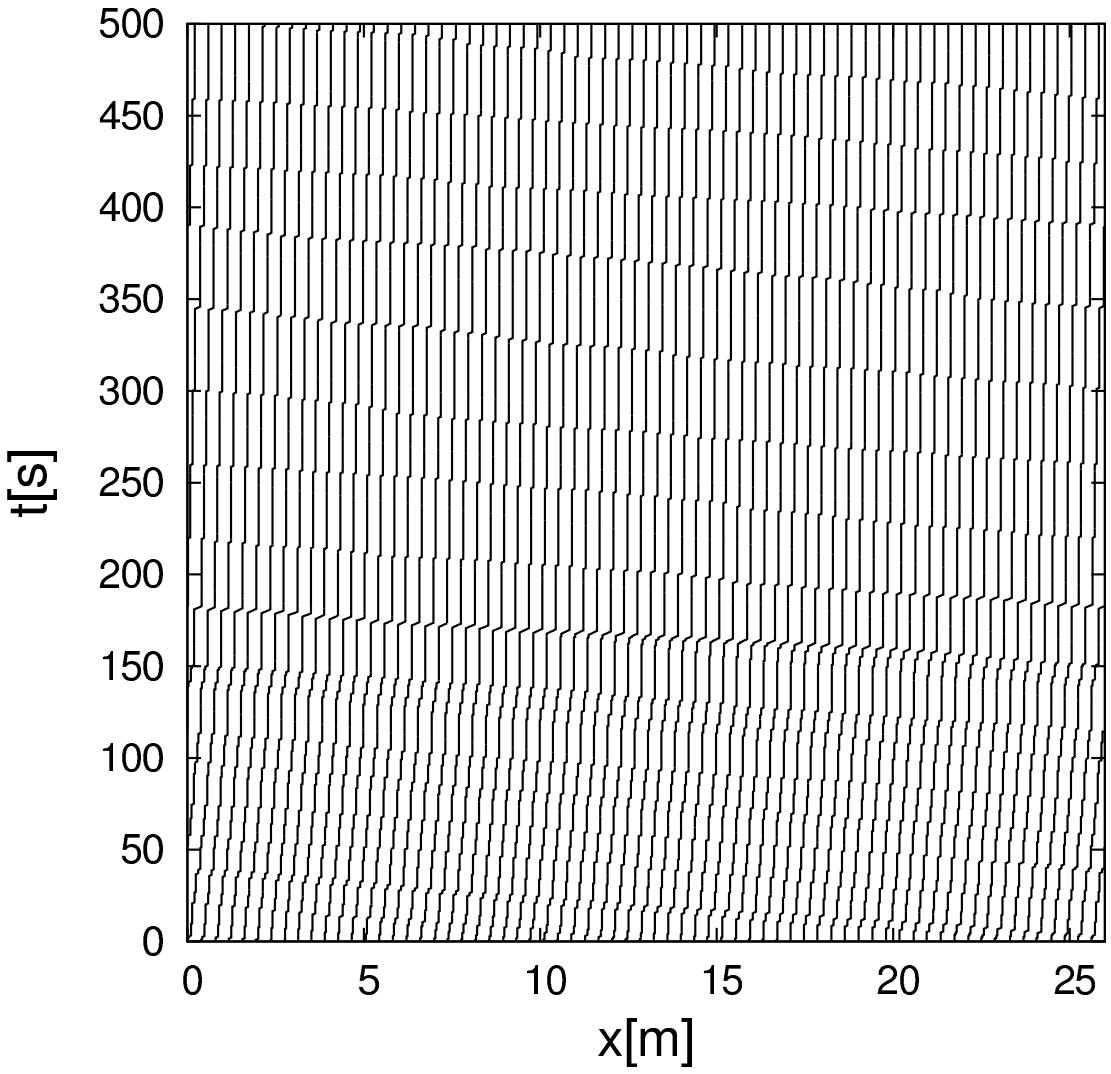

Figure A.3: Global trajectories of the SHDV model for $N = 67$, $\rho = 2.6$ m^{-1}.

APPENDIX B

Publications and talks

B.1 Publications

- A. Schadschneider, **C. Eilhardt**, S. Nowak, R. Will: Towards a calibration of the floor field cellular automaton, in *Pedestrian and Evacuation Dynamics 2010*, p. 557, Springer (2011)

- **C. Eilhardt**, S. Nowak, R. Will, A. Schadschneider: The Floor Field Model of Pedestrian Dynamics, in *Developments in Road Transportation*, p. 207, Macmillan Publ. India (2010)

- **C. Eilhardt**, A. Schadschneider: A simple model for phase separation in pedestrian dynamics, in *Traffic and Granular Flow '11*, p. 277, Springer (2013)

- A. Schadschneider, **C. Eilhardt**, S. Nowak, A.U. Kemloh Wagoum, A. Seyfried: HERMES - An evacuation assistent for large sports arenas based on microscopic simulations of pedestrian dynamics, in *Traffic and Granular Flow '11*, p. 287, Springer (2013)

- U. Kemloh, M. Chraibi, **C. Eilhardt**, S. Nowak, I. Kulkov, D. Weber, K. Sauer, H. Klüpfel, A. Schadschneider: Openpedsim: A framework for pedestrian flow analysis, in *Pedestrian and Evacuation Dynamics 2012*, p. 1323, Springer (2014)

- **C. Eilhardt**, A. Schadschneider: Stochastic Headway Dependent Velocity Model and Phase Separation in Pedestrian Dynamics, to be published in *Traffic and Granular Flow '13* (Springer)

- **C. Eilhardt**, A. Schadschneider: Stochastic headway dependent velocity model for 1d pedestrian dynamics at high densities, to be published in *Pedestrian and Evacuation Dynamics 2014* (Springer)

B.2 Talks

- *Towards a calibration of the floor field cellular automaton*
  Fifth International Conference on Pedestrian and Evacuation Dynamics (PED 2010), National Institute of Standards and Technology, Gaithersburg, MD USA, 9. März 2010

- *The Floor Field Model of Pedestrian Dynamics*
  International Conference on Developments in Road Transportation (DRT 2010), National Institute of Technology, Rourkela, Indien, 10. Oktober 2010

- *A Simple Model for Phase Separation in Pedestrian Dynamics*
  Traffic and Granular Flow '11 , MTUCI Congress Center, Moscow, Russia, 28. September 2011

BIBLIOGRAPHY

BIBLIOGRAPHY

[1] C. Burstedde, K. Klauck, A. Schadschneider, and J. Zittartz. Simulation of pedestrian dynamics using a two-dimensional cellular automaton. *Physica A*, 295:507, 2001. (Cited on pages 2, 3, 15, 19, 23, 25, 30, 51, 54, 63, and 71.)

[2] A. Kirchner and A. Schadschneider. Simulation of evacuation processes using a bionics-inspired cellular automaton model for pedestrian dynamics. *Physica A*, 312:260, 2002. (Cited on pages 2, 19, 21, 30, 51, 54, and 63.)

[3] A. Schadschneider, C. Eilhardt, S. Nowak, and R. Will. Towards a calibration of the floor field cellular automaton. In *Pedestrian and Evacuation Dynamics*, pages 557–566. Springer, 2011. (Cited on pages 2, 7, 19, 25, 30, 51, 54, and 63.)

[4] C. Eilhardt, A. Schadschneider, S. Nowak, and R. Will. The Floor Field Model of Pedestrian Dynamics. In *Developments in Road Transportation*, pages 207–214. Macmillan Publ. India, 2010. (Cited on pages 2, 19, and 54.)

[5] A. Schadschneider, C. Eilhardt, S. Nowak, U. Kemloh, and A. Seyfried. HERMES: An Evacuation Assistent for Large Sports Arenas Based on Microscopic Simulations of Pedestrian Dynamics. In *Traffic and Granular Flow 2011*, pages 287–298. Springer, 2013. (Cited on pages 2, 28, 54, and 56.)

[6] S. Holl and A. Seyfried. Hermes - an evacuation assistant for mass events. *inSiDE*, 7:60, 2009. (Cited on pages 2, 28, 54, and 56.)

[7] D. Helbing. Traffic and related self-driven many-particle systems. *Rev. Mod. Phys.*, 73:1067, 2001. (Cited on page 3.)

[8] D. Helbing, I. J. Farkas, P. Molnár, and T. Vicsek. Simulation of pedestrian crowds in normal and evacuation situations. In *Pedestrian and Evacuation Dynamics*, pages 21–58. Springer, 2002. (Cited on page 3.)

[9] A. Schadschneider, W. Klingsch, H. Klüpfel, T. Kretz, C. Rogsch, and A. Seyfried. Evacuation Dynamics: Empirical Results, Modeling and Applications. In *Encyclopedia of Complexity and System Science*, pages 3142–3176. Springer, 2009. (Cited on pages 3 and 7.)

[10] D. Helbing and P. Molnár. Social force model for pedestrian dynamics. *Phys. Rev. E*, 51:4282, 1995. (Cited on pages 3, 15, and 51.)

[11] D. Helbing. Collective phenomena and states in traffic and self-driven many-particle systems. *Comput. Mater. Sci.*, 30:180, 2004. (Cited on page 3.)

[12] S. P. Hoogendoorn and W. Daamen. Self-organization in pedestrian flow. In *Traffic and Granular Flow '03*, pages 373–382. Springer, 2005. (Cited on page 3.)

[13] J. Zhang, W. Klingsch, A. Schadschneider, and A. Seyfried. Ordering in bidirectional pedestrian flows and its influence on the fundamental diagram. *J. Stat. Mech.*, P02002, 2012. (Cited on pages 3 and 6.)

[14] S. Nowak and A. Schadschneider. Quantitative analysis of pedestrian counterflow in a cellular automaton model. *Phys. Rev. E*, 85:066128, 2012. (Cited on page 3.)

[15] D. Helbing, L. Buzna, A. Johansson, and T. Werner. Self-organized pedestrian crowd dynamics: Experiments, simulations, and design solutions. *Transport. Sci.*, 39:1, 2005. (Cited on page 3.)

[16] D. Yanagisawa and K. Nishinari. Mean-field theory for pedestrian outflow through an exit. *Phys. Rev. E*, 76:061117, 2007. (Cited on page 3.)

[17] M. Muramatsu, T. Irie, and T. Nagatani. Jamming transition in pedestrian counter flow. *Physica A*, 267:487, 1999. (Cited on page 3.)

[18] T. Kretz, M. Wölki, and M. Schreckenberg. Characterizing correlations of flow oscillations at bottlenecks. *J. Stat. Mech.*, P02005, 2006. (Cited on page 3.)

[19] D. Helbing, I. Farkas, and T. Vicsek. Simulating dynamical features of escape panic. *Nature*, 407:487, 2000. (Cited on page 3.)

[20] D. Helbing, I. J. Farkas, and T. Vicsek. Freezing by heating in a driven mesoscopic system. *Phys. Rev. Lett.*, 84:1240, 2000. (Cited on page 3.)

[21] D. Helbing and P. Molnár. Self-organization phenomena in pedestrian crowds. In *Self-Organization of Complex Structures: From Individual to Collective Dynamics*, pages 569–577. 1997. (Cited on page 3.)

[22] M. Muramatsu and T. Nagatani. Jamming transition of pedestrian traffic at crossing with open boundaries. *Physica A*, 286:377, 2000. (Cited on page 3.)

[23] J. Zhang. *Pedestrian fundamental diagrams: Comparative analysis of experiments in different geometries*. PhD thesis, Bergische Universität Wuppertal, 2012. (Cited on pages 5 and 36.)

[24] A. Seyfried, B. Steffen, W. Klingsch, T. Lippert, and M. Boltes. The Fundamental Diagram of Pedestrian Movement Revisited - Empirical Results and Modelling. In *Traffic and Granular Flow '05*, pages 305–314. Springer, 2007. (Cited on pages 6 and 10.)

[25] A. Seyfried, A. Portz, and A. Schadschneider. Phase coexistence in congested states of pedestrian dynamics. *Lecture Notes in Computer Science*, 6350:496, 2010. (Cited on pages 6, 9, 10, 12, and 58.)

[26] G. M. Voronoi. Nouvelles applications des paramètres continus à la théorie des formes quadratiques. *Journal für die reine und angewandte Mathematik*, 133:198, 1908. (Cited on page 6.)

[27] B. Steffen and A. Seyfried. Methods for measuring pedestrian density, flow, speed and direction with minimal scatter. *Physica A*, 389:1902, 2010. (Cited on pages 6 and 10.)

[28] J. Zhang, W. Klingsch, A Schadschneider, and A. Seyfried. Transitions in pedestrian fundamental diagrams of straight corridors and T-junctions. *J. Stat. Mech.*, P06004, 2011. (Cited on page 6.)

[29] J. Zhang, W. Klingsch, and A. Seyfried. High precision analysis of unidirectional pedestrian flow within the Hermes project. In *The Fifth Performance-based Fire Protection and Fire Protection Engineering Seminars*, 2010. (Cited on page 6.)

[30] M. Chraibi, A. Seyfried, and A. Schadschneider. The generalized centrifugal force model for pedestrian dynamics. *Phys. Rev. E*, 82:046111, 2010. (Cited on pages 7, 15, 30, 51, 56, and 71.)

[31] T. Meyer-König, H. Klüpfel, and M. Schreckenberg. Assessment and analysis of evacuation processes on passenger ships by microscopic simulation. In *Pedestrian and Evacuation Dynamics*, pages 297–302. Springer, 2002. (Cited on page 7.)

[32] U. Weidmann. Transporttechnik der Fussgänger. Technical Report Schriftenreihe des IVT 90, ETH Zürich, 1993. Zweite, ergänzte Auflage. (Cited on pages 7, 15, and 19.)

[33] D. Helbing, A. Johansson, and H. Z. Al-Abideen. Dynamics of crowd disasters: An empirical study. *Phys. Rev. E*, 75:046109, 2007. (Cited on page 7.)

[34] U. Chattaraj, A. Seyfried, and P. Chakroborty. Comparison of pedestrian fundamental diagram across cultures. *Adv. Complex Syst.*, 12:393, 2009. (Cited on page 7.)

[35] V. M. Predtechenskii and A. I. Milinskii. *Planning for Foot Traffic Flow in Buildings*. Amerind Publishing, New Dehli, 1978. (Cited on page 7.)

[36] D. Oeding. Verkehrsbelastung und Dimensionierung von Gehwegen und anderen Anlagen des Fußgängerverkehrs. Forschungsbericht 22, Technische Hochschule Braunschweig, 1963. (Cited on page 7.)

[37] B. Pushkarev and J. M. Zupan. Capacity of Walkways. *Transportation Research Record*, 538:1, 1975. (Cited on page 7.)

[38] F. D. Navin and R. J. Wheeler. Pedestrian flow characteristics. *Traffic Engineering*, 39:31, 1969. (Cited on page 7.)

[39] A. Seyfried, M. Boltes, J. Kähler, W. Klingsch, A. Portz, T. Rupprecht, A. Schadschneider, B. Steffen, and A. Winkens. Enhanced empirical data for the fundamental diagram and the flow through bottlenecks. In *Pedestrian and Evacuation Dynamics 2008*, pages 145–156. Springer, 2010. (Cited on pages 7, 9, and 10.)

[40] A. Seyfried and A. Schadschneider. Empirical results for pedestrian dynamics at bottlenecks. *Lecture Notes in Computer Science*, 6068:575, 2010. (Cited on page 7.)

[41] S. P. Hoogendoorn, W. Daamen, and P. H. L Bovy. Extracting microscopic pedestrian characteristics from video data. In *TRB 2003 Annual Meeting*. Washington DC: National Academy Press, 2003. (Cited on page 9.)

[42] Anders Johansson, Dirk Helbing, and Pradyumn K. Shukla. Specification of the social force pedestrian model by evolutionary adjustment to video tracking Data. *Advances in Complex Systems*, 10(2):271–288, 2007. (Cited on page 9.)

[43] A. Johansson, D. Helbing, H. Z. Al-Abideen, and S. Al-Bosta. From crowd dynamics to crowd safety: a video-based analysis. *Adv. Complex Syst.*, 11:497, 2008. (Cited on page 9.)

[44] X. Liu, W. Song, and J. Zhang. Extraction and quantitative analysis of microscopic evacuation characteristics based on digital image processing. *Physica A*, 388:2717, 2009. (Cited on page 9.)

[45] M. Boltes, A. Seyfried, B. Steffen, and A. Schadschneider. Automatic Extraction of Pedestrian Trajectories from Video Recordings. In *Pedestrian and Evacuation Dynamics 2008*, pages 43–54. Springer, 2010. (Cited on pages 9 and 10.)

[46] M. Boltes, A. Seyfried, B. Steffen, and A. Schadschneider. Using stereo recordings to extract pedestrian trajectories automatically in space. In *Pedestrian and Evacuation Dynamics*, pages 751–754. Springer, 2011. (Cited on pages 9, 10, and 37.)

[47] S. P. Hoogendoorn, W. Daamen, and R. Landman. Microscopic calibration and validation of pedestrian models - cross-comparison of models using experimental data. In *Pedestrian and Evacuation Dynamics 2005*, pages 329–340. Springer, 2007. (Cited on page 9.)

[48] T. Kretz, S. Hengst, and P. Vortisch. Pedestrian flow at bottlenecks - validation and calibration of vissim's social force model of pedestrian traffic and its empirical foundations. In *International Symposium of Transport Simulation 2008*. Monash University, 2008. (Cited on pages 9 and 15.)

[49] S. P. Hoogendoorn and W. Daamen. A novel calibration approach of microscopic pedestrian models. In *Pedestrian Behavior: Models, Data Collection and Applications*, page 195. Emerald, 2009. (Cited on page 9.)

[50] D. R. Parisi, M. Gilman, and H. Moldovan. A modification of the social force model can reproduce experimental data of pedestrian flows in normal conditions. *Physica A*, 388:3600, 2009. (Cited on page 9.)

[51] A. Seyfried, B. Steffen, W. Klingsch, and M. Boltes. The fundamental diagram of pedestrian movement revisited. *J. Stat. Mech.*, P10002, 2005. (Cited on page 9.)

[52] BaSiGo, 2014.
`http://www.basigo.de/`. (Cited on page 13.)

[53] A. Schadschneider, D. Chowdhury, and K. Nishinari. *Stochastic Transport in Complex Systems. From Molecules to Vehicles*. Elsevier Science Publishing Co Inc., 2010. (Cited on pages 14, 15, 51, 52, 53, 54, and 97.)

[54] W. J. Yu, L.Y. Chen, R. Dong, and S.Q. Dai. Centrifugal force model for pedestrian dynamics. *Phys. Rev. E*, 72:026112, 2005. (Cited on page 15.)

[55] A. Seyfried, B. Steffen, and T. Lippert. Basics of modelling the pedestrian flow. *Physica A*, 368:232, 2006. (Cited on page 15.)

[56] S. Wolfram. Statistical mechanics of cellular automata. *Rev. Mod. Phys.*, 55:601, 1983. (Cited on page 15.)

[57] V. J. Blue and J. L. Adler. Cellular Automata Microsimulation of Bidirectional Pedestrian Flows. *Transportation Research Record*, 1678:135, 1999. (Cited on page 15.)

[58] T. Kretz and M. Schreckenberg. The F.A.S.T.-Model. *Lecture Notes in Computer Science*, 4173:712, 2006. (Cited on pages 15 and 25.)

[59] M. Davidich and G. Köster. Towards automatic and robust adjustment of human behavioral parameters in a pedestrian stream model to measured data. In *Pedestrian and Evacuation Dynamics*, pages 535–536. Springer, 2010. (Cited on pages 15 and 26.)

[60] D. Hartmann. Adaptive pedestrian dynamics based on geodesics. *New J. Phys.*, 12:043032, 2010. (Cited on pages 15 and 26.)

[61] G. Köster, M. Seitz, F. Treml, D. Hartmann, and W. Klein. On the modelling the influence of group formations in a crowd. *Contemporary Social Science*, 6:397, 2011. (Cited on pages 15 and 26.)

[62] M. Davidich and G. Köster. Towards automatic and robust adjustment of human behavioral parameters in a pedestrian stream model to measured data. *Safety Science*, 50:1253, 2012. (Cited on pages 15 and 26.)

[63] E. W. Dijkstra. A note on two problems in connexion with graphs. *Numerische Mathematik*, 1:269, 1959. (Cited on page 20.)

[64] B. Holldobler and E. Wilson. *The ants*. Belknap, 1990. (Cited on page 20.)

[65] A. Kirchner. *Modellierung und statistische Physik biologischer und sozialer Systeme*. PhD thesis, Universität zu Köln, 2002. (Cited on pages 23 and 25.)

[66] A. Kirchner, K. Nishinari, and A. Schadschneider. Friction effects and clogging in a cellular automaton model for pedestrian dynamics. *Phys. Rev. E*, 67:056122, 2003. (Cited on page 23.)

[67] A. Kirchner, H. Klüpfel, K. Nishinari, A. Schadschneider, and M. Schreckenberg. Discretization effects and the influence of walking speed in cellular automata models for pedestrian dynamics. *J. Stat. Mech.*, 10:P10011, 2004. (Cited on page 25.)

[68] K. Nishinari, A. Kirchner, A. Namazi, and A. Schadschneider. Extended floor field CA model for evacuation dynamics. *IEICE Trans. Inf. and Syst.*, E87-D(3):726, 2004. (Cited on pages 25 and 26.)

[69] K. Nishinari, A. Kirchner, A. Namazi, and A. Schadschneider. Simulations of evacuation by an extended floor field ca model. In *Traffic and Granular Flow 03*, pages 405–410. Springer, 2005. (Cited on page 26.)

[70] C. M. Henein and T. White. Agent-based modelling of forces in crowds. *Lecture Notes in Computer Science*, 3415:173, 2005. (Cited on page 26.)

[71] C. M. Henein and T. White. Macroscopic effects of microscopic forces between agents in crowd models. *Physica A*, 373:694, 2007. (Cited on page 26.)

[72] Image courtesy of Düsseldorf Congress Sport & Event GmbH, 2014. (Cited on page 28.)

[73] U. Kemloh. *Route Choice Modelling and Runtime Optimisation for Simulation of Building Evacuation*. PhD thesis, Bergische Universität Wuppertal, 2012. (Cited on pages 29, 41, and 46.)

[74] PTV Group. PTV Visum, 2013. `http://vision-traffic.ptvgroup.com/de/produkte/ptv-visum/`. (Cited on page 30.)

[75] TraffGo HT GmbH. Pedgo, 2013. `http://www.traffgo-ht.com/de/pedestrians/products/pedgo/index.html`. (Cited on page 30.)

[76] J. Zhang, W. Song, and X. Xu. Experiment and multi-grid modeling of evacuation from a classroom. *Physica A*, 387:5901, 2008. (Cited on page 32.)

[77] A. Schadschneider and A. Seyfried. Empirical Results for Pedestrian Dynamics and their Implications for Cellular Automata Models. In *Pedestrian Behavior: Data Collection and Applications*, pages 27–43. Emerald, 2009. (Cited on page 33.)

[78] R. Will. *Simulation von Fußgängerströmen*. Staatsexamen, Universität zu Köln, 2009. (Cited on page 33.)

[79] T. Kretz. Pedestrian traffic: on the quickest path. *J. Stat. Mech.*, P03012, 2009. (Cited on pages 33 and 43.)

[80] S. Burghardt. *Dynamik von Personenströmen in Sportstadien*. PhD thesis, Bergische Universität Wuppertal, 2013. (Cited on page 36.)

[81] E. Kirik, T. Yurgel'yan, and D. Krouglov. The Shortest Time and/or the Shortest Path Strategies in a CA FF Pedestrian Dynamics Model. *Journal of Siberian Federal University. Mathematics & Physics*, 2:271, 2009. (Cited on page 43.)

[82] E. Kirik, T. Yurgel'yan, and D. Krouglov. On realizing the shortest time strategy in a ca ff pedestrian dynamics mode. *Cybernet. Syst.*, 42:1, 2011. (Cited on page 43.)

[83] T. Kretz, A. Große, S. Hengst, L. Kautzsch, A. Pohlmann, and P. Vortisch. Quickest paths in simulations of pedestrians. *Adv. Complex Syst.*, 14:733, 2011. (Cited on page 43.)

[84] D. Ellsberg. Risk, ambiguity, and the savage axioms. *Q. J. Econ.*, 75:643, 1961. (Cited on page 45.)

[85] F. Spitzer. Interaction of markov processes. *Adv. Math.*, 5:246, 1970. (Cited on page 51.)

[86] R. Barlovic, L. Santen, A. Schadschneider, and M. Schreckenberg. Metastable states in cellular automata for traffic flow. *EPJ B*, 5:793, 1998. (Cited on pages 51 and 53.)

[87] J. Krug. Phase separation in disordered exclusion models. *Braz. J. Phys.*, 30:97, 2000. (Cited on page 52.)

[88] K. Nagel and M. Schreckenberg. A cellular automaton model for freeway traffic. *J. Phys. I France*, 2:2221, 1992. (Cited on pages 53 and 71.)

[89] F. L. Hall, B. L. Allen, and M. A. Gunter. Empirical analysis of freeway flow-density relationships. *Transp. Res. A*, 20:197, 1986. (Cited on page 54.)

[90] M. Chraibi. In preparation. (Cited on page 58.)

[91] A. Portz and A. Seyfried. Modeling stop-and-go waves in pedestrian dynamics. *Lecture Notes in Computer Science*, 6068:561, 2010. (Cited on page 58.)

[92] A. Portz and A. Seyfried. Analyzing stop-and-go waves by experiment and modeling. In *Pedestrian and Evacuation Dynamics*, pages 577–586. Springer, 2011. (Cited on page 58.)

[93] C. Eilhardt and A. Schadschneider. A Simple Model for Phase Separation in Pedestrian Dynamics. In *Traffic and Granular Flow 2011*, pages 277–286. Springer, 2013. (Cited on pages 60 and 125.)

[94] M. Chraibi and A. Seyfried. Pedestrian dynamics with event-driven simulation. In *Pedestrian and Evacuation Dynamics 2008*, pages 713–718. Springer, 2010. (Cited on page 67.)

[95] C. Eilhardt and A. Schadschneider. Stochastic Headway Dependent Velocity Model and Phase Separation in Pedestrian Dynamics. In *Traffic and Granular Flow 2013*. Springer, estimated 2015. (Cited on page 71.)

[96] C. Eilhardt and A. Schadschneider. Stochastic headway-dependent velocity model for 1d pedestrian dynamics at high densities. In *Transportation Research Procedia: The Conference in Pedestrian and Evacuation Dynamics 2014 (PED2014)*. Elsevier, estimated 2015. (Cited on page 71.)

[97] M. Bando, K. Hasebe, A. Nakayama, A. Shibata, and Y. Sugiyama. Structure stability of congestion in traffic dynamics. *Jpn. J. Ind. Appl. Math.*, 11:203, 1994. (Cited on page 71.)

[98] M. Bando, K. Hasebe, A. Nakayama, A. Shibata, and Y. Sugiyama. Dynamical model of traffic congestion and numerical simulation. *Phys. Rev. E*, 51:1035, 1995. (Cited on pages 71 and 74.)

[99] V. J. Blue and J. L. Adler. Cellular automata microsimulation for modeling bi-directional pedestrian walkways. *Transp. Res. B*, 35:293, 2001. (Cited on page 71.)

[100] Z. Fang, W. Song, X. Liu, W. Lv, J. Ma, and X. Xiao. A continuous distance model (cdm) for the single-file pedestrian movement considering step frequency and length. *Physica A*, 391:307, 2012. (Cited on page 71.)

[101] S. Tadaki, M. Kikuchi, Y. Sugiyama, and S. Yukawa. Noise induced congested traffic flow in coupled map optimal velocity model. *J. Phys. Soc. Jpn*, 68(9):3110–3114, 1999. (Cited on page 71.)

[102] S. C. Benjamin, N. F. Johnson, and P. M. Hui. Cellular automata models of traffic flow along a highway containing a junction. *J. Phys. A*, 29:3119, 1996. (Cited on page 71.)

[103] M. Takayasu and H. Takayasu. 1/f noise in a traffic model. *Fractals*, 1:860, 1993. (Cited on page 71.)

[104] Y. S. Ikura, E. Heisler, A. Awazu, H. Nishimori, and S. Nakata. Collective motion of symmetric camphor papers in an annular water channel. *Phys. Rev. E*, 88:012911, 2013. (Cited on page 84.)

[105] D. Böde. *Simulation von Fußgängerbewegung durch eindimensionale Dynamik im Zellularautomaten*. Bachelorarbeit, Universität zu Köln, 2013. (Cited on page 84.)

[106] E. Üstüner. *Modifikation des CDM-Modells zur Fußgängerdynamik*. Bachelorarbeit, Universität zu Köln, 2013. (Cited on page 84.)

[107] D. Miedema, A. de Wijn, and P. Schall. A criterion for condensation in kinetically constrained one-dimensional transport models. *arXiv:1402.6220*, 2014. (Cited on pages 121 and 122.)

[108] U. Kemloh, M. Chraibi, C. Eilhardt, S. Nowak, I. Kulkov, D. Weber, K. Sauer, H. Klüpfel, and A. Schadschneider. OpenPedSim: A Framework for Pedestrian Flow Analysis. In *Pedestrian and Evacuation Dynamics 2012*, pages 1323–1330. Springer, 2014. (Not cited.)

ERKLÄRUNG

Ich versichere, dass ich die von mir vorgelegte Dissertation selbständig angefertigt, die benutzten Quellen und Hilfsmittel vollständig angegeben und die Stellen der Arbeit – einschließlich Tabellen, Karten und Abbildungen –, die anderen Werken im Wortlaut oder dem Sinn nach entnommen sind, in jedem Einzelfall als Entlehnung kenntlich gemacht habe; dass diese Dissertation noch keiner anderen Fakultät oder Universität zur Prüfung vorgelegen hat; dass sie – abgesehen von unten angegebenen Teilpublikationen – noch nicht veröffentlicht worden ist sowie, dass ich eine solche Veröffentlichung vor Abschluss des Promotionsverfahrens nicht vornehmen werde. Die Bestimmungen der Promotionsordnung sind mir bekannt. Die von mir vorgelegte Dissertation ist von Prof. Dr. Andreas Schadschneider betreut worden.

Christian Eilhardt, den 06. August 2014